INTENSIFICATION OF MIXING AND HOMOGENISATION OF CULTURE MEDIUM IN PHOTOBIOREACTORS FOR MICROALGAE PRODUCTION

VOJTĚCH BĚLOHLAV

INTENSIFICATION OF MIXING AND HOMOGENISATION OF CULTURE MEDIUM IN PHOTOBIOREACTORS FOR MICROALGAE PRODUCTION

Author: **Vojtěch Bělohlav**
Supervisors: Tomáš Jirout, Enrica Uggetti

2021

CTU CZECH TECHNICAL UNIVERSITY IN PRAGUE

UPC UNIVERSITAT POLITÈCNICA DE CATALUNYA BARCELONATECH

Doctoral Degree Under Co-Tutoring Agreement Between

Czech Technical University in Prague

and

Universitat Politècnica de Catalunya

PhD Thesis

INTENSIFICATION OF MIXING AND HOMOGENISATION OF CULTURE MEDIUM IN PHOTOBIOREACTORS FOR MICROALGAE PRODUCTION

Vojtěch Bělohlav

2021

Czech Technical University in Prague (CTU), Faculty of Mechanical Engineering
Department of Process Engineering
and
Universitat Politècnica de Catalunya (UPC), Department of Civil and Environmental Engineering
GEMMA – Group of Environmental Engineering and Microbiology

THESIS DISSERTATION OF THE PHD TITLE

INTENSIFICATION OF MIXING AND HOMOGENISATION OF CULTURE MEDIUM IN PHOTOBIOREACTORS FOR MICROALGAE PRODUCTION

Author: Vojtěch Bělohlav
Graduated in Mechanical Engineering specialized in Process Engineering
Graduated in Agricultural Engineering specialized in Technologies for the Food and Bioprocessing Industry

Supervisors: Tomáš Jirout
Enrica Uggetti
Co-supervisors: Lukáš Krátký
Tutor: Joan García Serrano

PhD program: Design and Process Engineering (CTU)
Environmental Engineering (UPC)

Prague and Barcelona, 2021

Acknowledgements

I am thankful to my supervisors Tomáš Jirout and Enrica Uggetti for their valuable guidance and support in scientific matters throughout my studies. I am equally thankful to Lukáš Krátký, Rubén Díez-Montero, and Joan García Serrano for being helpful with experimental measurements and for willing to provide critical feedback and insightful suggestions.

I would also like to express my gratitude to my parents, Zdeněk and Ivana for their guidance during my previous studies and for supporting me all the time. Last but not least, I would like to thank my beloved Jana for her unconditional support and her calmness helped me keep a positive outlook during these years, and together with our dog Chaplin, tolerated my weekends spent with the thesis.

Preface

The current thesis is framed within the context of two Czech grants:

This work was supported by the Ministry of Education, Youth and Sports of the Czech Republic under OP RDE grant number CZ.02.1.01/0.0/0.0/16_019/0000753 “Research centre for low-carbon energy technologies”.

This work was supported by the Grant Agency of the Czech Republic University in Prague (grant no. SGS18/129/OHK2/2T/12).

This work was supported by the European Commission project - INCOVER (GA 689242).

Abstract

Generally, the parameters important for microalgae growth include light irradiation, temperature and nutrients and CO_2 concentrations in the culture medium. However, during the scaling-up, these parameters are often limiting factors for microalgae growth. Due to the large volume of the processed medium in pilot or industrial systems, it is difficult to illuminate the entire layer of the culture medium, which results in the formation of dark zones. Due to insufficient mixing, also an unbalanced utilization of nutrients contained in the culture medium or formation of temperature gradients can occur. Microalgal biofilm formation attached to the transparent walls of closed photobioreactors (PBRs) is also a significant limitation associated with scaling-up, since it can significantly reduce the intensity of incident light.

According to those factors, the hydrodynamic conditions of the culture medium are an important parameter in the scaling-up of cultivation systems, since it affects the mixing and the homogeneity of the culture medium. Efficient mixing can: 1) allow all microalgal cells to reach the irradiated area (light zone) of the culture medium; 2) prevent the formation of temperature gradients or sedimentation of microalgal cells; 3) intensify mass transfer resulting in more efficient utilization of nutrients. Moreover, the intensification of flow in the area close to the transparent walls of the cultivation system can also result in an increase of shear forces close to the wall and a reduction of biofilm formation.

The aim of this thesis was to study the influence of hydrodynamic conditions on parameters affecting the production of microalgae in two cultivation systems: a hybrid horizontal tubular photobioreactor (HHT PBR) and a closed flat panel photobioreactor (FP PBR). To this end, a multi-physical model was created to study the effect of hydrodynamic conditions on microalgae cultivation. Solutions were then proposed to intensify the mixing of the culture medium in order to ensure the homogeneity of hydrodynamic conditions in the entire volume of the culture medium and to increase the microalgae production.

Based on the experimental measurements, a numerical model simulating the hydrodynamic conditions in transparent HHT PBR tubes was validated. Using the particle tracking model, it was possible to simulate the movement of microalgae cells in transparent tubes according to different operating configurations. Through the model, the influence of different operating conditions on the mixing of the culture medium was investigated. When the flow rate of the culture medium increased, the dead zones in the retention tanks were eliminated. The model indicated that the shear stress, which is especially important in terms of biofilm formation, increased in accordance with flow velocities.

A multi-physical model was created integrating particles distribution data under different operating conditions into a mechanistic model simulating the microalgae cultivation process. The developed multi-physical model allowed to investigate the influence of operating conditions on the distribution of light in the culture medium and the production of microalgae. The model was calibrated and validated based on the data from two intensive experimental campaigns. The multi-physical model considered the effect of the distance from the microalgae cells to the irradiated wall of the HHT PBR, which is significantly influenced by the mixing conditions of the culture medium. The model showed that, in systems working with a large layer of culture medium or a high concentration of microalgae, the intensification of mixing increases the production of microalgae. To do this, the hydrodynamic conditions in the cultivation system should be brought as close as possible to the state where the entire volume of the culture medium is ideally mixed. This state can be achieved by increasing the flow rate in the tubes or by using static mixers installed in the tubes of the PBR.

Hydrodynamics in FP PBR were more complex than in HHT PBR. By changing the inflow and outflow configuration in FP PBR, it was possible to change the hydrodynamics of the culture medium in the irradiated area of the PBR. The effect of flow rate on mixing and homogenization was investigated under several inlet and outlet configurations. By comparing the created hydrodynamic model with experimental measurements, the influence of hydrodynamics on the prevention of biofilm formation was specified as well. The created hydrodynamic model allowed to optimize the operating and design parameters of the FP PBR.

The results showed that even by changing the configuration of the inlet and outlet, and the flow rate of the culture medium, the formation of dead zones in the culture medium could not be completely eliminated. Then, in order to intensify the mixing and homogenize the flow of the culture medium in the FP PBR, a static mixer was designed. A numerical model of FP PBR with the static mixer was validated based on experimental measurements. Compared to the empty FP PBR chamber, the homogenization time was reduced and the homogenous flow in the chamber was ensured by the installed static mixer.

The multi-physical model developed in this thesis has proved to be an efficient tool to understand the influence of hydrodynamic conditions on microalgae production. Based on experimental measurements and numerical models, the operating conditions of HHT PBR and FP PBR were optimized. To further intensify the mixing and homogenize the flow of the culture medium, a static mixer was designed, which demonstrated a positive effect on the hydrodynamic conditions of the culture system. Overall, the created numerical model is a useful tool to improve existing cultivation systems, to acquire knowledge during the scale-up of cultivation systems, or for designing novel PBRs.

Abstrakt

Mezi nejdůležitější provozní parametry zajišťující správnou kultivaci mikrořas patří světelné záření, vhodná teplota kultivačního média, koncentrace živin a CO_2 v kultivačním médiu. Při zvětšování měřítka kultivačních systémů jsou však právě tyto parametry limitujícím faktorem. Vzhledem k velkému objemu zpracovávaného média v poloprovozních či průmyslových systémech je obtížně prosvětlit celou vrstvu kultivačního média, což vede k tvorbě tmavých zón, v kterých nejsou mikrořasy dostatečně osvětlovány. V důsledku nedostatečného míchání může také docházet k nerovnoměrnému využívání živin obsažených v kultivačním médiu nebo může docházet ke vzniku teplotních gradientů. Častým problémem je při zvětšování měřítka systému také tvorba biofilmu na transparentních plochách fotobioreaktorů, což dále snižuje intenzitu působícího světelného záření.

Všechny tyto provozní parametry jsou výrazně ovlivňovány hydrodynamickými podmínkami v kultivačních systémech. Studium hydrodynamických podmínek je důležitá zejména při zvětšování měřítka kultivačních systémů. Efektivní promíchávání kultivačního média může: 1) umožnit, aby se všechny buňky mikrořas dostaly do ozařovaného prostoru (světlá zóna) kultivačního média; 2) zabránit vzniku teplotních gradientů nebo sedimentaci buněk mikrořas; 3) zintenzivnit přenos hmoty, což vede k účinnějšímu využívání živin. Intenzivnější promíchávání v blízkosti transparentních ploch může dále zvýšit lokální hodnoty smykového napětí, které ovlivňuje tvorbu biofilmu.

Cílem této práce bylo studium vlivu hydrodynamických podmínek na parametry ovlivňující produkci mikrořas ve dvou kultivačních systémech: hybridní horizontální trubkový fotobioreaktor a uzavřený deskový fotobioreaktor. Za tímto účelem byl vytvořen multifyzikální model, který umožňuje detailně studovat vliv hydrodynamických podmínek na proces kultivace mikrořas. Na základě studia stávajících konstrukcí fotobioreaktorů byla navržena řešení pro zintenzivnění míchání kultivačního média s cílem zajistit homogenitu hydrodynamických podmínek v celém objemu zpracovávaného kultivačního média a zvýšit tak produkci mikrořas.

Na základě experimentálního měření byl validován numerický model simulující hydrodynamické podmínky v transparentních trubkách hybridního trubkového fotobioreaktoru. Pomocí modelu trasování pohybu částic bylo možné simulovat pohyb buněk mikrořas pro různé provozní konfigurace. Pomocí vytvořeného modelu byl zkoumán vliv různých provozních podmínek na míchání kultivačního média. Při navýšení průtoku kultivačního média byly eliminovány zóny v zadržovacích tancích, kde médium proudí nízkou rychlostí a mohli by zde docházet k sedimentaci buněk mikrořas. Model ukázal, že smykové napětí, které je důležité zejména z hlediska tvorby biofilmu, se zvyšuje v závislosti na rostoucí rychlosti proudění.

Výsledky distribuce částic byly integrovány do multifyzikálního modelu, který dokáže predikovat vliv hydrodynamických podmínek na proces kultivace mikrořas. Vytvořený multifyzikální model tak umožňuje zkoumat vliv provozních podmínek na distribuci světla v kultivačním médiu a produkci mikrořas. Model byl kalibrován a validován na základě údaje ze dvou intenzivních experimentálních kampaní. Multifyzikální model zohledňuje vliv vzdálenosti proudících buněk mikrořas od ozařované stěny fotobioreaktoru, která je výrazně ovlivňována promícháváním kultivačního média. Model ukázal, že v systémech pracujících s velkou vrstvou kultivačního média nebo s vysokou koncentrací mikrořas zvyšuje intenzifikace míchání celkovou produkci mikrořas. Z tohoto důvodu je potřeba hydrodynamické podmínky kultivačního média co nejvíce přiblížit stavu, kdy je celý objem média ideálně promícháván. Tohoto stavu lze v případě trubkového fotobioreaktoru dosáhnout zvýšením průtoku nebo použitím statických směšovačů, které by byly instalovány v transparentních trubkách.

Hydrodynamické podmínky v deskovém fotobioreaktoru jsou v porovnání s hybridním trubkovým fotobioreaktorem výrazně komplikovanější. Změnou konfigurace nátoku a odtoku z komory deskového fotobioreaktoru je možné sledovat vliv geometrie a provozních podmínek na hydrodynamiku tohoto systému. Porovnáním vytvořeného hydrodynamického modelu s experimentálními měřeními bylo možné zkoumat vliv hydrodynamiky na prevenci tvorby biofilmu. Vytvořený hydrodynamický model dále umožnil optimalizovat provozní a konstrukční parametry deskového fotobioreaktoru.

Výsledky ukázaly, že pouhou změnou konfigurace vstupního a výstupního hrdla nebo změnou průtoku kultivačního média nelze zcela eliminovat tvorbu mrtvých zón v komoře deskového fotobioreaktoru. Za účelem eliminace těchto zón byl navržen statický směšovač, který byl instalován v komoře fotobioreaktoru. Numerický model hydrodynamických podmínek v komoře se statickým směšovačem byl validován na základě experimentálních měření. Ve srovnání s prázdnou komorou deskového fotobioreaktoru se při použití statického směšovače zkrátila doba homogenizace a proudění média bylo rovnoměrně distribuováno po celém průřezu komory.

Na základě experimentálních měření a numerických modelů byly optimalizovány provozní podmínky v hybridním horizontálním trubkovém fotobioreaktoru a deskovém fotobioreaktoru. Pro další zintenzivnění míchání a homogenizaci proudění kultivačního média byl navržen statický směšovač, který prokázal pozitivní vliv na hydrodynamické podmínky kultivačního systému. Vytvořený numerický model prokázal, že je užitečný nástroj využitelný k optimalizaci stávajících kultivačních systémů, k studiu provozních parametrů při zvětšování měřítka kultivačních systémů nebo pro návrh nových fotobioreaktorů.

Resumen

Generalmente, los factores más importantes para el crecimiento de microalgas incluyen la luz, temperatura, y concentración de nutrientes y CO_2 en el medio de cultivo. Sin embargo, al aumentar la escala del cultivo, estos factores suelen ser limitantes para el crecimiento de las microalgas. Debido al gran volumen de los sistemas piloto o industriales, es difícil iluminar todo el volumen del medio de cultivo, lo que da lugar a la formación de zonas en sombra. También puede producirse una utilización desequilibrada de los nutrientes contenidos en el medio de cultivo o la formación de gradientes de temperatura si la mezcla es deficiente. La formación de biopelículas de microalgas adheridas a las paredes transparentes de fotobiorreactores cerrados (PBR) es también una limitación significativa asociada con el escalado, ya que puede reducir significativamente la intensidad de la radiación de luz incidente.

De acuerdo con estas limitaciones, un factor determinante en el escalado de los sistemas de cultivo son las condiciones hidrodinámicas en el mismo, ya que afectan al mezclado y la homogeneidad del medio de cultivo. Una mezcla eficiente puede: 1) permitir que todas las células alcancen el volumen iluminado del medio de cultivo; 2) prevenir la formación de gradientes de temperatura o la sedimentación de células; 3) intensificar la transferencia de masa dando como resultado una utilización más eficiente de los nutrientes. Además, la intensificación del flujo en la zona cercana a las paredes transparentes del sistema de cultivo da lugar a un aumento del esfuerzo cortante en la pared y una reducción de la formación de biopelículas.

El objetivo de esta tesis ha sido estudiar la influencia de las condiciones hidrodinámicas sobre los parámetros que afectan a la producción de microalgas en dos sistemas de cultivo: un fotobiorreactor tubular horizontal híbrido (HHT PBR) y un fotobiorreactor cerrado de placa plana (FP PBR). Con este fin, se construyó un modelo multifísico para estudiar el efecto de las condiciones hidrodinámicas en el cultivo de microalgas. Posteriormente, se propusieron soluciones para intensificar la mezcla del medio de cultivo con el fin de asegurar la homogeneidad de las condiciones hidrodinámicas en todo el volumen y aumentar la producción de microalgas.

Se construyó un modelo numérico que simula las condiciones hidrodinámicas en tubos transparentes HHT PBR, el cual fue validado a partir de mediciones experimentales. Utilizando el modelo de seguimiento de partículas, fue posible simular el movimiento de células de microalgas en el interior de los tubos con diferentes configuraciones de operación. Mediante el modelo, se investigó la influencia de diferentes condiciones operativas en la mezcla del

medio de cultivo. Al aumentar el caudal en el medio de cultivo, se eliminaron las zonas muertas en los tanques de retención. El modelo indicó que el esfuerzo cortante en la pared, que es especialmente importante en términos de formación de biopelículas, aumentó al incrementar la velocidad de flujo.

Se creó un modelo multifísico que combina la distribución de partículas en diferentes condiciones operativas con un modelo mecanicista que simula el proceso de cultivo de microalgas. El modelo multifísico desarrollado permitió evaluar la influencia de las condiciones operativas en la distribución de la luz en el medio de cultivo y la producción de microalgas. El modelo fue calibrado y validado utilizando los resultados de dos campañas experimentales intensivas. Gracias al modelo desarrollado se ha podido estudiar el efecto de la distancia entre las células de microalgas y la pared iluminada del HHT PBR, que está significativamente influenciada por las condiciones de mezcla en el medio de cultivo. El modelo mostró que, en sistemas que trabajan con una gran profundidad de medio de cultivo o una alta concentración de microalgas, la intensificación de la mezcla aumenta la producción de microalgas. Para ello, las condiciones hidrodinámicas en el sistema de cultivo deben aproximarse lo más posible al estado de mezcla ideal en todo el volumen del medio de cultivo. Este estado se puede lograr aumentando el caudal circulante en los tubos o utilizando mezcladores estáticos instalados en los tubos del PBR.

La hidrodinámica en el FP PBR es más compleja que en el HHT PBR. Al cambiar la configuración de entrada y salida en el FP PBR, fue posible modificar la hidrodinámica en el medio de cultivo en la zona iluminada del PBR. Se evaluó el efecto del caudal sobre la mezcla y la homogeneización en varias configuraciones de entrada y salida. Al comparar las simulaciones del modelo hidrodinámico con mediciones experimentales, también evaluó la influencia de la hidrodinámica en la prevención de la formación de biopelículas. El modelo hidrodinámico desarrollado permitió optimizar los parámetros operativos y de diseño del FP PBR.

Los resultados mostraron que, incluso cambiando la configuración de la entrada y la salida, así como la velocidad de flujo del medio de cultivo, no se pudo eliminar por completo la formación de zonas muertas en el medio de cultivo. Entonces, para intensificar el mezclado y homogeneizar el flujo del medio de cultivo en el FP PBR, se diseñó un mezclador estático. En comparación con la cámara del FP PBR vacía, mediante la instalación del mezclador estático se redujo el tiempo de homogeneización y se aseguró el flujo homogéneo en la cámara.

El modelo multifísico desarrollado en esta tesis ha demostrado ser una herramienta eficaz para comprender la influencia de las condiciones hidrodinámicas en la producción de microalgas en fotobiorreactores. Basándose en mediciones experimentales y modelos numéricos, se han optimizado las condiciones de funcionamiento de HHT PBR y FP PBR.

Para intensificar aún más la mezcla y homogeneizar el flujo del medio de cultivo, se diseñó un mezclador estático, que demostró tener un efecto positivo sobre las condiciones hidrodinámicas del sistema de cultivo. En definitiva, el modelo numérico creado es una herramienta útil para optimizar la operación de los sistemas de cultivo existentes, para adquirir conocimientos durante el escalado de los sistemas de cultivo y para diseñar nuevos PBR.

Acronyms and Abbreviations

ASM3	Activated Sludge Model No. 3
CFD	Computational fluid dynamic
COD	Chemical oxygen demand
CTU	Czech Technical University in Prague
DO	Dissolved oxygen
FM	Flowmeter
FP PBR	Flat panel photobioreactor
GEMMA	Research Group of Environmental Engineering and Microbiology
HHT PBR	Hybrid horizontal tubular photobioreactor
HRT	Hydraulic retention time
HS	pH sensor
L/D	Light and dark cycle
LES	Large eddy simulation
LS	Level sensor
NS	Turbidity sensor
OS	Dissolved oxygen sensor
PBR	Photobioreactor
PFD	Process flow diagram
PMMA	Polymethylmethacrylate
PS	Pressure sensor
PVC	Polyvinyl chloride
RANS	Reynolds Averaged Navier-Stokes
RMSE	Root mean square error
RNG	Re-Normalisation Group
RTD	Residence time distribution
RWQM1	River Water Quality Model 1
TIN	Total inorganic nitrogen
TS	Temperature sensor
TSS	Total suspended solids
UPC	Universitat Politècnica de Catalunya – BarcelonaTech
VSS	Volatile suspended solids

List of symbols

A	(m^2)	Cross-sectional area
B	(-)	Constant
b	(m)	Distance to the nearest wall
C	(g m^{-3})	Concentration of tracer in culture medium
$C_{1\varepsilon}$	(-)	Model constant
$C_{1\varepsilon}$	(-)	Model constant
C_i	(g m^{-3})	Concentration of tracer in culture medium in discrete form
COD	(gO_2 m^{-3})	Chemical oxygen demand concentration
C_μ	(-)	Model constant
d	(m)	Tube inner diameter
d_1	(m)	Tube diameter of HHT PBR
d_2	(m)	Tube diameter of geometrically similar PBR
D_{ax}	(-)	Dimensionless axial dispersion coefficient
D_{diff}	(m^2 s^{-1})	Diffusion coefficient
d_h	(m)	Hydraulic diameter
E	(s^{-1})	Residence time distribution
E_θ	(-)	Dimensionless residence time distribution
$f_{T,FS}$	(-)	Thermic photosynthetic factor
G_b	(kg m^{-1} s^{-3})	Generation of turbulence kinetic energy due to buoyancy
G_k	(kg m^{-1} s^{-3})	Generation of turbulence kinetic energy due to the mean velocity gradient
H	(m)	Distance of the particle from the irradiated wall
h_1	(m)	Culture medium level in discharge section of retention tank
h_2	(m)	Culture medium level in suction section of retention tank
I_{av}	(W m^{-2})	Average light intensity
$I_{CO2,ALG}$	(g m^{-3})	Carbon dioxide inhibition constant
I_o	(W m^{-2})	Incident light intensity
k	(m^2 s^{-2})	Turbulent kinetic energy
k^*	(-)	Relative roughness
$K_{C,ALG}$	(g m^{-3})	Saturation constant for carbon species
$k_{death,ALG}$	(s^{-1})	Decay constant of microalgae
$k_{death,H}$	(s^{-1})	Decay of heterotrophic bacteria
k_{eq}	(s^{-1})	Dissociation constant of reaction
K_I	(m^2 g^{-1})	Extinction coefficient
k_La_{CO2}	(s^{-1})	Volumetric mass transfer coefficient for carbon dioxide
k_La_{NH3}	(s^{-1})	Volumetric mass transfer coefficient for ammonia
k_La_{O2}	(s^{-1})	Volumetric mass transfer coefficient for oxygen
$K_{N,ALG}$	(g m^{-3})	Saturation constant for nitrogen species

$K_{O2,ALG}$	(g m^{-3})	Saturation constant for oxygen species
$k_{resp,ALG}$	(s^{-1})	Rate of endogenous respiration
k_s	(m)	Roughness
L	(m)	Length of the tube
l_m	(m)	Mixing length
L_s	(m)	Length of the static mixer
n	(-)	Dimensionless constant in power-law velocity profile
Pe	(-)	Péclet number
Q	(m^3 s^{-1})	Volume flow rate
R	(m)	Inner tube radius
r	(m)	Radial coordinate
Re	(-)	Reynolds number
Re_t	(-)	Turbulent Reynolds number
S_{CO2}	(gCO_2-C m^{-3})	Dissolved carbon dioxide concentration
S_{CO3}	(gCO_3^{2-}-C m^{-3})	Carbonate concentration
S_{eq}	(g m^{-3})	Concentration at equilibrium
S_H	(gH^+ m^{-3})	Hydrogen ions concentration
S_{HCO3}	(gHCO_3^--C m^{-3})	Bicarbonate concentration
S_I	(gCOD m^{-3})	Inert soluble organic matter concentration
S_{NH3}	(gNH_3-N m^{-3})	Ammonia nitrogen concentration
S_{NH4}	(gNH_4^+-N m^{-3})	Ammonium nitrogen concentration
S_{NO2}	(gNO_2^--N m^{-3})	Nitrite nitrogen concentration
S_{NO3}	(gNO_3^--N m^{-3})	Nitrate nitrogen concentration
S_{O2}	(gO_2 m^{-3})	Dissolved oxygen concentration
S_{OH}	(gOH^--H m^{-3})	Hydroxide ions concentration
S_{PO4}	(gPO_4^--P m^{-3})	Phosphate phosphorus concentration
S_S	(gCOD m^{-3})	Readily biodegradable soluble organic matter concentration
S^{WAT}	(g m^{-3})	Saturation concentration of gas in the water
t	(s)	Time
t_D	(s)	Retention time in dark zone
t_i	(s)	Time in discrete form
t_L	(s)	Retention time in light zone
t_m	(s)	Mean residence time
TSS	(gCOD m^{-3})	Total suspended solids concentration
$\bar{u}$	(m s^{-1})	Mean velocity
$u*$	(m s^{-1})	Friction velocity
u_i	(m s^{-1})	Velocity
u_{max}	(m s^{-1})	Centreline velocity
VSS	(gCOD m^{-3})	Volatile suspended solids concentration
X_{ALG}	(gCOD m^{-3})	Microalgae biomass concentration
X_{AOB}	(gCOD m^{-3})	Ammonium oxidizing bacteria concentration
X_C	(gCOD m^{-3})	Sum of particulate components concentration

X_H	(gCOD m^{-3})	Heterotrophic bacteria concentration
X_I	(gCOD m^{-3})	Inert particulate organic matter concentration
X_{NOB}	(gCOD m^{-3})	Nitrite oxidizing bacteria concentration
X_S	(gCOD m^{-3})	Slowly biodegradable particulate organic matter concentration
y^+	(-)	Dimensionless distance from the wall
z	(m)	Depth of culture medium in PBR
z_{tank}	(m)	Depth of culture medium in retention tank
τ_{lam}	(Pa)	Shear stress in laminar flow
τ_{tur}	(Pa)	Shear stress in turbulent flow
α_k	(-)	Inverse effective Prandtl number
α_k	(-)	Inverse effective Prandtl number
β	(-)	Constant
Δh	(m)	Difference of culture medium level
Δp	(Pa)	Pressure drop
Δp_s	(Pa)	Pressure drop of the static mixer
Δt	(s)	Time difference
ε	(m^2 s^{-3})	Dissipation rate
ε_L	(-)	Light fraction
η_{PS}	(-)	Photosynthetic factor
θ	(-)	Normalized time
λ	(-)	Friction coefficient
μ	(Pa s)	Dynamic viscosity
μ_{ALG}	(s^{-1})	Maximum growth rate of microalgae
μ_H	(s^{-1})	Maximum growth rate of heterotrophic bacteria
μ_t	(Pa s)	Turbulent viscosity
ν	(m^2 s^{-1})	Kinematic viscosity
ξ	(-)	Local loss coefficient
ρ	(kg m^{-3})	Density
ρ_i	(kg m^{-3} s^{-1})	Process rate corresponding to process *i*
τ	(Pa)	Shear stress
τ_w	(Pa)	Wall shear stress
σ^2	(-)	Dimensionless variance of the RTD function
σ_t^2	(s^2)	Variance of the RTD function

List of contents

1

Introduction

Fossil fuels are the largest source of greenhouse gases. Mitigation strategies are therefore required to neutralize the excess of carbon dioxide (CO_2). The 2015 United Nations Climate Change Conference was held in Paris, where the participating 195 countries agreed to reduce emissions as part of the method for reducing greenhouse gas. The members agreed to reduce their CO_2 outputs and to do their best to decrease global warming (The Paris Agreement 2020). The Paris Agreement was followed in 2018 by the Katowice Climate Change Conference, which further confirmed the direction (The Katowice climate package: Making the Paris Agreement work for all 2020). The European Green Deal is a package of measures by the European Commission, presented in December 2019, which should ensure the transition of citizens and companies in the European Union to a more sustainable economy. The European Green Deal aims to transform the European economy so that it can grow without increasing the use of natural resources (A European Green Deal 2020).

1.1 Biotechnological potential of microalgae

New strategies are required for energy security as well as to mitigate emissions. Therefore, renewable energy technologies expand and receive a lot of attention. Microalgae biomass can be used for the production of high-value products in the food or pharmaceutical industry. However, microalgae has also the potential to replace fossil fuels in form of biofuels and it is possible to use them to mitigate the CO_2 emission from the atmosphere. Nevertheless, challenges to commercialize the production at a large scale need to be solved. The demand for biofuels is not that high due to the low market price of fossil fuels, the high cost of the biofuels produced from microalgae, and the slow return of investment. Moreover, the investment costs are also high in the cultivation systems for the production of microalgal high-value products. Taking into account the previously mentioned influences, it is necessary to optimize and improve technologies before microalgae production can become economically viable (Milano et al., 2016). This should be accomplished together with political and economic support by governments, which will probably increase due to the outcomes of the United Nation agreement.

Microalgae biomass is classified as a third-generation feedstock and has a potential for biofuel, food, feed and chemical production. The main benefit of microalgae is their growth yields and the low land requirement. Microalgae are possible to grow with the large diversity of biomass content on wastewater as well (Slegers et al., 2013). Microalgae are part of a large and diverse group of simple aquatic organisms (Slade and Bauen, 2013). The characteristic of microalgae is that they are able to convert sunlight, CO_2, and nutrients into biomass through photosynthesis in the same way as other plants. However, microalgae have higher photosynthetic efficiency than other crops, which leads to a higher conversion of CO_2 to

microalgae biomass. They can grow at a faster rate than other land-based crops and can live in a diverse environment with basic nutrient requirements (Milano et al., 2016).

1.2 Microalgae cultivation systems

Microalgae can be cultivated in various aqueous systems that can be divided into two main groups: open cultivation systems and closed photobioreactor systems (PBRs). The literature describes widely the advantages and disadvantages of individual cultivation systems for microalgae production (Mata et al., 2010; Olivieri et al., 2014; Wang et al., 2012). Many papers are focused not only on cultivation itself but also on the design of cultivation systems.

Open cultivation systems

There is a number of open pond system configurations used for microalgae cultivation such as raceway ponds (Mohd Udaiyappan et al., 2017) or thin-layer cascade (Masojídek, 2014). In such systems, nutrients are normally supplied by channeling runoff water from land areas, industrial disposal water or urban wastewater treatment plant.

The most commonly used open cultivation system is the raceway pond (Figure 1.2.1a). The microalgae, water and nutrients are circulated around a racetrack using paddle wheels to keep microalgae suspended in water and to allow the utilization of CO_2 from the atmosphere. Generally, the pond is shallow (0.3 m) to provide a light penetration into microalgae culture to maximize the photosynthetic effect. The main drawback of those systems is that it is difficult to control surrounding environmental conditions such as medium temperature, weather and the possibility of contamination with different microalgae species (Masojídek, 2014). These conditions can significantly affect microalgae biomass production due to temperature fluctuation in microalgae growth, CO_2 deficiencies, inefficient agitation and light limitation (Milano et al., 2016).

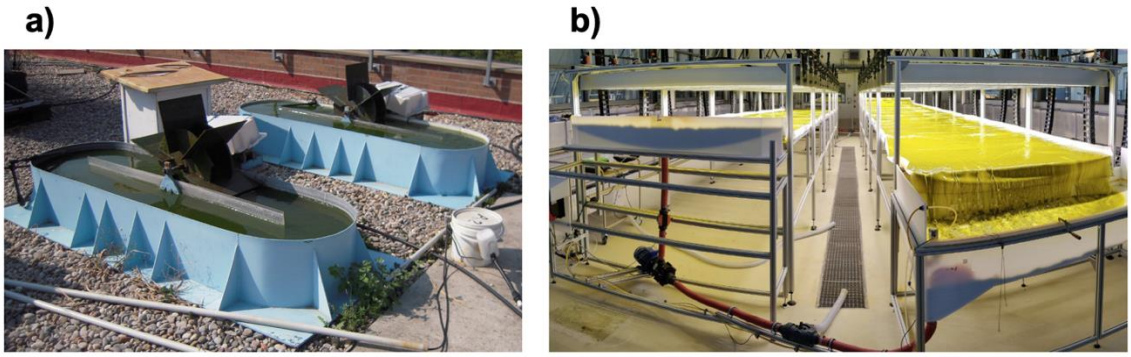

Fig. 1.2.1. Open cultivation systems – a) raceway pond system (Matamoros et al., 2015) and b) thin-layer cascade system (Schädler et al., 2021).

Another kind of open cultivation system is the thin-layer cascade (Figure 1.2.1b). This system consists of a basin, a retention tank connected by a pump and pipelines to a horizontal sloping cascade plate. Microalgal suspension flows in a thin layer (25 mm) from the basin over a slightly sloping cascade that is exposed to light radiation. After exposure, the suspension is collected in a retention tank. Finally, the suspension is pumped back to the basin from the retention tank via tubes. The thickness of the layer in the plate can be regulated by a baffle located at the end of the cascade (Jerez et al., 2014). This feature excludes light limitation in comparison with the raceway pond system, leading to easier penetration into the medium.

Closed cultivation systems

To overcome the problems associated with the open pond system, closed PBRs are nowadays used for microalgae cultivation. The main advantage of such systems is the high productivity thanks to effective control of the operating conditions, such as temperature, CO_2 concentration, or pH. Moreover, it is possible to reduce the risk of contamination of the culture medium from the environment. Therefore, also microalgae species that are more sensitive to environmental and operating conditions can be processed (Molina et al., 2001). The investment costs of closed PBRs are higher than open systems (Milano et al., 2016). Moreover, also operating and maintenance costs are significantly higher due to the need for additional equipment that ensures the circulation of the culture medium and the control of different parameters. There are many types of closed PBR systems such as tubular PBR (Massart et al., 2014), flat panel PBR (Wang et al., 2012), or column PBR (Xu et al., 2009).

The tubular PBR consists of an array of transparent tubes that capture light radiation. Tubular PBR can be distinguished by their arrangement: horizontal (Figure 1.2.2a), vertical (Figure 1.2.2b), inclined or helix. Microalgae are recirculated either by a pump or by an airlift system that can intensify absorption and desorption of CO_2 and O_2 between the liquid medium and injected gas. Injected gas can also provide agitation, which is very important to enhance the gas exchange and avoid biomass sedimentation. On the other hand, it is necessary to consider the possibility of biofilm formation and high operating costs. The irradiated part of the tubular PBR consists of tubes allowing the light to penetrate efficiently thanks to a high surface/volume ratio (Brennan and Owende, 2010). However, the length of the tubes is limited in order to avoid dissolved O_2 accumulation. Gómez-Pérez et al. (2015) defined an optimal tube length according to the chosen volumetric flow of the culture medium and the oxygen production rate.

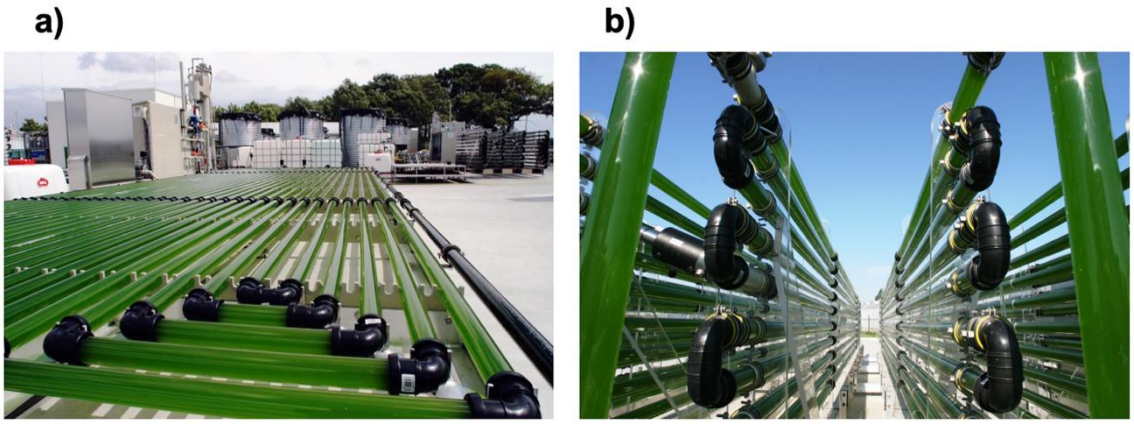

Fig. 1.2.2. Closed cultivation systems – a) tubular horizontal PBR (Bosma et al., 2014) and b) tubular vertical PBR (Slegers et al., 2013).

Flat panel PBRs are made of transparent plates for maximum solar energy capture. High radiation absorbance is secured by a thin layer of dense culture flowing across the flat plates. The productivity is significantly influenced by shading and diffuse light penetration between the single panels. The fresh medium is fed by a pump and a suspension of water and microalgae cultures is withdrawn from the plate and collected in a retention vessel. The main advantage of flat panel PBR is the large surface area exposed to illumination (Sforza et al., 2014).

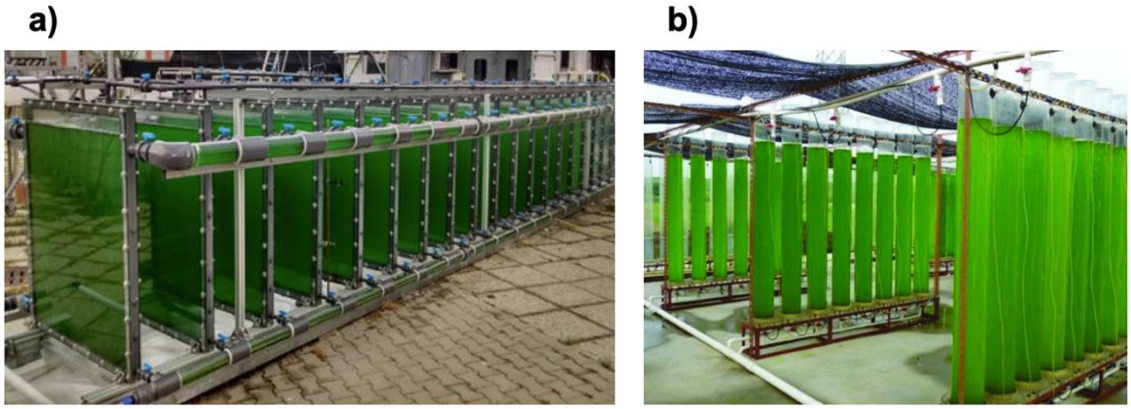

Fig. 1.2.3. Closed cultivation systems – a) flat panel PBR (Lindblad et al., 2019) and b) column PBR (Huo et al., 2018).

Column PBR is a vertical cylinder aerated from the bottom and illuminated through transparent walls. The illumination area is smaller in comparison with the tubular and flat panel PBR and, therefore, internal illumination can be used. Generally, column PBR function is similar to tubular PBR, but the construction is more sophisticated and thus more expensive (Brennan and Owende, 2010). The main benefit of column PBR is the efficient agitation, high volumetric mass transfer rates and controllable growth conditions. Moreover, columns require less energy for cooling because of the low surface to volume ratio. Moreover, the aerated PBR ensures the circulation of the microalgae culture without moving parts or mechanical pumping, which

leads to low shear stress and consequently low stressing of microalgae cells. A vertical orientation of the construction decreases requirements for the land area (Kunjapur and Eldridge, 2010).

Hybrid cultivation systems

The hybrid systems partially combine the two previous groups. Part of the hybrid cultivation system is closed, and part of the system is open. Hybrid systems thus use the possibility to increase the ratio of surface to total volume through closed transparent components.

The main benefits and drawbacks of the mentioned design alternatives are shown in Table 1.2.1.

Table 1.2.1. Advantages and disadvantages of cultivation system design alternatives.

Cultivation system	Advantages	Disadvantages
Raceway pond	Large capacity of culture medium Low investment, operation and maintenance costs	Sedimentation of microalgae Ineffective irradiation of medium Medium contamination Low surface to volume ratio
Thin-layer cascade	Effective irradiation of medium	Low capacity of culture medium Medium contamination
Tubular PBR	Effective irradiation of medium Prevention of contamination Large surface to volume ratio	Maintenance requirements High investment costs
Flat panel PBR	Large capacity of culture medium Effective irradiation of medium Prevention of contamination Large surface to volume ratio	Maintenance requirements Hight investment costs
Column PBR	Large capacity of culture medium Prevention of contamination	Ineffective irradiation of medium Sedimentation of microalgae Maintenance requirements Hight investment costs

2

State of the art

Given the global strategy to implement a circular economy based on streamlining the processes of using all residual materials to generate byproducts and renewable energy sources, the microalgae cultivation technology appears to be very beneficial with potential for use in a wide range of processes. In order to reach a full industrial scale for microalgal biomass processing technologies and for final products to be competitive on the market, it is necessary to increase the efficiency of the cultivation process itself and to optimize the systems for microalgae cultivation.

2.1 Operating parameters to be considered for scale-up

Multiple operating parameters have a significant influence on the scale-up of cultivation system design. The intensification of the process should necessarily take into account aspects such as light, temperature, mass transfer, heat transfer, and shear forces on the transparent plates. These aspects are crucial for transport phenomena specification and the subsequent scale-up design methodology. Proper microalgae growth and biomass productivity depend on several operational and design factors. Generally, microalgae need light, nutrients, a carbon source, and a certain temperature to grow properly. However, too high intensity light, ammonium or oxygen level can inhibit microalgae growth. Such parameters are strictly connected with the particular microalgae species, some of them grow well at low temperatures and low light intensities, whereas others need higher irradiance (Masojídek, 2014).

Light

In all microalgae cultivation systems, the light source and light intensity are critical factors affecting the condition of autotrophic microalgae growth. For outdoor cultivation systems, sunlight can be used as the source of light, whereas artificial light sources are used for indoor cultivation systems. On the other hand, it is also possible to use sunlight as a source for indoor systems by transmitting solar energy from outside to illuminate indoor systems with the help of optical fiber systems (Mata et al., 2010). The fluctuations in sunlight can be avoided by the application of artificial light sources. The main benefit is that artificial source is stable, controllable and it allows more choices in location. For this reason, the light utilization efficiency and microalgae biomass productivity are usually higher under artificial light sources, if compared with natural sunlight. On the other hand, the investment costs and operating costs are higher than for the sunlight cultivation system, which leads to higher final production costs (Wang et al. 2014). Maximum specific growth rate, specific respiration rate, and the light saturation constant are defined properties of a given microalgal strain and the mass specific light absorption coefficient is estimated from the light absorption levels with different cell concentrations of microalgal cultures (Li et al., 2015).

Another important feature of microalgae is their resistance to photoinhibition. Indeed, excess radiation can inhibit their growth and decrease the production of the system. According to the microalgal species, the needs for exposure to irradiance and relaxing in the calm section vary, and so does the ratio of light and dark periods. It means that microalgae also need a non-irradiated section to calm and further develop their growth. Data of acceptable light and dark ratio for various microalgae species are mentioned in the literature (Huang et al., 2014; Phillips & Myers, 1954). This ratio affects not only the growth rate but also has an impact on the development of microalgae and their structure (Mata et al., 2010). Due to this fact, for systems irradiated by sunlight, where it is not possible to regulate the intensity of light radiation, it is necessary to design a cultivation system with variable retention times in the light and dark zones of the photobioreactors. Modification of design can allow further exploration of the influence of light/dark ratio. As a relaxation zone, a retention vessel can be used to prevent radiation. Another option is the possibility to create dark zones directly in the irradiated area of the photobioreactor. Therefore, it is important to ensure sufficient mixing of the culture medium in order to provide the appropriate ratio between light and dark. In the case of the application of artificial light, it is also possible to regulate the irradiance intensity according to the microalgae needs or to change the light and dark ratio by flashing light (Abu-Ghosh et al., 2016).

Temperature

Microalgae culture growth rate varies according to the temperature of culture medium changes. Although microalgae can grow at a variety of temperatures, the optimal range of most of them is between 15 and 30°C. However, some microalgae species tolerate a broad range of temperatures between 15 and 45°C (Masojídek, 2014). Transparent components of the closed photobioreactors partially reflect light radiation into the environment, nevertheless, most of the light radiation passes into the culture medium. The PBR transparent components absorb the incident energy, which causes the heating of the culture medium to a certain temperature. At the same time, the culture medium is also affected by the surrounding environment.

Mass transfer and pH

Besides light and nutrients, also CO_2 is a necessary component for proper photosynthetic cultivation. The utilization of CO_2 by microalgae for their growth can be divided into two main stages: the absorption of CO_2 by the mass transfer and the fixation of CO_2 by photosynthesis. The aim of the absorption is to reduce the mass transfer resistance. The fixation of CO_2 means uptake by microalgae for its growth and it can increase with increasing CO_2 retention time in the cultivation system. Therefore, the time for CO_2 absorption from gas by water should be similar to the time required for the fixation of CO_2 by microalgae (Vasumathi et al., 2012).

However, the mechanism must be suitable for O_2 removal from microalgae as well, because the high level of O_2 around microalgae cells is undesirable. The source of CO_2 may be the surrounding air with a CO_2 concentration of about 0.04 %. To intensify the growth, the flue gas with a concentration of CO_2 ranging between 0.04 and 15 % can be used (Kunjapur and Eldridge, 2010). Each microalgae species has its narrow optimal range of pH. The optimal pH of most cultured microalgae species is in the range of 7-9. However, some species have their optimal pH value in acid or basic ranges. The pH of the medium is connected to the concentration of CO_2. Since pH is so fundamental, it is necessary to control it during the growth (Wang et al., 2012).

Biofilm formation

Another important factor accompanied by the scale-up of the cultivation system is the formation of biofilm. The biofilm is the thin layer, with a thickness of the magnitude of units up to hundreds of millimeters, formed on the photobioreactor surfaces. Thus, the ability of the culture medium to be irradiated is reduced when the biofilm is formed on transparent walls of PBR (Huang et al., 2016). Biofilm removal has an important role in closed cultivation systems. The biofilm is visible as a thin viscous layer of sediments, and its thickness reaches units up to hundreds of micrometers. Biofilm formation reduces light intensity in the system (Zippel and Neu, 2005). The study of Huang et al., (2016) showed that the biofilm density exceeds 40 g m^{-2}, and almost no light passes through the layer. Schnurr et al., (2014) referred that the cells in the culture medium received only 20 µmol m^{-2} s^{-1} of light intensity, from the original 100 µmol m^{-2} s^{-1} if the biofilm thickness was 150 µm. Based on this information, it can be considered that the biofilm significantly affects the limitation of the light into the system, reduces the photosynthetic efficiency of the culture system, and, consequently, the productivity of microalgal biomass. The presence of biofilm also leads to other undesirable phenomena, namely loss of cell pigmentation, contamination by microbes and bacteria, and encrustation of the PBR surface (Zeriouh et al., 2017). The most important processing parameter for the growth of microalgae is light radiation (Cicci et al., 2014). Therefore, the removal of biofilm on the transparent walls of the PBR is one of the most important steps for the performance efficiency of bioprocesses in PBRs.

Biofilm formation is influenced especially by material, adhesion, microalgae species, their physicochemical properties, nutrients chemical composition, by the geometry of the PBR and the hydrodynamics (Barros et al., 2019). The process of biofilm formation on the transparent wall of the PBR consists of several stages. It begins with the colonization of the support material, so the microalgae cells begin to adhere to the surface due to the effect of adhesive forces. Biofilm formation is affected by the force effects that act on the cell. When the cells remain adhered on the surface, adhesive forces are higher than other force effects dependent

on the surface properties of the wall. As the microalgae layer matures, the thickness of the biofilm increases as well. The final stage of biofilm formation involves the release of the microalgae cells and other microorganisms into the culture medium (Vanysacker et al., 2014). Factors supporting the biofilm formation can be optimized to reach the biofilm elimination or removal on the illuminated surface of the PBR.

Methods of biofilm removal can be divided into three main groups. Nowadays, the most common method is mechanical cleaning. Another option to eliminate biofilm formation is to optimize the geometry of the system in order to ensure appropriate hydrodynamic conditions (Ting et al., 2017). The geometric optimizations can provide appropriate mixing intensity, which can ensure the prevention of sedimentation, mass transfer, gas exchange, and elimination of the dead zones. Other available methods are, for example, the use of ozone, ultrasonic technology, removal by sand, or the use of various chemicals. Comparing the previously mentioned methods, geometric optimization and hydrodynamics seem to be the most appropriate methods for biofilm removal (Zakova et al., 2019). The most important parameter of those methods is to find the critical value of the wall shear stress. If the value of the shear stress is over 80 to 100 Pa, microalgal cells are damaged or completely destroyed (Wang & Lan, 2018). However, if the value is too low, the biofilm remains attached to the transparent wall. Therefore, a suitable wall shear stress value is an important processing parameter.

Hydrodynamic characterization and mixing

Hydrodynamic conditions are important for proper microalgae cultivation. It is necessary to prevent sedimentation of microalgae cells and ensure that all cells will have a uniform average exposure time to light and nutrients. Flow regime or mixing should also increase mass transfer conditions and, furthermore, facilitate heat transfer and thus avoid the formation of the thermal gradient. The flow regime is also important in terms of microalgal biofilm formation on transparent components of closed cultivation systems that would decrease irradiation of culture medium. Therefore, it is necessary to provide sufficient shear forces on the walls of the transparent components. On the other hand, excessively high flow velocities should be avoided to prevent cell stress (Acién Fernández et al., 2001) and to avoid unnecessary energy consumption. The selection of the optimal operating condition of the system can reduce the cultivation system costs (Gómez-Pérez et al., 2015).

Microalgae cultivation is a very complex process that is influenced by several operating parameters. From the mentioned operating parameters, it can be stated that hydrodynamics is the most important since it influences all operating parameters of cultivation systems. Hydrodynamic conditions affect the intensity of light that microalgae cells need for their growth. By suitable mixing, it is possible to ensure that all microalgal cells are irradiated evenly and also the formation of thermal gradients in the culture medium is eliminated. Hydrodynamic

conditions are also very important in terms of mass transfer, which intensifies the utilization of nutrients and CO_2 for the growth of microalgae. The study of hydrodynamic conditions in cultivation systems is crucial for scale-up, optimization, and general design of cultivation systems.

2.2 Hydrodynamics influence on microalgae cultivation

As the hydrodynamics of the culture medium is very important for streamlining the process of microalgae cultivation in PBRs, an overview of studies aimed at modeling and investigation of the influence of hydrodynamic conditions on microalgae cultivation is presented here.

2.2.1 Microalgae models

A number of different models have been developed to describe the photosynthesis and process of microalgae cultivation, which can be specified in terms of biomass growth, nutrients utilization, or the influence of light, temperature or pH. Most of these models using the Monod formulation for the description of microalgae processes.

Nikolaou et al. 2016

The principle of the model is based on the combination of a semi-mechanistic model and a Lagrangian particle tracking model. The semi-mechanistic model describes microalgal growth, photoregulation, photoinhibition or photoacclimation. Imperfect mixing of the culture medium is described by the particle tracking model. Nikolaou et al. (2016) presented a modeling methodology for the prediction of microalgae cultivation in raceway ponds with imperfect mixing conditions. The work demonstrates the effect of mixing intensification on the increasing production of microalgae. The microalgal growth model takes into account the basics of photosystem II (RCII) and photoregulation activity (NPQ), which predict fluorescence fluxes. The fluxes are described more in detail in Bernardi et al. (2015). The growth model consists of 13 equations defining the processes of growth. These equations provide the minimum complexity of the system for accurate prediction of *Nannochloropsis gaditana* growth.

The hydrodynamic model was created in the ANSYS 15 software. A transient *k-ε* model with a time step of 0.01 s was used to simulate the movement of particles in the raceway PBR. The movement of particles was monitored in the PBR and the position of the particles was recorded every second. To integrate hydrodynamic conditions into the growth model, a vertical position of the particles as a function of time was generated. This made it possible to monitor the distance of the particles from the level of the culture medium which is irradiated with the light source. The reduction of incident light radiation through the culture medium is described using Beer-Lambert's law. From the generated distance of the particles from the irradiated surface, it is possible to determine the intensity of the light radiation that the individual particles receive

under the selected operating conditions. Using a hydrodynamic model, it was possible to observe the different behavior of microalgal particles depending on their initial position in the PBR. This results in imperfect mixing in the entire cross-section and dead zones are created where the degree of mixing is minimal. The paddle wheel had a significant effect on the movement of individual particles. The created model showed a significant effect on the production of microalgae when considering the ideal mixing, ie the variant where all cells are evenly exposed to light radiation so all cells are identical in terms of their photosynthetic states. The model also studied the effect of dilution on the production of microalgae according to imperfect and perfect mixing conditions.

Blanken et al. 2016

The kinetic model can be used to predict the growth of microalgae in systems with limited light supply. The model combines a mathematical description of photoautotrophic sugar production and aerobic chemoheterotrophic biomass growth. The rate of phototrophic sugar production depends on the light intensity. The aerobic model defines the use of the sugar produced in the light reaction for the formation of biomass. The attenuation of incident light radiation is described using Beer-Lambert's law. The effect of incident light radiation can also be investigated for different wavelengths. The model was developed based on five measurable parameters: molar mass of the microalgae, specific light absorption coefficient per wavelength, sugar yield on photons, biomass yield on sugar, maintenance-related specific sugar consumption rate, and maximal specific sugar production rate. All these parameters can also be obtained from the literature for various types of culture media. The kinetic model takes into account only the thickness of the layer of the culture medium and its effect on the reduction of the intensity of incident light radiation. However, it does not take into account the effect of mixing the culture medium on the ability of irradiation of microalgal cells in the culture medium. Blanken et al. (2016) validated a kinetic model based on experimental data that can simulate the cultivation process of *Chlorella sorokiniana*.

Suh and Lee 2003

The importance of light radiation for microalgae cultivation has been described in chapter 2.1. Suh and Lee (2003) developed a model describing the distribution of light radiation in tubular systems with an internal light source. Using the model, it is possible to predict the intensity of light radiation on the cells contained in the culture medium. The model is based on Beer-Lambert's law, which describes the reduction of light radiation propagating through the culture medium. Using the model, the distribution of light intensity for different geometries of tubular PBR in different design arrangements with an internal light source can be simulated. The distribution of light radiation can then be used to determine the effect on the growth of

microalgae. The developed model was validated on the basis of experimental measurements of light distribution in the radial direction in the internally irradiated PBR tube.

Papacek et al. 2018

The model describes the effect of operating parameters on the growth of microalgae. The growth of microalgae cells is affected by heterogeneous environmental conditions such as light irradiation or mixing of the culture medium. This model consists of three main parts. The first part defines the model of microalgae growth in a cultivation system. The model of microalgae growth consists of the advection-diffusion-reaction system with a phenomenological model of photosynthesis and photoinhibition. The model brings together the dynamics of three basic states that occur in cultivation systems: cell growth, photoinhibition, and photosynthetic reactions in light and dark cycles. The second part of the model specifies the hydrodynamics by fluid flow Navier-Stokes equations. This part of the model can describe the hydrodynamics also as a multiphase flow. The third part describes the irradiance field in the cultivation system by Beer-Lambert law. Papacek et al., (2018) integrated this multidisciplinary model within CFD Ansys Fluent software. The application of the model was validated on a simplified 2D cavity.

Huesemann et al. 2016

The model can predict biomass production in open pond cultivation systems. The model takes into account the utilization of nutrients for the growth of microalgae depending on the variable intensity of incident light and for changing the temperature of the culture medium. The model can be used for batch or continuous operation. Different thicknesses of the culture medium and varying concentrations of the culture medium are taken into account in the model using Beer-Lambert's law. The culture medium is thus divided into separate layers, which receive different intensities of light radiation. The model assumes that the biomass concentration in each layer increases exponentially over time. Biomass growth is affected by a specific growth rate. Specific growth is influenced by model input parameters. As the input parameters, the intensity of incident light radiation and the temperature of the culture medium, are used in the model. Furthermore, data describing the properties of the microalgae strain in the culture medium are also inserted into the model. Experimentally determined strain input parameters are growth rate as a function of light intensity and temperature, biomass loss rate in the dark as a function of temperature and light intensity during the preceding light period, and the scatter-corrected biomass light absorption coefficient. The model assumes that light radiation and the temperature of the culture medium are key factors influencing the microalgae cultivation process. On the contrary, the effect of varying nutrient concentrations in the culture medium, the amount of CO_2, and the mixing of the culture medium are neglected. Another assumption is that the pH remains constant throughout the process and the cultivation is not limited by inhibition by photosynthetic oxygen or other compounds. Huesemann et al. (2016)

validated a model for three different species: *Chlorella sorokiniana*, *Nannochloropsis salina*, and *Picochlorum species*. The model was designed to investigate the effect of fluctuations in incident light intensity and temperature of the culture medium. The model demonstrated the ability to simulate a time-dependent increase in biomass production and the development of photosynthetic oxygen according to different culture medium temperatures. Using the created model, it is possible to investigate the effect of light radiation and the temperature of the culture medium on different types of microalgae. However, the model does not take into account the influence of hydrodynamic conditions on operating parameters and the process of cultivation.

Numerical modeling can be used for the simulation of the cultivation process. Nikolaou et al. (2016) presented a modeling methodology for the prediction of microalgae cultivation in raceway ponds with imperfect mixing conditions. The work demonstrates the effect of mixing intensification on the increasing production of microalgae. Blanken et al. (2016) validated a kinetic model based on experimental data that can simulate the cultivation process of *Chlorella sorokiniana*. Suh and Lee (2003) developed a model able to simulate the degree of illumination of indoor illuminated reactors. The distribution of light radiation can then be used to determine the effect on the growth of microalgae. Huesemann et al. (2016) validated a model for predicting microalgal biomass production in outdoor open ponds. The model was designed to investigate the effect of fluctuations in incident light intensity and temperature on the culture medium. The developed model also takes into account the effect of the thickness of the layer of the culture medium, which reduces the penetration of light radiation in the culture medium. However, the model does not take into account the influence of hydrodynamic conditions. Solimeno et al. (2017a) created a BIO_ALGAE mechanistic model that describes the complex function of a system for the cultivation of microalgae and bacteria. Based on the input parameters, this model can simulate the production of microbial biomass and it is thus possible to study the composition of microorganisms in the system as well. However, the model does not include the effect of hydrodynamics on operating conditions and the cultivation process (Solimeno and García, 2019).

Most of the created models are focused either on the biological part of the microalgae cultivation process or on the hydrodynamics in culture systems. The created models are always applied to a specific type of cultivation system or for a specific application in a given technology. However, as the scale is increased or the geometry of the culture system is changed, hydrodynamics will have a greater and greater effect on the microalgae cultivation process itself. Therefore, it is necessary to take into account the complexity of the microalgae cultivation process during creating models. An important aspect is also the versatility of its use and the possibility of adapting to various operating conditions or design parameters.

Solimeno et al. 2017

Solimeno et al. (2017a) created a BIO_ALGAE mechanistic model that describes the complex function of a system for the cultivation of microalgae and bacteria. Based on the input parameters, this model can simulate the production of microbial biomass and it is thus possible to study the composition of microorganisms in the system as well. However, the model does not include the effect of hydrodynamics on operating conditions and the cultivation process (Solimeno and García, 2019). BIO_ALGAE is the mechanistic model that combines the most important physical, chemical and biokinetic processes that describe microalgae cultivation. The model was developed as part of Solimeno's PhD thesis (Solimeno, 2017) at the Universitat Politècnica de Catalunya. By using the model, it is possible to understand more in detail the interaction of microalgae and bacteria occurring when wastewater is used for microalgae growth. The BIO_ALGAE model consists of River Water Quality Model 1 (RWQM1) and a modified Activated Sludge Model No. 3 (ASM3).

Table 2.2.1.1. BIO_ALGAE model components (Solimeno et al., 2017).

Particulate components	
X_{ALG}	Microalgae biomass
X_H	Heterotrophic bacteria
X_{AOB}	Ammonium oxidizing bacteria
X_{NOB}	Nitrite oxidizing bacteria
X_S	Slowly biodegradable particulate organic matter
X_I	Inert particulate organic matter
Dissolved components	
S_{NH4}	Ammonium nitrogen
S_{NH3}	Ammonia nitrogen
S_{NO3}	Nitrate nitrogen
S_{NO2}	Nitrite nitrogen
S_{PO4}	Phosphate phosphorus
S_{O2}	Dissolved oxygen
S_{CO2}	Dissolve carbon dioxide
S_{HCO3}	Bicarbonate
S_{CO3}	Carbonate
S_H	Hydrogen ions
S_{OH}	Hydroxide ions
S_S	Readily biodegradable soluble organic matter
S_I	Inert soluble organic matter

The model includes the most important operating parameters such as temperature, photorespiration, pH, light irradiation, light attenuation, and transfer of gases to the atmosphere. The model works with 6 particulate and 13 dissolved components, which are implicated as variables (Table 2.2.1.1) in the physical, chemical, and biokinetic processes (Solimeno et al., 2017).

The BIO_ALGAE model consists of microalgal and bacterial processes, chemical equilibrium equations and equations describing the transfer of gases into the atmosphere. The growth rate of microalgal biomass per unit time is expressed as the product of their maximum specific growth rate μ_{ALG} (s^{-1}), their concentration at a given point in time X_{ALG} (g m^{-3}), dimensionless thermic photosynthetic factor $f_{T,FS}$, which takes into account the effect of temperature on growth of microalgae, dimensionless photosynthetic factor η_{PS}, which takes into account the effects of light intensity and excess of oxygen on photosynthesis, and concentration of dissolved components (Table 2.2.1.1). The rate of microalgae growth on ammonia is defined

$$\rho_{1a} = \mu_{ALG} \cdot f_{T,PS} \cdot \eta_{PS} \cdot \frac{S_{CO2} + S_{HCO3}}{K_{C,ALG} + S_{CO2} + S_{HCO3} + \frac{{S_{CO2}}^2}{I_{CO2,ALG}}} \cdot \frac{S_{NH3} + S_{NH4}}{K_{N,ALG} + S_{NH3} + S_{NH4}} \cdot \frac{S_{PO4}}{K_{P,ALG} + S_{PO4}} \cdot X_{ALG} \tag{2.1}$$

where $I_{CO2,ALG}$ (g m^{-3}) is the carbon dioxide inhibition constant, and $K_{C,ALG}$ (g m^{-3}) is the saturation constant for carbon species. The rate of microalgae growth on nitrate is defined

$$\rho_{1b} = \mu_{ALG} \cdot f_{T,PS} \cdot \eta_{PS} \cdot \frac{S_{CO2} + S_{HCO3}}{K_{C,ALG} + S_{CO2} + S_{HCO3} + \frac{{S_{CO2}}^2}{I_{CO2,ALG}}} \cdot \frac{S_{NO3}}{K_{N,ALG} + S_{NO3}} \cdot \frac{K_{N,ALG}}{K_{N,ALG} + S_{NH3} + S_{NH4}} \cdot \frac{S_{PO4}}{K_{P,ALG} + S_{PO4}} \cdot X_{ALG} \tag{2.2}$$

where $K_{N,ALG}$ (g m^{-3}) is the saturation constant for nitrogen species. The rate of endogenous respiration is specified by the rate of endogenous respiration of microalgae $k_{resp,ALG}$ (s^{-1}), the concentration of microalgae X_{ALG}, thermic photosynthetic factor $f_{T,FS}$, and saturation constant for oxygen species $K_{O2,ALG}$ (g m^{-3}) as expressed in Eq. (2.3)

$$\rho_2 = k_{resp,ALG} \cdot f_{T,FS} \cdot \eta_{PS} \cdot \frac{S_{O2}}{K_{O2,ALG} + S_{O2}} \cdot X_{ALG} \tag{2.3}$$

The rate of microalgae inactivation is expressed as

$$\rho_3 = k_{death,ALG} \cdot f_{T,FS} \cdot X_{ALG} \tag{2.4}$$

where $k_{death,ALG}$ (s^{-1}) is the decay constant of microalgae. Chemical equilibria affect carbon, nitrogen and also the balance of hydrogen and hydroxide ions. The rate of chemical equilibrium reactions is defined by Eq. (2.5) to (2.8)

$$CO_2 \leftrightarrow HCO_3^-: \qquad \rho_4 = k_{eq.1} \cdot \left(S_{CO2} - S_{eq,1}\right) \tag{2.5}$$

$$HCO_3^- \leftrightarrow CO_3^{2-}: \qquad \rho_5 = k_{eq.2} \cdot \left(S_{HCO3} - S_{eq,2}\right) \tag{2.6}$$

$$NH_4^+ \leftrightarrow NH_3: \qquad \rho_6 = k_{eq.3} \cdot \left(S_{NH4} - S_{eq,3}\right) \tag{2.7}$$

$$H^+ \leftrightarrow OH^-: \qquad \rho_7 = k_{eq.w} \cdot \left(1 - S_{eq,w}\right) \tag{2.8}$$

where $k_{eq,i}$ (s^{-1}) are dissociation constant of reaction *i*, and $S_{eq,i}$ (g m^{-3}) is the concentration of component *i* at equilibrium. Transfer rates of gases (oxygen, carbon dioxide, ammonia) to the atmosphere is defined by Eq. (2.9) to (2.11)

$$\rho_8 = k_L a_{O2} \cdot \left(S_{O2}^{WAT} - S_{O2}\right) \tag{2.9}$$

$$\rho_9 = k_L a_{CO2} \cdot \left(S_{CO2}^{WAT} - S_{CO2}\right) \tag{2.10}$$

$$\rho_{10} = k_L a_{NH3} \cdot \left(S_{NH3}^{WAT} - S_{NH3}\right) \tag{2.11}$$

where $k_L a_i$ (s^{-1}) is the volumetric mass transfer coefficient of gas *i*, and S_i^{WAT}(g m^{-3}) is the saturation concentration of gas *i* in the water (Solimeno et al., 2015). BIO_ALGAE model using Monod kinetics for bacterial processes in the same way as for microalgae processes. All processes, parameters and constants are described in detail in Solimeno et al., (2017).

By using this model, it is possible to predict microalgae production for different operating conditions. The growth of microalgae depends on the intensity of light irradiation, temperature, which are the most limiting factors in cultivation systems. However, the model can describe the dependence of microalgae growth on the utilization of nutrients as well. The model needs to be carefully calibrated based on the maximum growth rate of microalgae (μ_{ALG}), the maximum growth rate and the decay of heterotrophic bacteria (μ_H and $k_{death,H}$) and the transfer of gases to the atmosphere ($k_L a_{O2}$, $k_L a_{CO2}$ and $k_L a_{NH3}$). Photorespiration is also implemented in the model, which can describe the accumulation of dissolved oxygen in closed cultivation systems. According to this, it is possible to monitor in which part of the PBR the produced microalgae cells may be inhibited due to the excessive amount of produced oxygen (Solimeno and García, 2019).

Using the model, the effect of microalgae concentration in the culture medium on growth efficiency can be monitored. Due to the increasing concentration, the light source may not be able to effectively illuminate the entire layer of the culture medium. In this case, the model considers the increasing concentration of microalgae and the depth of the culture medium in the system. Light attenuation in this case can limit microalgae growth by 60 % (Solimeno et al., 2017).

The BIO_ALGAE model works on the assumption that the culture medium is ideally mixed. The light is thus ideally distributed, and the temperature of the culture medium is homogeneous throughout the volume of the PBR. The PBR also works ideally in terms of nutrient utilization and mass transfer. All these assumptions can be considered for simplification in laboratory

systems and pilot PBRs. However, with the transition to a larger scale device, the usability of BIO_ALGAE may be limited. In the conclusions of the dissertation thesis, Solimeno (2017) states that the aim of further work should be to integrate the influence of hydrodynamic conditions on the process of microalgae cultivation. Application of Computational fluid dynamics (CFD) simulations can provide information that would further refine the homogeneity of the concentration of individual components important for the growth of microalgae. CFD model can reflect the influence of hydrodynamic conditions on the intensity of light irradiation and subsequently on microalgal cells distribution as well. Details about the BIO_ALGAE model can be found in Solimeno (2017) and Solimeno et al. (2017). The PBR geometry in BIO_ALGAE model is represented in a 1D domain divided into two parts: one part represents the open components, and the second part represents the closed transparent components. The ratio of both parts corresponds to the volume of culture medium in open and closed components. The model assumes that each cell of the microalgae receives the same quantity of photons since the model does not consider non-ideal mixing. Therefore, the light attenuation in the model is calculated from average light intensity representing any point of the culture medium. The exponential decrease of light intensity as it penetrates into the depth of culture medium was described by average light intensity I_{av} (W m^{-2}) using Lambert-Beer's Law

$$I_{av} = \frac{I_O \cdot \left(1 - e^{(-K_I \cdot X_C \cdot z)}\right)}{K_I \cdot X_C \cdot z} \tag{2.12}$$

where I_o (W m^{-2}) is the incident light intensity, K_I (m^2 g^{-1}) is the extinction coefficient, and z (m) is the depth of culture medium in HHT PBR. Average light intensity is attenuated by the particulate components from Table 2.2.1.1.

$$X_C = X_{ALG} + X_I + X_S + X_{AOB} + X_{NOB} \tag{2.13}$$

A detailed description of the equations used in the BIO_ALGAE model is reported in Solimeno (2017).

2.2.2 Hydrodynamic conditions in cultivation systems

It is important to ensure sufficient mixing of the culture medium in cultivation systems (Huang et al., 2014). Mixing affects the mass transfer and subsequently to the utilization of nutrients and carbon dioxide for the growth of microalgae. It is important to ensure that no sedimentation of microalgae cells occurs. It is also necessary to provide homogenous light irradiation of cells in the culture medium. Due to the higher biomass concentrations or large layer thicknesses of the culture medium, scattering can occur, which can significantly affect the efficiency of the cultivation system (Perner-Nochta and Posten, 2007). This can lead to the formation of dark zones in the culture medium, where the cells do not receive a sufficient amount of light radiation

(Zhang et al., 2013). Moreover, achieving a sufficiently intensive mixing of the culture medium can be complicated due to the scale-up complexity as well (Schreiber et al., 2017).

There are two ways to scale-up tubular systems. The first option for increasing the volume of culture medium in the tubular system is to extend the lengths of the transparent tubes. However, this leads to higher demands for the built-up area. During the extension of tubes, it is necessary to take into account also the increasing concentration of produced oxygen, which could inhibit the produced microalgae (Camacho Rubio et al., 1999). The second option is to increase the diameter of the transparent tubes. The advantage is lower demands in the built-up area. However, as the diameter of the tubes increases, the layer of the culture medium increases as well. Increasing the thickness of the culture medium layer can result in reduced penetration of incident light radiation into the culture medium and subsequent formation of dark zones. Thus, when increasing the diameter of the transparent tubes, it is necessary to ensure sufficient mixing of the culture medium so all microalgal cells can be irradiated.

The scale-up of a flat panel PBR is a complex process. The height of the plates is limited by hydrostatic pressure, which would place more emphasis on the robustness of the structure. The distance between the transparent plates is limited by the light ability to penetrate through the culture medium layer. Janssen et al. (2003) and Zhu et al. (2013) report that a gap greater than 50 mm between transparent plates results in a reduction in total microalgae production. Thus, it seems that the only way to effectively scale-up the FP PBR is to install parallel panels side by side. However, for scaling-up by enlarging the gap between the transparent plates, it is necessary to ensure sufficient mixing of the culture medium in order to provide homogenous light irradiation of all microalgae cells. Huang et al. (2014) in their work investigated the influence of internal mixing elements on the total production of microalgae in the FP PBR with a gap between transparent plates of 150 mm. By installing internal static mixers, an increase in the residence time in the irradiated area was achieved, which also resulted in an overall increase in the production of microalgae. Wang et al. (2014) described the increase in the production of microalgae depending on the installation of internal mixing elements that intensify the mixing of the culture medium in the chamber with a distance between transparent plates of 80 mm. The installed static mixers caused not only the increase of microalgae production but also provided the uniform growth conditions of microalgae cells at different locations inside the PBR chamber. Degen et al. (2001) confirmed the positive effect of internal mixing elements on the production of microalgae in the culture medium. However, it is stated in the work that it is important to ensure uniform mixing in the entire volume of the culture medium in order to prevent the formation of static dead zones in the PBR chamber.

The Computational fluid dynamic (CFD) method, which allows to simulate parameters affecting the hydrodynamics in the system, can be used for a detailed description of hydrodynamic

conditions in the PBRs. CFD is a tool based on the fluid dynamics theory. Fluid flows are described by partial differential equations and CFD replaces these equations with algebraic equations, which can be subsequently numerically solved. These equations describe how the single operating parameters are related. The application of a numerical model can replace complex experimental measurements (Pires et al., 2017). Using the numerical simulations, it is possible to investigate the formation of dead zones in the culture medium (Gómez-Pérez et al., 2015), or the influence of the geometry and internal modifications, such as static mixers, on the process of cultivation (Perner-Nochta and Posten, 2007). The results of numerical simulations can help to optimize the geometry of the cultivation system (Bitog et al., 2011), however, each numerical model needs to be validated using basic experiments that can determine whether the model corresponds to real hydrodynamic conditions (Pires et al., 2017). From the definition of numerical models, it is possible to define the limitations, which need to be considered during the evaluation of the results.

Gómez-Pérez et al. (2015) and Pires et al. (2017) described CFD applications to model the operation of PBRs in recent years. Most of these studies are focused on a reduction in energy consumption and operating costs. Further studies are focused on the effect of flow velocity on biofilm formation in the dead zones of the PBRs. Zhang et al. (2013) and Perner-Nochta and Posten, (2007) described the influence of static mixers application in tubular PBR tubes on operating conditions and energy consumption. Bitog et al. (2011) review the status of CFD modeling for PBRs and the application of CFD in the design of PBR for microalgae production in different cultivation systems as well. The CFD can not only provide a quantitative description of the flow characteristics but can also simulate the motion of particles in multiphase flow (Su et al., 2010).

CFD appears to be a suitable tool for the detailed study of local hydrodynamic conditions in cultivation systems. Using a validated CFD model, it is possible to investigate the influence of various operating and design parameters on the hydrodynamics of the culture medium. The results of numerical simulations can be subsequently used to optimize the operation of existing PBRs or to design a novel cultivation system.

2.3 Conclusions

For scaling-up a cultivation system from a laboratory or pilot scale to an industrial scale, it is necessary to ensure sufficient hydrodynamic conditions. Crucial inhomogeneities in the culture medium can cause the formation of temperature gradients or inefficient utilization of nutrients can occur during the scale-up. Also, the formation of dead zones, where the culture medium is not sufficiently mixed, can result in sedimentation of the produced microalgae and the formation of biofilm. In systems operating with a large thickness or with the concentrated culture medium, it is difficult to irradiate the entire layer due to the reduction of incident light

radiation during the penetration in the culture medium. Reduction of incident light radiation can cause the formation of dead zones, which reduce the efficiency of the whole microalgae cultivation process. Therefore, during the scaling-up, it is necessary to optimize the operating and geometric parameters of the cultivation system in order to ensure suitable hydrodynamic conditions for the cultivation of microalgae in the entire volume of the PBR culture medium.

To optimize the operating and design parameters of existing PBRs, it is important to investigate the influence of operating conditions on the microalgae cultivation process. For this purpose, it is appropriate to use numerical models that allow a detailed study of local hydrodynamic conditions in the culture medium and their subsequent effect on microalgae growth. It is possible to predict the influence of hydrodynamic conditions on light distribution in culture medium and microalgae production. Using validated numerical models, it is possible to specify the design modifications or to adjust operating conditions. Numerical models can then be used for scale-up or design of novel cultivation systems as well.

3

Objectives and thesis outline

The overall objective of the present PhD thesis was to study and optimize the operating conditions of two cultivation systems in order to intensify microalgae production. A hybrid horizontal tubular photobioreactor (HHT PBR) and a closed flat panel photobioreactor (FP PBR) were selected for the study. The majority of existing cultivation systems work efficiently only on a laboratory scale. However, as their design is scaled-up, significant operational problems arise and their applicability on a pilot or industrial scale is limited. Hydrodynamics in cultivation systems has a strong influence during scaling-up, since it affects all parameters important for microalgae cultivation. For this reason, the first objective was to study the hydrodynamic conditions of existing cultivation systems creating a mechanistic model to simulate microalgae cultivation. Experimental measurements were then performed to calibrate and validate the model. Finally, the results of the model were used to optimize the operating conditions and design parameters of the studied PBRs.

3.1 Objectives

The specific objectives of this research were:

- Calibrate a mechanistic model simulating the process of microalgae cultivation in HHT PBR based on the intensive experimental campaigns.
- Calibrate and validate the Computational fluid dynamic (CFD) model simulating hydrodynamic conditions in HHT PBR based on the experimental measurements.
- Integrate the influence of hydrodynamic conditions into a mechanistic model that would consider the influence of hydrodynamics in HHT PBR on the microalgae cultivation process.
- Specify the influence of different operating conditions on the hydrodynamics of the culture medium and the process of microalgae cultivation in HHT PBR.
- Validate the CFD model simulating hydrodynamic conditions in FP PBR based on the experimental measurements.
- Specify the influence of different operating configurations on the hydrodynamics in FP PBR and influence on the formation of biofilm as the key factor affecting the scale-up of cultivation systems.
- Optimize the operating conditions of HHT PBR and FP PBR according to the results of experimental measurements and numerical simulations in terms of the intensification of microalgal biomass production.
- Optimize the design of the FP PBR chamber concerning the intensification of mixing and homogenization of the culture medium. Based on experimental measurements and the created CFD models, verify the usability of internal installations in FP PBR chamber for intensification of mixing and homogenization of culture medium flow.

3.2 Thesis outline

The work on the thesis was carried out under a co-tutoring agreement between Czech Technical University in Prague (CTU) and Universitat Politècnica de Catalunya (UPC). The first part was focused on the study of HHT PBR, which is installed at UPC. The second part was focused on the study of FP PBR installed at CTU. The PhD thesis is based on fifteen scientific articles (thirteen of which have been already published, see CV at the end of this document). The thesis is divided into two main parts. The thesis consists of the following chapters:

Chapter 4: Modeling of hybrid horizontal tubular PBR performance and hydrodynamics

Based on two intensive measurement campaigns, a mechanistic BIO_ALGAE model simulating the process of microalgae cultivation in HHT PBR was calibrated and validated. Furthermore, a CFD model simulating hydrodynamic conditions was created. The CFD model was validated using data from experimental measurements of hydrodynamic conditions. Then it was used to simulate fluid dynamics and particle tracking.

Chapter 5: Multi-physical model integrating the hydrodynamics and PBR performance

Hydrodynamic conditions in the HHT PBR were integrated into the mechanistic BIO_ALGAE model. The developed integrated multi-physical model was calibrated and validated based on the experimental data.

Chapter 6: Hydrodynamics influence on microalgae production and light regime

Hydrodynamic conditions on the microalgae cultivation process were investigated using the integrated multi-physical model. Furthermore, the influence of operating conditions on the light regime in the culture medium, and the formation of light and dark zones in HHT PBR transparent tubes were studied.

Chapter 7: Hydrodynamics of flat panel PBR

The CFD model simulating hydrodynamic conditions in FP PBR was validated based on experimental measurements. Using the model and measured data, the influence of different operating conditions on the mixing intensity, homogenization of the culture medium, and biofilm formation on transparent walls of FP PBR was monitored.

Chapter 8: Homogenization and mixing of flow in flat panel PBR

The FP PBR chamber was optimized in order to intensify the homogenization of the culture medium in the irradiated area of the FP PBR. Using the developed CFD numerical model, the influence of the static mixer on the hydrodynamic conditions was studied.

4

Modeling of hybrid horizontal tubular PBR performance and hydrodynamics

This chapter is based on articles:

Belohlav, V., Uggetti, E., García, J., Jirout, T., Kratky, L., Díez-Montero, R. (2021). Assessment of hydrodynamics based on Computational Fluid Dynamics to optimize the operation of hybrid tubular photobioreactors. *Journal of Environmental Chemical Engineering*, 9, 105768.

Díez-Montero, R., Belohlav, V., Ortiz, A., Uggetti, E., García-Galán, M. J., García, J. (2020). Evaluation of daily and seasonal variations in a semi-closed photobioreactor for microalgae-based bioremediation of agricultural runoff at full-scale. *Algal Research*, 47, 101859.

Belohlav, V., Uggetti, E., Montero, R. D., García, J., Jirout, T., Kratky, L. (2018). Numerical investigation of hydrodynamic conditions in a pilot tubular photobioreactor. In European Biomass Conference and Exhibition Proceedings; ETA – Florence, pp 183–190.

García, J., Ortiz, A., Álvarez, E., Belohlav, V., García-Galán, M. J., Díez-Montero, R., Álvarez, J. A., Uggetti, E. (2018). Nutrient removal from agricultural run-off in demonstrative full scale tubular photobioreactors for microalgae growth. *Ecological Engineering*, 120.

Belohlav, V., Jirout, T., Kratky, L., Uggetti, E., Díez-Montero, R., García, J. (in preparation). Integration of hydrodynamics in cultivation model of hybrid horizontal tubular photobioreactor.

A hybrid horizontal tubular PBR was used to study the influence of hydrodynamic conditions on the cultivation process. In order to study the influence of hydrodynamic conditions on the cultivation process, it is necessary to create a model that will be able to predict microalgal biomass growth depending on different operating conditions. For this purpose, it is necessary to create a validated hydrodynamic model, which will be able to simulate in detail the local hydrodynamic parameters. The results of the hydrodynamic model can be subsequently integrated into a numerical model that is able to predict microalgal biomass production. For this purpose, the numerical BIO_ALGAE model, which was created at the Universitat Politècnica de Catalunya, can be used. However, before the integration itself, BIO_ALGAE model needs to be validated based on the experimental data from an intensive measurement campaign in hybrid horizontal tubular PBR. Using the integrated model and hydrodynamic model, it is possible to subsequently optimize the operating and design parameters of the PBR.

4.1 Photobioreactor design and system operation

Three hybrid horizontal tubular photobioreactors (HHT PBRs) are located in the Agròpolis experimental campus of the Universitat Politècnica de Catalunya – BarcelonaTech (UPC) (41.288N, and 2.043 E UTM) close to Barcelona's airport. The HHT PBRs are part of the bio-refinery concept designed to process wastewater and further generate reusable water and different high-value bioproducts. The aim of the biorefinery concept is to change the current wastewater treatment concept towards a bioproduct recovery industry (Uggetti et al., 2018).

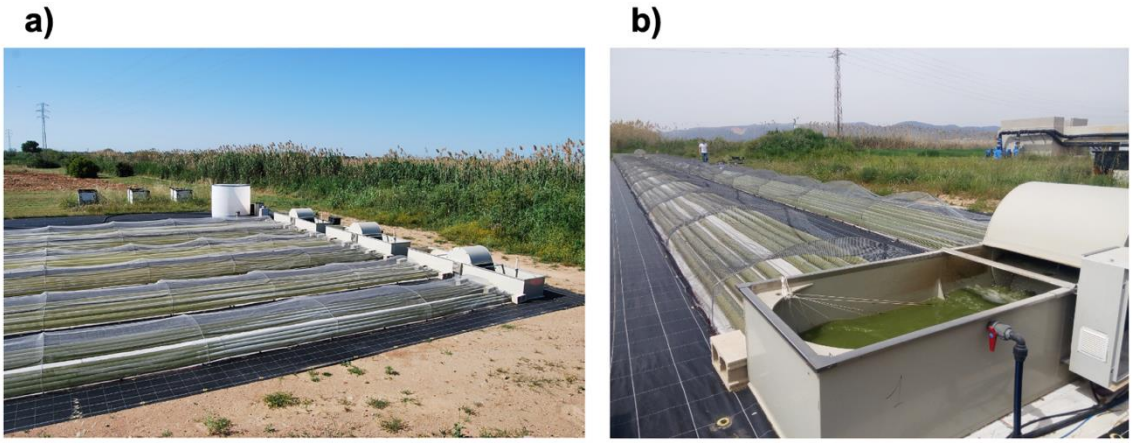

Fig. 4.1.1. HHT PBR in Agròpolis experimental campus - a) three parallel PBRs and b) detail view on retention tank with paddle wheel.

The PBRs and their support elements and equipment were designed and constructed by the Research Group of Environmental Engineering and Microbiology (GEMMA) of the UPC in collaboration with the company Disoltech S.L. Each HHT PBR (Figure 4.1.1) consists of two open retention tanks connected through 16 low-density polyethylene transparent tubes with *d*=125 mm inner diameter. The total volume of the culture medium in each PBR is 11.7 m^3.

Both tanks are equipped with a paddle wheel, which is powered by a 0.25 kW engine. The paddle wheel speed is varied by a frequency converter in the range of 0 to 12 rpm.

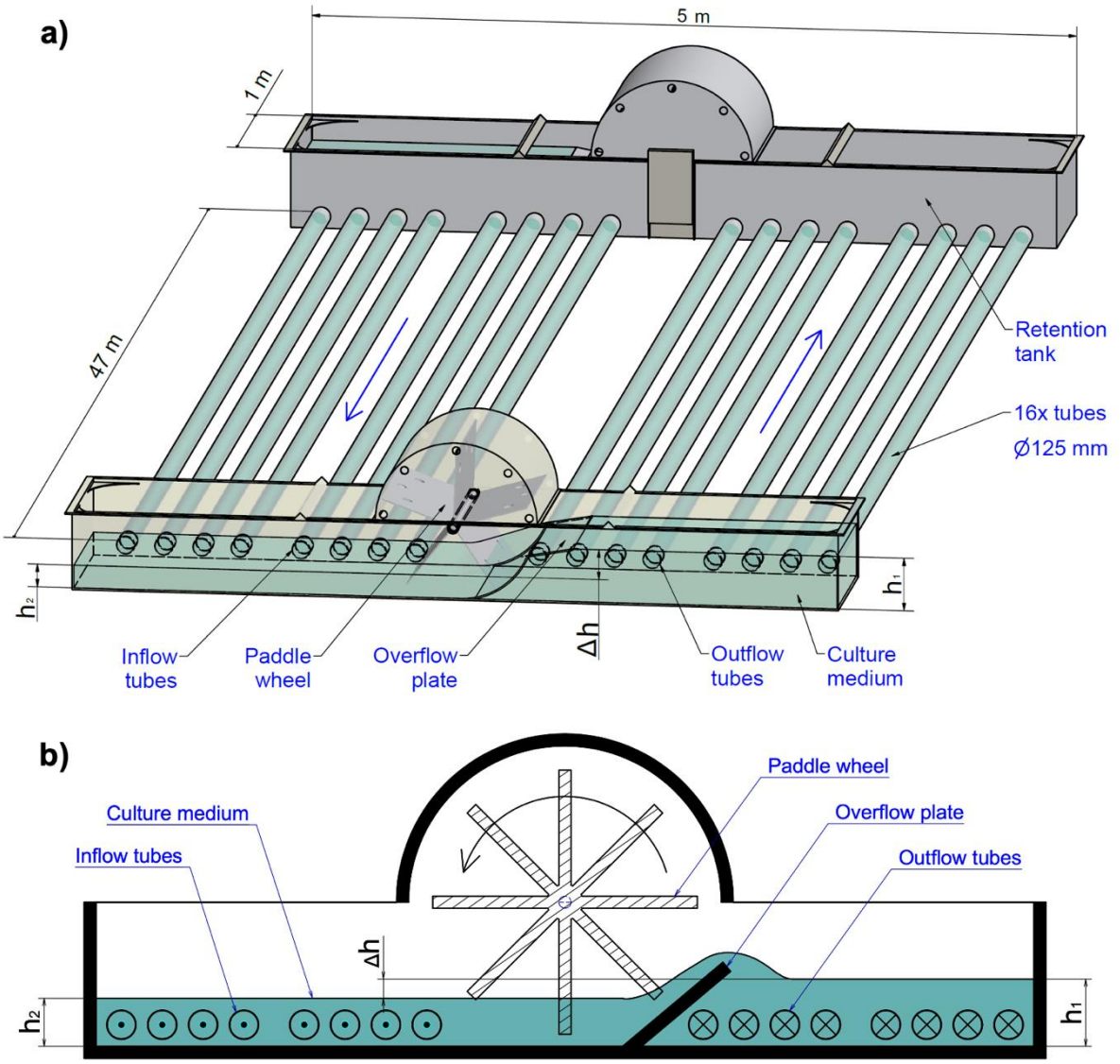

Fig. 4.1.2. Scheme of HHT PBR - a) 3D isometric view of HHT PBR and b) lateral section view of open retention tank.

The overflow plate is located in each tank below the paddle wheel. The paddle wheel moves the culture medium from one side of the tank over the overflow to the other side. The overflow plate, thus, causes the creation of the difference of culture medium levels Δh (m). The scheme of PBR and section of open retention tank is shown in Figure 4.1.2. The speed of rotation of the paddle wheel determines the level of the culture medium in the suction and discharge section of the paddle wheel, h_2 (m) and h_1 (m) respectively. A higher level in one of the tanks causes the flow of culture medium through the transparent tubes. In the second tank, the medium is moved through the overflow again, thus, continuous circulation in PBR is ensured.

Open tanks allow also releasing the excess of oxygen produced from photosynthesis and accumulated along the closed tubes.

The PBRs operation was followed up by means of online sensors of dissolved oxygen (DO) (Neurtek, Spain), pH (Hatch Lange SL., Spain), and temperature (Campbell Scientific Inc., USA) installed in one of the two open tanks. Measured data are continuously recorded and stored in a datalogger (Campbell Scientific Inc., USA). The PBRs were also equipped with water level sensors (Wras, UK) connected to the pumps to control the daily feeding and emptying of the PBRs. The three HHT PBRs were installed in winter 2017 and inoculated by the end of April 2017 with 10 L of a microalgae-dominated mixed culture (microalgae, bacteria, protozoa, and small metazoans) grown in urban wastewater and mostly dominated by green microalgae *Chlorella* sp. and *Stigeoclonium* sp., and diatoms *Nitzschia* sp. and *Navicula* sp. (Díez-Montero et al., 2020). After inoculation, the three PBRs were operating in parallel and fed with a mixture of agricultural run-off and domestic wastewater (2.3 m^3 d^{-1} for each PBR) (García et al., 2018).

Treated domestic effluent was obtained from an aerated septic tank which receives the wastewater of the main building of the campus Agròpolis (~20 persons, without overnight stay), whereas agricultural wastewater comes from a drainage collection channel. Figure 4.1.3 shows a process flow diagram (PFD) of the PBR and their support equipment. The daily operation cycle starts at 4:30 AM when the treated domestic wastewater, stored in a cylindrical glass fiber tank (TK-103, 1 m^3) discharges in a cylindrical polyethylene homogenization tank (HT-102, 10 m^3, provided with a sampling port) through stream 3. This operation was done by means of a centrifugal pump P-104 (14.4 m^3 h^{-1}) during a maximum time of 30 min. Treated domestic wastewater continuously reaches TK-103 by the stream line 2, which conveys treated wastewater to the tank thanks to a submersible pump located in the aerated septic tank. When more than 1 m^3 of domestic wastewater was produced per day, TK-103 remains full and the remaining wastewater gets out through a weir, reaching a general by-pass. Note that the amount of treated domestic wastewater was often lower than 1 m^3 (i.e., during the weekends).

At 5:00 AM, 6 m^3 of agricultural run-off are pumped by a submersible pump (P-101), from the nearby channel to the homogenization tank during a period of approximately 3 h (stream 1). Agricultural run-off and domestic wastewater are mixed in that tank and discharged in a unique outflow at 8:00 AM (streams 4a, 4b, and 4c) to the three PBRs by means of three centrifugal pumps (P-201, P-202 and P-203, time and level (LS) controlled) during a period ranging from 1 to 1.5 h. The homogenization tank has an internal recirculation pump to ensure the complete stirring of the tank. Note that streams 1 and 3 have flow meters (FM) installed (Siemens, Germany). The homogenization tank has the necessary tubing and valves for maintenance

and discharge to the general by-pass. At 7:00 AM, and before filling the PBRs with fresh wastewater, a designed volume of 2.3 m^3 of the culture medium of each PBR are simultaneously discharged to three circular glass fiber outflow storage tanks (TK-301, TK-302, and TK-303, 2.3 m^3 each) through streams 5a, 5b, and 5c. This operation is done by three centrifugal pumps (P-204, P-205, and P-206) which provide a constant flow of approximately 3 m^3 h^{-1}. Therefore, that volume is evacuated from the PBRs daily in 45 min approximately. Each outflow storage tank has two different water level sensors (LS, located at the top and the bottom) that control the filling and emptying pumps, as well as internal submerged pumps for the complete stirring of the tanks and different sampling ports. As a result of the operation procedure described above, PBR functioning is done in parallel and semi-continuous mode. Note that the emptying and filling processes are done early in the morning (once a day) in order to promote biomass growth when sunlight is available. PBR theoretical hydraulic retention time (HRT) is 5 d.

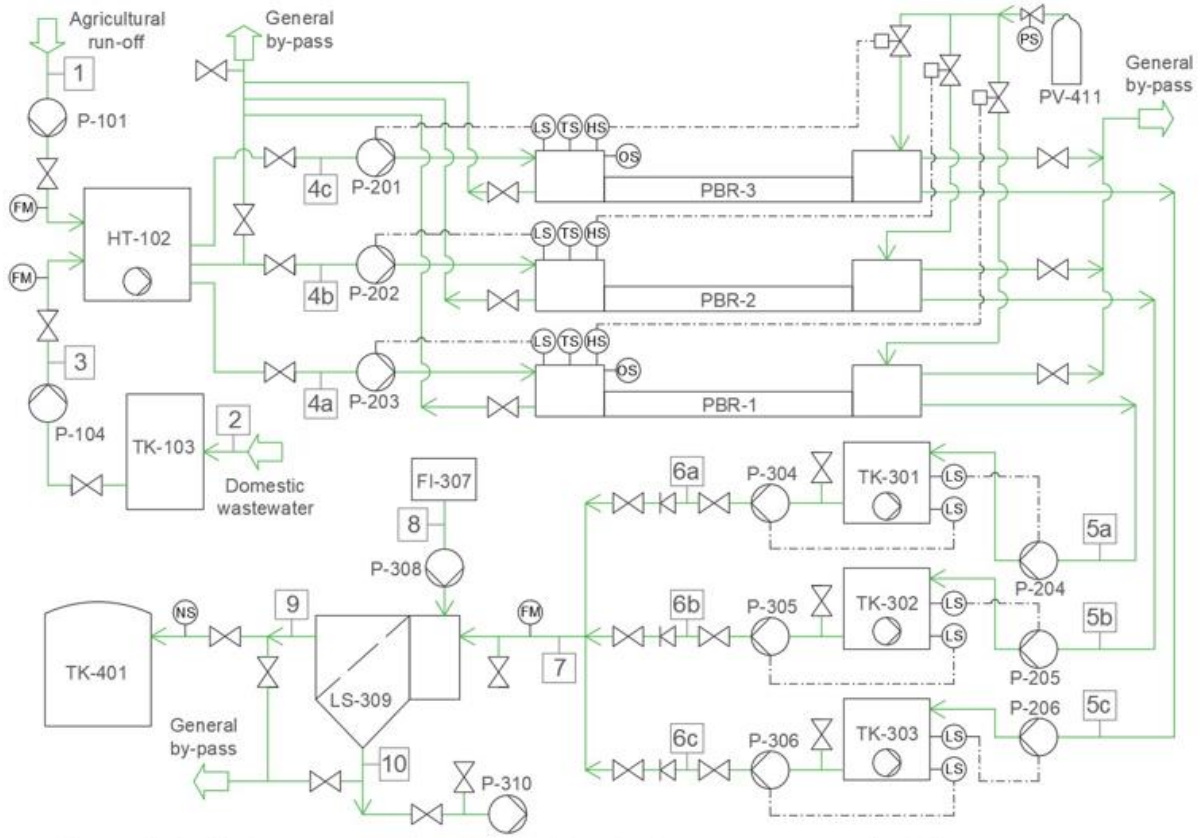

P-101	Centrifugal pump	P-206	Centrifugal pump
HT-102	Wastewater homogenization tank	TK-301	PBR-1 outflow storage tank
TK-103	Domestic wastewater storage tank	TK-302	PBR-2 outflow storage tank
P-104	Centrifugal pump	TK-303	PBR-3 outflow storage tank
P-201	Centrifugal pump	P-304	Centrifugal pump
P-202	Centrifugal pump	P-305	Centrifugal pump
P-203	Centrifugal pump	P-306	Centrifugal pump
PBR-1	Photobioreactor 1	FI-307	CI
PBR-2	Photobioreactor 2	P-308	Dosing pump
PBR-3	Photobioreactor 3	LS-309	Lamella settler
P-204	Centrifugal pump	P-310	Peristaltic pump
P-205	Centrifugal pump	TK-401	Clarified effluent tank

TS Temperature sensor
LS Level sensor
HS pH sensor
OS Dissolved oxygen sensor
PS Pressure sensor
NS Turbidity sensor
FM Flow meter

Fig. 4.1.3. Process flow diagram of the HHT PBRs and their support equipment – streams in green color.

PBRs have the necessary tubing and valves installed for maintenance and discharge to the general by-pass. Water from the storage tanks reaches the polypropylene static lamella settler (LS-309, 0.675 m^3, Moral Torralbo S.L.U., Spain) through streams 6a, 6b, 6c, and 7, the last one provided with a sampling port. The apparent critical settling velocity within the settler is 1.14 m h^{-1} at a flow of 0.4 m^3 h^{-1}. Peristaltic pumps P-304, P-305 and P-306 (0.4 m^3 h^{-1}) work one after the other, starting at 8:00 AM, 3:00 PM, and 10:00 PM (storage tanks are therefore emptied in this order). A flowmeter (FM, Siemens, Germany) in stream 7 allows checking the flow rate to the settler. The settler has one internal mixing chamber (0.05 m^3) for coagulation-flocculation where polyaluminium chloride (PAX-18 (Al^{3+} at 9 %), Kemira Water Solutions Inc., Spain) is added at a concentration that usually ranges from 2 to 10 mg Al^{3+} per liter, by means of a diaphragm pump (stream 8, P-308), which is activated simultaneously with the peristaltic pumps. The internal stirring of this chamber is provided by a motorized propeller (0.09 kW). The coagulant is stored in a plastic tank (FI-307, 0.1 m^3). The water is discharged from the lamella chamber of the settler by stream 9, provided with an online turbidimeter (Digimed, Brazil), to one clarified effluent tank (TK-401), and from there to other units that are not described in this PFD. The coagulant doses are adjusted by means of jar tests using the methods described in Gutiérrez et al. (2015), which are carried out when it is observed that the effluent turbidity from the settling tank is higher than 5 UNT. The biomass harvested in the settler is taken out through stream 10 with a peristaltic pump (P-310) to the other units neither described in the PFD. There is a sampling port for the harvested biomass, and the settler has the necessary tubing and valves for maintenance and discharge to the general by-pass (García et al., 2018).

4.2 Calibration and validation of BIO_ALGAE model

The microalgae-based bioremediation systems for urban and municipal wastewater treatment have been reported to have strong internal daily changes due to the daily rhythms of microalgae photosynthetic activity (García et al., 2006). In these systems, dissolved oxygen (DO) and pH values peak during diurnal hours and decrease at night, therefore influencing the contaminant removal efficiency throughout the day. Indeed, pH-dependent processes such as ammonia volatilization and phosphorus precipitation are greatly affected by this variation (García et al., 2000). The main objective of the present study was to evaluate the daily variations in the performance of HHT PBR for culturing wastewater-borne microalgae, fed with agricultural runoff in different seasons. The results of intensive experimental campaigns can then be used to calibrate and validate the BIO_ALGAE model simulating the microalgae cultivation process.

4.2.1 Monitoring of the PBR performance

Daily changes in the performance were studied in one of the three PBRs during two intensive sampling campaigns carried out in late winter (19^{th}-22^{nd} March 2018) and in mid-spring (8^{th}-11^{th} May 2018). In each campaign, grab samples of the mixed culture medium were collected from one of the two open tanks for three consecutive days every 3 hours, resulting in 8 samples per day. The grab samples were considered representative of the whole volume of the PBR. Additionally, one influent sample was collected every sampling day. Both campaigns started at 12:00 p.m. and finished at 9:00 p.m.

Influent wastewater and effluent culture medium samples from the PBR were analyzed for temperature, pH, electrical conductivity, turbidity, alkalinity, total suspended solids (*TSS*), volatile suspended solids (*VSS*) and nutrients: orthophosphate (PO_4^{3-}-P), ammonium (NH_4^+-N), nitrate (NO_3^--N) and nitrite (NO_2^--N). Total inorganic nitrogen (TIN) was calculated as the sum of nitrate, nitrite, and ammonium. Due to the very low amounts of organic fractions present in the samples, as observed in previous studies (Gutiérrez et al., 2015), dissolved organic carbon, nitrogen, and phosphorus were not measured. Temperature, pH, electrical conductivity and alkalinity were measured immediately after sampling in an in-situ field laboratory. Temperature and electrical conductivity were measured in the lab using an Endress+Hauser meter. Turbidity and pH were measured using a Hanna Instruments meter. Alkalinity, *TSS* and *VSS* were analyzed following Standard Methods for the Examination of Water and Wastewater (American Public Health Association et al., 2005). NH_4^+-N was analyzed according to the methods described in (Solórzano, 1968). PO_4^{3-}-P, NO_3^--N, and NO_2^--N were measured by means of an ion chromatograph DIONEX ICS1000 (Thermo-Scientific). Meteorological data were gathered from the recordings of the Catalan Meteorological Service (Servei Meteorològic de Catalunya 2018). Microalgal biomass concentration and variation were evaluated through *TSS* and *VSS* analyses. Microalgae evaluation through pigment measurements (chlorophyll *a*) probably would give a more accurate measurement of biomass concentration. However, in this study *TSS* and *VSS* were used since microalgae production in culture systems is usually expressed as biomass weight (Ansari et al., 2017) and for the sake of simplicity. Few samples from the PBRs were observed at the bright light microscope (Motic) equipped with a camera (Fi2, Nikon) and a fluorescence microscope (Eclipse E200, Nikon) using the NIS-Element viewer® software. Different taxonomic books and databases were used to identify and classify the species of microalgae and cyanobacteria growing in the culture medium of the PBR (On-line database of cyanobacterial genera 2018).

For both measuring campaigns, the speed of rotation of the paddle wheels was set by the frequency converter so the mean velocity of the culture medium in the transparent tubes was 0.25 m s^{-1}.

Environmental and operational conditions

The daily variation of air and culture medium temperature are presented in Figure 4.2.1.1 and Figure 4.2.1.2, respectively. Air temperature oscillated between 2°C and 16°C in winter and between 12°C and 25°C in spring. This corresponded to temperatures in the culture medium of 5 to 23°C in winter and 12 to 36°C in spring. It should be noted that, even in the case of a semi-closed HHT PBR, the daily temperature range, i.e. the difference between the maximum and the minimum daily temperature, is significantly high: around 15°C in winter and around 20°C in spring. The behavior of the temperature variation seems similar in both seasons. The temperature during daylight increases over the air temperature, being the tubes exposed to the solar radiation.

The open tanks provide a cooling effect, avoiding the extremely high temperatures that would be reached in completely closed tubular PBRs. Indeed, quite similar variation patterns were observed compared to those obtained in open ponds by Posadas et al. (2015). The cooling effect continued during the night, decreasing the culture medium temperature to that the air temperature was reached just before sunrise. This fact highlights the role and capability of the open tanks, and the mixing inside them, as a cooling element in semi-closed PBRs.

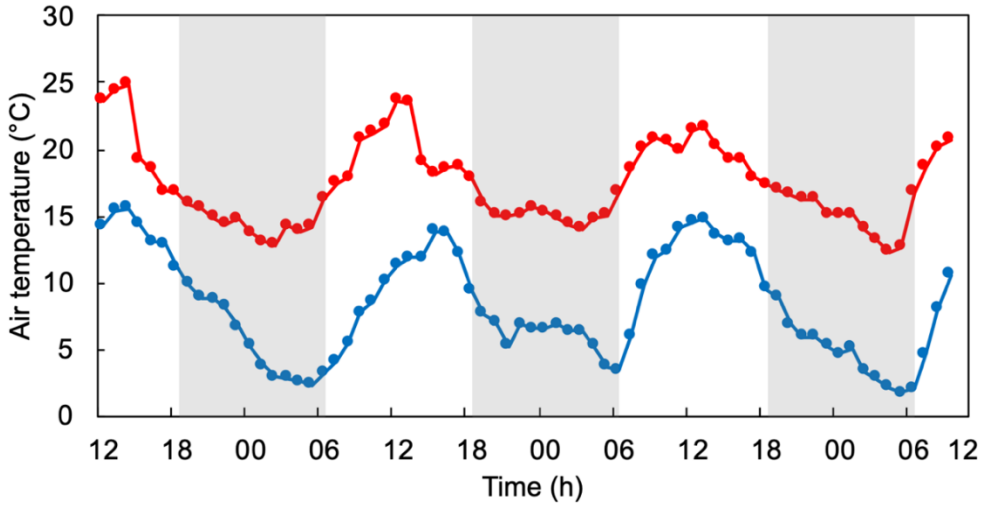

Fig. 4.2.1.1. Air temperature – blue represents winter values (March), red indicates spring values (May). The vertical white and grey stripes represent the daylight and night periods.

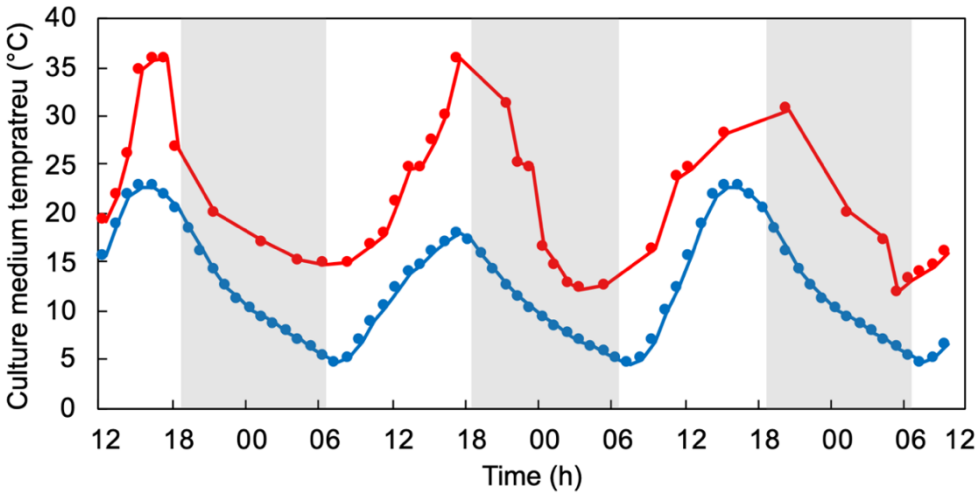

Fig. 4.2.1.2. Culture medium temperature – blue represents winter values (March), red indicates spring values (May). The vertical white and grey stripes represent the daylight and night periods.

Solar radiation also showed a great variation during the day, as shown in Figure 4.2.1.3, with peaks of 900 W m^{-2} and 800 W m^{-2} at around 12:00 p.m. in spring and winter, respectively. In general, solar radiation was similar in both campaigns, just slightly higher in spring. The evolution of DO concentration is shown in Figure 4.2.1.4. DO variations are the result of the microalgal activity and the values observed in the HHT PBR are similar in both seasons. The lower photosynthetic activity at night was reflected by lower DO concentrations (8 g m^{-3}), which were doubled at midday (16 g m^{-3}). This daily variation pattern is typical in microalgae-based wastewater treatment systems. However, in this case, the DO concentrations are significantly high at night. Microalgae-based systems treating wastewaters with higher influent organic load have reported lower oxygen concentration and even oxygen depletion during the night due to the lack of photosynthesis and the intense microbial respiration (Solimeno et al., 2017; Solimeno & García, 2019). However, the low influent organic load in the present study allowed for a significant concentration of DO during the whole day. On the other hand, the open tanks of the PBR allowed for oxygen release to the atmosphere, keeping the dissolved oxygen concentration below 17 g m^{-3} (168 % of air saturation). This is of high importance since dissolved oxygen concentration above 300 to 400 % of air saturation value can inhibit microalgae activity and damage algal cells (Chisti, 2007; Molina et al., 2001), which usually represents an issue in closed PBRs.

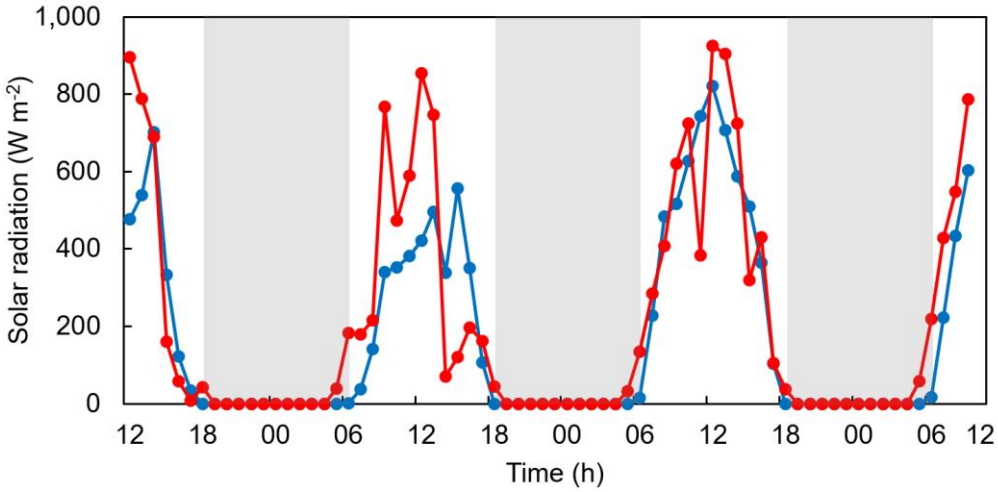

Fig. 4.2.1.3. Solar radiation – blue represents winter values (March), red indicates spring values (May). The vertical white and grey stripes represent the daylight and night periods.

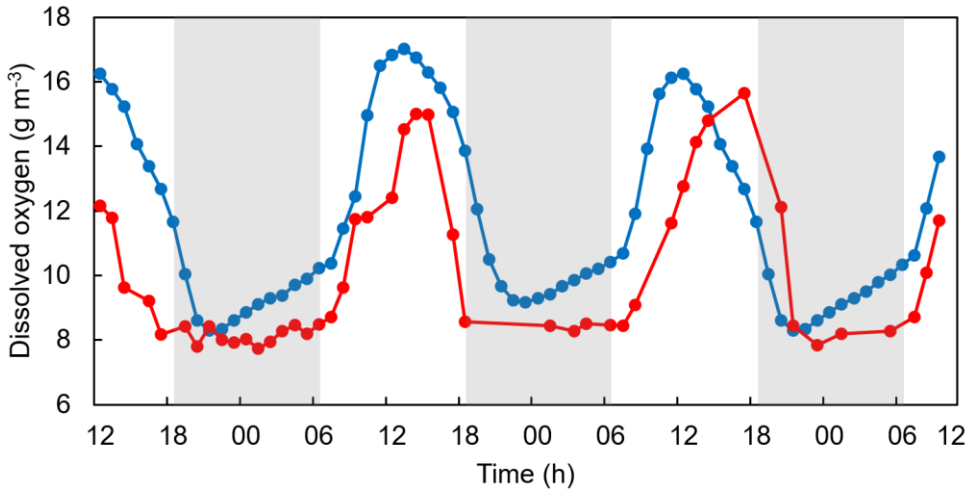

Fig. 4.2.1.4. Dissolved oxygen – blue represents winter values (March), red indicates spring values (May). The vertical white and grey stripes represent the daylight and night periods.

While the excess oxygen produced during photosynthesis is released in the open tanks, the paddle wheels can aerate the system when the DO concentration is below the saturation value. At the low temperatures observed at night in the culture medium, the DO saturation value is increased. In the winter campaign, the paddle wheels aeration provided more oxygen than the requirements for microbial respiration, increasing the DO concentration towards the saturation value (12.8 g m^{-3} at 5°C). This effect was not so evident in the spring campaign (Figure 4.2.1.4, red curve), due to the lower saturation value (10.1 g m^{-3} at 15°C).

Regarding pH, it was recorded in both campaigns, but some interference occurred during the spring campaign, resulting in random and inconsistent measurements and records. However, the shape of the pH curve for the spring campaign is evident, but it is not possible to take the

data as relevant. Figure 4.2.1.5 shows the evolution and variation recorded in the winter and spring campaigns. As for DO, pH variations are the result of microalgal activity. A clear increase during daylight and a decrease during the night was observed and repeated each day, as expected due to the photosynthetic activity. The pH achieved high values, ranging between a minimum of 9.3 at the end of the night and a maximum of 11.2 at the end of daylight.

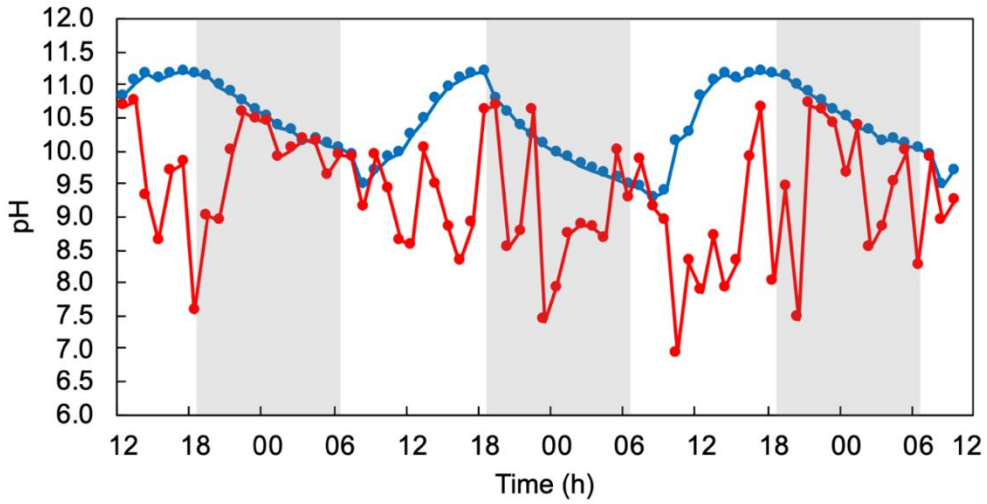

Fig. 4.2.1.5. pH recorded in the HHT PBR – blue represents winter values (March), red indicates spring values (May).

Concentration and production of biomass

The evolution of *TSS* and *VSS* concentrations in the culture medium are shown in Figure 4.2.1.6. Higher concentrations were observed in spring compared to those in winter since the environmental conditions were more favorable for microalgae growth in spring. Taking into account that the most distinguishing environmental factor between the winter and spring campaigns was the water temperature (the solar radiation was not extremely different in both campaigns), it evidences that this parameter was the most limiting factor for microalgae growth during winter. Indeed, with the low water temperature observed in winter (as low as 5°C) it is not expected to achieve a notable biomass growth. The favorable water temperature in spring, with a significant increase compared to winter, allowed for a fast biomass rise.

In winter, *TSS* concentration showed a certain increase after feeding, almost constant values during the day, and a slight decrease in the evening after sunset (around 7:00 p.m.), with an average concentration of 96 g_{TSS} m^{-3} (Figure 4.2.1.6, blue curve). There is no clear reason for this decrease, but it could be attributed to a lower *TSS* resuspension after sunset due to a lower presence of oxygen bubbles produced by photosynthesis. The observation underlying this hypothesis is that DO concentration was above the saturation value before sunset, and below the saturation value after sunset. Therefore, oxygen bubbles could rise up and

resuspend the *TSS* before sunset, but not after sunset. In spring, the daily cyclical variation of *TSS* concentration was less evident (average of 358 g_{TSS} m^{-3}), whereas an increased concentration was observed, which is consistent with the increasing biomass trend observed in the seasonal monitoring (Figure 4.2.1.6, red curve). The ratio *VSS*/*TSS* was similar and almost constant in both campaigns, slightly lower in spring (0.67 ± 0.08 in winter and 0.56 ± 0.08 in spring). This could be attributed to a higher content of solid inorganic precipitates in spring compared to winter, due to higher values of pH deriving from higher photosynthetic activity. Note that the *TSS* concentration in the influent wastewater slightly increased from an average value of 72 g_{TSS} m^{-3} in winter to 115 g_{TSS} m^{-3} in spring, as well as the ratio *VSS*/*TSS*, from 0.31 ± 0.08 to 0.44 ± 0.09.

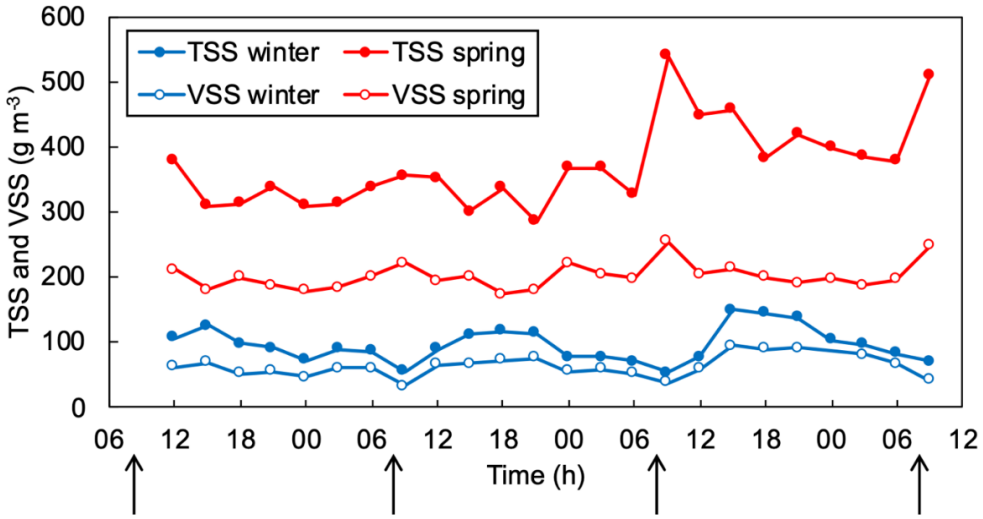

Fig. 4.2.1.6. Evolution of total suspended solids (*TSS*) and volatile suspended solids (*VSS*) concentrations in the two campaigns in the culture medium of the HHT PBR. Arrows indicate feeding time.

Microscopy observation of the culture medium of the HHT PBR revealed the presence of green microalgae but mainly the dominance of cyanobacteria, in both campaigns. In the winter campaign, cyanobacteria from filamentous species resembling to *Oscillatoria* sp. and *Leptolyngbya* sp. were identified. There was also the presence of coccoid cyanobacteria resembling to *Chroococcus* sp., *Synechococcus* sp. and *Synechocystis* sp. during the winter campaign. In the spring campaign, a higher dominance of *Synechococcus* sp. was observed with some presence of *Pseudanabaena* sp.

Dynamics of nutrients concentration and removal

Regarding the evolution of nitrogen species, NH_4^+-N and NO_3^--N concentrations in the culture medium of the PBR in the two campaigns are presented in Figure 4.2.1.7. The NH_4^+-N concentration in the influent wastewater sample in winter was 3.5 g_N m^{-3}, 1.5 g_N m^{-3}, and 1.6 g_N m^{-3} each of the three consecutive days. As it can be observed in Figure 4.2.1.7 (blue

full dots), the effect of feeding was reflected by the culture medium concentrations, which suffered an increase immediately after feeding. However, NH_4^+-N was rapidly removed, keeping a concentration close to zero during the rest of the day. NH_4^+-N removal can be attributed to microalgae uptake, but also to ammonia stripping taking into account the high pH reached in the PBR during daylight (García et al., 2000). A similar pattern was observed in spring (Figure 4.2.1.7, red full dots), when picks proportional to the NH_4^+-N concentration in the influent (0.5 g_N m^{-3}, 1.3 g_N m^{-3}, and 7.3 g_N m^{-3}, in the three days) were also detected. In this case, NH_4^+-N concentration dropped down in the few following hours, being negligible during the rest of the day. NH_4^+-N removal was performed in only a small fraction of time. These results confirm that the PBR was underloaded and it has a much higher NH_4^+-N removal capacity than that utilized in this study.

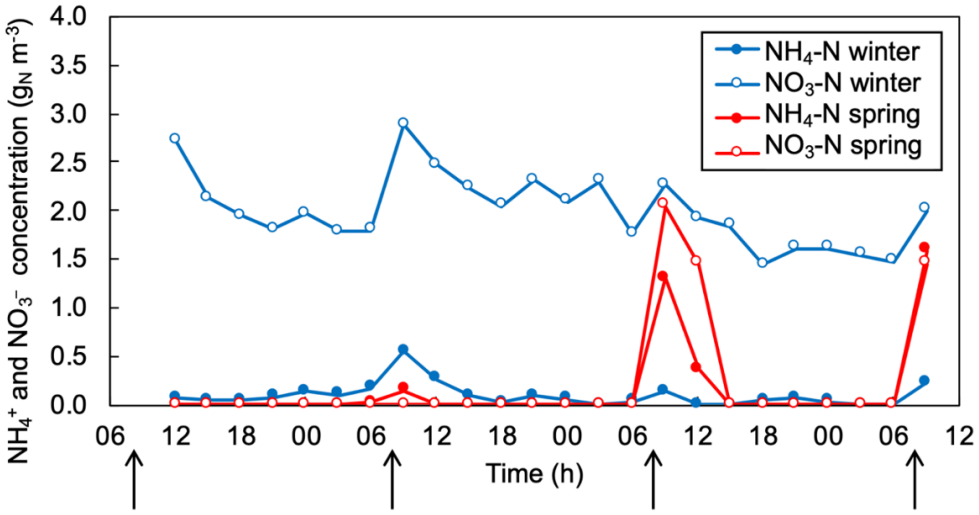

Fig. 4.2.1.7. Ammonium (NH_4^+) and nitrate (NO_3^-) concentrations measured in the two campaigns in the culture medium of the HHT PBR. Arrows indicate feeding time.

Concerning NO_3^--N, concentrations were significantly higher in winter than in spring, as shown in Figure 4.2.1.7. With the warmer conditions in spring, the system was able to immediately remove NO_3^--N after feeding (Figure 4.2.1.7, red empty circles and line). The influent NO_3^--N concentrations were 1.8 g_N m^{-3}, 1.6 g_N m^{-3}, and 3.5 g_N m^{-3} in the three consecutive days, while the NO_3^--N concentration in the HHT PBR was negligible in every record except two values after feeding the third day. The influent concentrations during the winter campaign were slightly higher, 5.0 g_N m^{-3}, 2.5 g_N m^{-3} and 4.1 g_N L^{-3}, and NO_3^--N was only partially removed in the PBR, resulting in concentrations ranging between 1.4 g_N m^{-3} and 2.9 g_N m^{-3} (Figure 4.2.1.7, blue empty circles and line). These results are consistent with the biomass concentration and activity observed in the PBR in the different seasons, being microalgae uptake the main way for NO_3^--N removal. It can be concluded that NO_3^--N was completely removed in the warm seasons, being the PBR fed below its full capacity. Biomass growth was likely limited by the

low concentration of nutrients in the HHT PBR during most part of the day, therefore lessening the production of oxygen (Figure 4.2.1.4). On the contrary, the permanent availability of nitrogen (as NO_3^--N) during winter indicates that biomass growth could be limited by the low water temperature, as stated previously.

Regarding phosphorus, PO_4^{3-}-P concentration in the PBR was very low in both campaigns due to the low concentration in the influent wastewater, which ranged between 0.2 and 1.6 $g_P\ m^{-3}$. Therefore, PO_4^{3-}-P concentration in the PBR was practically negligible, always below 0.2 $g_P\ L^{-3}$ except the third sampling day in spring after feeding, when an influent of 1.6 $g_P\ m^{-3}$ gave rise to a short and isolated peak up to 0.4 $g_P\ L^{-3}$. These results are consistent with the weekly monitoring and the analysis of the seasonal average, confirming that phosphorus was a limiting factor for biomass growth during the whole period.

In spite of the low influent loading of nutrients in this study, it is considered of special interest that the influent wastewater was real agricultural runoff, collected from an agricultural drainage system in a suburban area in Barcelona. Similar conditions are expected to happen in other agricultural areas and locations. A different type of wastewater would have probably led to different results. According to the results of this study, it is suggested that in cases with a higher concentration of nutrients in the influent wastewater, higher biomass growth would have been observed. This would lead to a higher concentration of biomass in the HHT PBR, more production of oxygen during daylight through photosynthesis, and more consumption of oxygen during the night through respiration.

Dynamics of alkalinity and carbon uptake

The evolution of total alkalinity during the three days of experimental campaigns in winter and spring are shown in Figure 4.2.1.8. Influent wastewater alkalinity ranged from approximately 160 to 270 g m^{-3} as $CaCO_3$ in winter, and around 270 $g_{CaCO3}\ m^{-3}$ in spring. Concentration in the culture medium increased after feeding events, but the alkalinity provided by the influent was reduced during the day indirectly by microalgal activity, resulting in an almost constant concentration during the night, which ranged between 80 and 100 $g_{CaCO3}\ m^{-3}$ in winter, and between 50 and 70 $g_{CaCO3}\ m^{-3}$ in spring. This pattern is linked to culture medium pH behavior because high pH during daylight causes carbonate precipitation and alkalinity reduction. At night, there is no photosynthesis, and respiration does not affect alkalinity.

The daily reduction of alkalinity during the experimental campaigns ranged between 28 and 56 g $m^{-3}\ d^{-1}$ as $CaCO_3$. In winter, the alkalinity decrease was quite stable with an average of 31 ± 3 $g_{CaCO3}\ m^{-3}\ d^{-1}$. In spring, a higher daily alkalinity decrease was observed (47 ± 11 $g_{CaCO3}\ m^{-3}\ d^{-1}$), which is consistent with the higher microalgal activity and biomass growth during that season. The higher daily alkalinity decrease was observed in spring and the

low values of alkalinity eventually reached, suggest that the culture could be carbon limited during the spring campaign due to bicarbonate depletion.

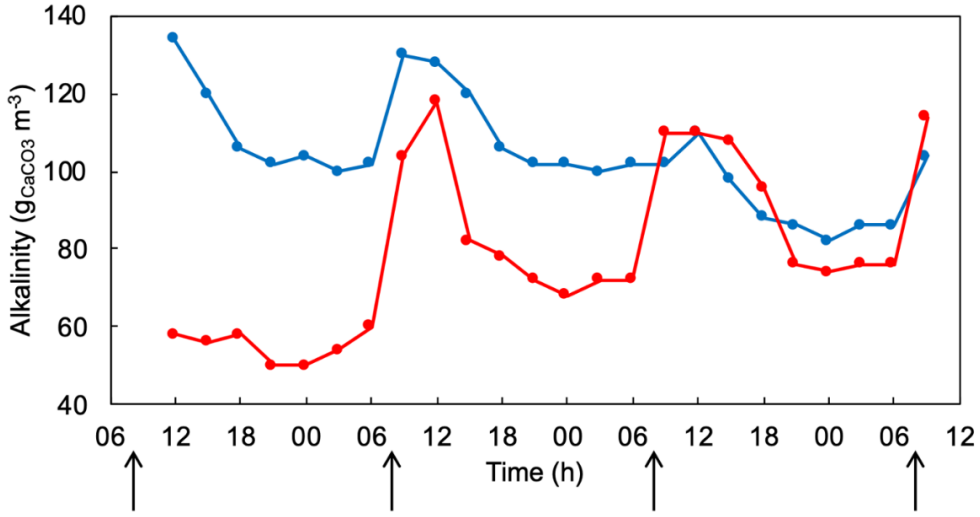

Fig. 4.2.1.8. Evolution of total alkalinity (measured from unfiltered samples) in the culture medium of the HHT PBR in the two campaigns – blue represents winter values (March), red indicates spring values (May), arrows indicate feeding time.

However, with the results of this study, it cannot be concluded that inorganic carbon limitation actually occurred, since limitation by nutrients was clear in spring. In cases with a higher concentration of nutrients in the influent wastewater, higher consumption of inorganic carbon is expected. The influent bicarbonate could be depleted, and inorganic carbon would become limiting, requiring the supply of an external source or inorganic carbon. CO_2 addition could provide an alternative source of inorganic carbon and give rise to an increase in biomass production. Also, pH control at values around 8.5 would avoid carbon losses by conversion of bicarbonate to carbonate and subsequent precipitation. In fact, Weissman et al. (1988) reported that maintaining a pH of 8.5 is suitable for the high productivity of biomass of some microalgae. Moreover, CO_2 injection also would avoid or reduce nitrogen losses by ammonia volatilization and carbon precipitation as carbonate. Altogether, pH control would lead to a lower biomass growth limitation by nitrogen and/or inorganic carbon. Increases in biomass production between 24 % and 100 % have been reported when the microalgae-based systems are supplied with CO_2 (Azov et al., 1982; de Godos et al., 2016). CO_2 injection in the PBR could be implemented by bubbling flue gases within the horizontal tubes or in the open tanks prior to entering the tubes. It could be also implemented by bubbling biogas in an external carbonation column used for the upgrade to biomethane of the biogas produced in the anaerobic digestion of the microalgal biomass, as studied by Marín et al. (2019) in the same HHT PBR.

4.2.2 Model calibration and validation

The BIO_ALGAE model was implemented in COMSOL Multiphysics™ version 5.4. The model was calibrated using measured data from the first (winter) experimental campaign, which are shown in chapter 4.2.1. The applicability of the calibrated model was validated using the measured data in the second (spring) experimental campaign. The values of the influent parameters for calibration and validation are shown in Table 4.2.2.1. These parameters were determined according to Henze et al. (2015), where the ratios of parameters were defined based on the measured influent value of chemical oxygen demand *COD* ($gO_2\ m^{-3}$). The distribution of parameters was defined as follows: 50 % X_S, 22 % S_S, 10 % S_I, 10 % X_H, and 8 % X_I.

Table 4.2.2.1. Influent wastewater parameters for model calibration.

Parameter		Concentration					
		Influent 1		Influent 2		Influent 3	
		Winter	Spring	Winter	Spring	Winter	Spring
COD	($gO_2\ m^{-3}$)	59	87	50	76	54	79
X_S	($gCOD\ m^{-3}$)	29.3	43.5	24.9	38	27.0	39.5
S_S	($gCOD\ m^{-3}$)	12.9	19.1	10.9	16.7	11.9	17.4
X_H	($gCOD\ m^{-3}$)	5.9	8.7	5.0	7.6	5.4	7.9
X_I	($gCOD\ m^{-3}$)	4.7	7.0	4.0	6.1	4.3	6.3
NH_4^+-N	($g\ m^{-3}$)	2.30	0.05	3.51	1.31	1.50	7.3
NO_3^--N	($g\ m^{-3}$)	6.8	2.4	3.4	2.2	5.5	4.7
Alkalinity	($gCaCO_3\ m^{-3}$)	272	272	248	266	156	270

The initial concentrations of the components in the HHT PBR are shown in Table 4.2.2.2. The measured values were firstly used as the initial values of the particulate components. Subsequently, some of the parameters were adjusted according to the first test numerical calculations of the model. At the same time, the measured values of the culture medium temperature in HHT PBR (Figure 4.2.1.2) and the intensity of solar radiation (Figure 4.2.1.3) were used in the model as well. The total calculation was repeated several times after the time corresponding to the length of the measurement campaign. The calculation was repeated until all parameters in the model had stabilized. The total calculation thus simulated the cultivation process in the order of tens of days.

Table 4.2.2.2. Initial concentration of the components for model calibration.

Components		Concentration	
		Winter	Spring
S_{NH4}	(gNH_4-N m^{-3})	0.09	0.11
S_{NH3}	(gNH_3-N m^{-3})	0.09	0.11
S_{NO3}	(gNO_3-N m^{-3})	0.200	0.206
S_{NO2}	(gNO_2-N m^{-3})	0.0045	1E-6
S_{HCO3}	($gHCO_3$-C m^{-3})	80	17
S_{CO2}	(gCO_2-C m^{-3})	0.055	0.150
S_{CO3}	(gCO_3-C m^{-3})	11.0	5.4
S_{O2}	(gO_2 m^{-3})	14.00	9.35
S_H	(gH m^{-3})	3.16E-8	3.16E-8
S_{OH}	(gOH-H m^{-3})	1.47E-7	1.47E-7
TSS	(gCOD m^{-3})	95	371
X_{ALG}	(gCOD m^{-3})	57	223
X_S	(gCOD m^{-3})	13	129
S_S	(gCOD m^{-3})	26	76
X_H	(gCOD m^{-3})	20	26
X_I	(gCOD m^{-3})	27	21
X_{AOB}	(gCOD m^{-3})	0.02	0.07
X_{NOB}	(gCOD m^{-3})	0.03	0.13

The model was calibrated using the mentioned calibration parameters: μ_{ALG}, μ_H, $k_{death,H}$, k_La_{O2}, k_La_{CO2}, and k_La_{NH3}. The resulting values of these parameters are shown in Table 4.2.2.3. The numerical model was calibrated by comparing the generated graphic data from the model with the measured curves. The following parameters were used for calibration: S_{O2}, TSS, and S_{NH4}. The resulting curves of the calibrated model are shown in Figures 4.2.2.1 to 4.2.2.3.

Table 4.2.2.3. Calibrated parameters.

Parameter	Description	Value (d^{-1})
μ_{ALG}	Maximum specific growth rate of microalgae	1.7
μ_H	Maximum specific growth rate of heterotrophic bacteria	1.3
$k_{death,H}$	Inactivation constant of heterotrophic bacteria	0.3
k_La_{O2}	Volumetric mass transfer coefficient for oxygen	3.4
k_La_{CO2}	Volumetric mass transfer coefficient for carbon dioxide	3.0
k_La_{NH3}	Volumetric mass transfer coefficient for ammonia	0.7

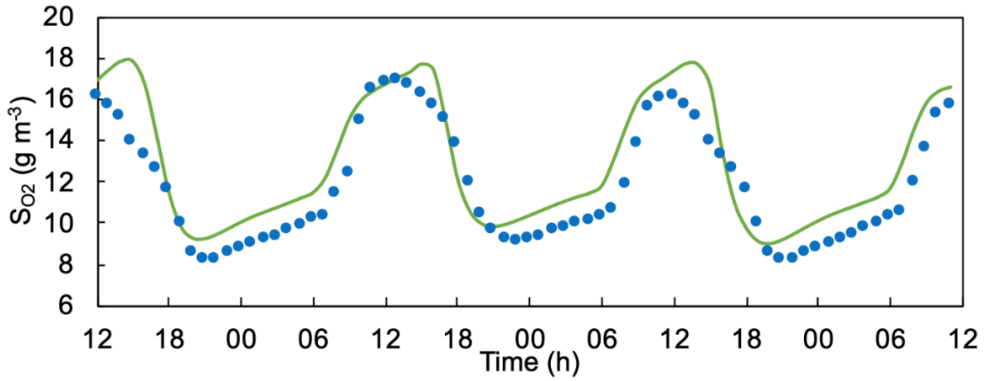

Fig. 4.2.2.1. Calibration of dissolved oxygen in HHT PBR. Simulated (green line) and experimental (blue dots) data during winter measuring campaign.

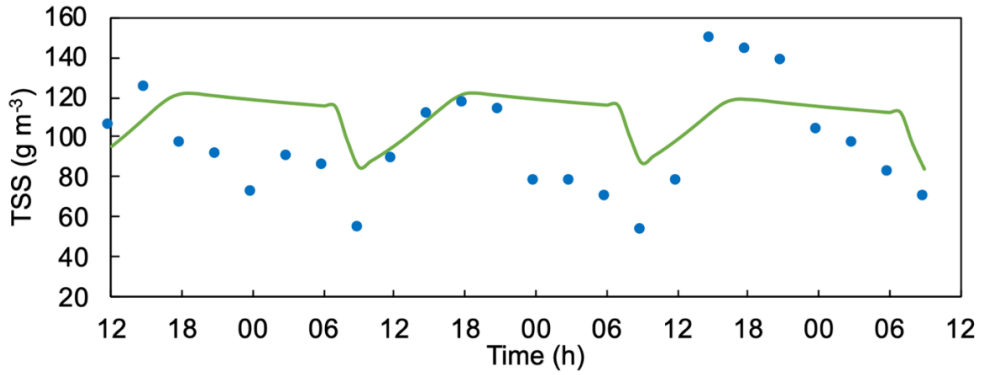

Fig. 4.2.2.2. Calibration of TSS in HHT PBR. Simulated (green line) and experimental (blue dots) data during winter measuring campaign.

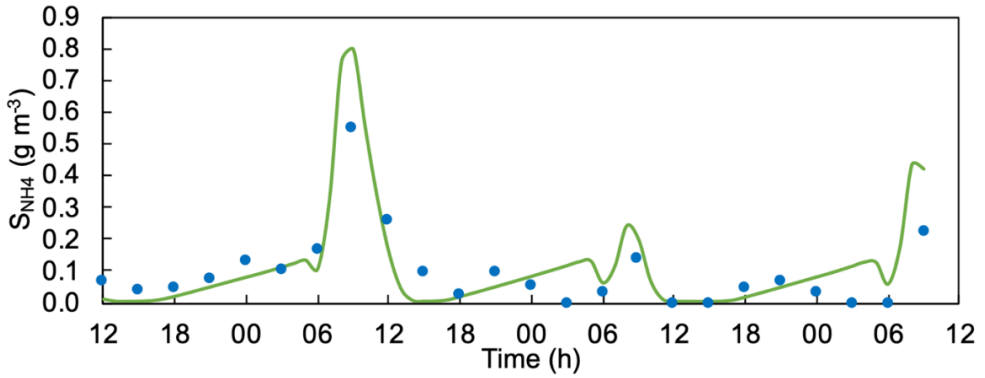

Fig. 4.2.2.3. Calibration of ammonium nitrogen in HHT PBR. Simulated (green line) and experimental (blue dots) data during winter measuring campaign.

Calibration was performed in order to minimize the root mean square error (RMSE). The RMSE of the calibrated model for each component was: $RMSE_{SO2}$ = 1.52 gO_2 m^{-3}, $RMSE_{TSS}$ = 9.48 gTSS m^{-3} and $RMSE_{NH4}$ = 0.05 gNH_4-N m^{-3}. The higher value of $RMSE_{TSS}$ is due to the model considering respiration at the end of the night, resulting in a steep drop in biomass. The decrease in experimentally measured TSS during the night cycle is due to low oxygen production in the culture medium, which keeps the biomass buoyant. However, it is

difficult to eliminate this deficiency by automatic sampling and the culture medium would need to be homogenized before. The model was validated according to experimental data from the second (spring) campaign. Validation was conducted using the calibrated parameters shown in Table 4.2.2.3. The influent parameters (Table 4.2.2.1), initial conditions (Table 4.2.2.2), culture medium temperature (Figure 4.2.1.2), and solar radiation (Figure 4.2.1.3) were slightly different in comparison with winter values. Experimental data matched well with simulated data. The global error of the simulations was slightly higher in comparison with calibration. Validation of dissolved oxygen is shown in Figure 4.2.2.4 with $RMSE_{SO2}$ = 2.43 gO_2 m^{-3}. Validation of microalgae production and ammonium nitrogen are shown in Figure 4.2.2.5 and Figure 4.2.2.6. The RMSE value of each component was: $RMSE_{TSS}$ = 21.19 gTSS m^{-3} and $RMSE_{NH4}$ = 0.08 gNH_4-N m^{-3}. TSS values were influenced by influent parameters in addition to respiration and oxygen production during the night. The model is not sensitive enough to capture such a step change and showed only a gradual increase.

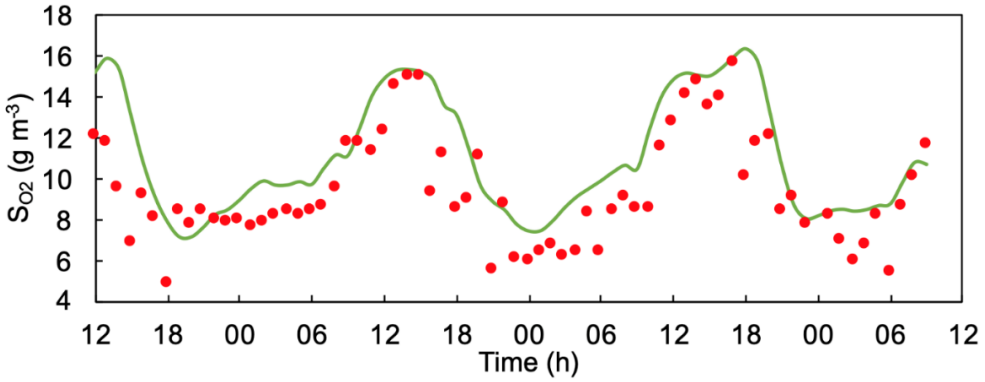

Fig. 4.2.2.4. Validation of dissolved oxygen in HHT PBR. Simulated (green line) and experimental (red dots) data during winter measuring campaign.

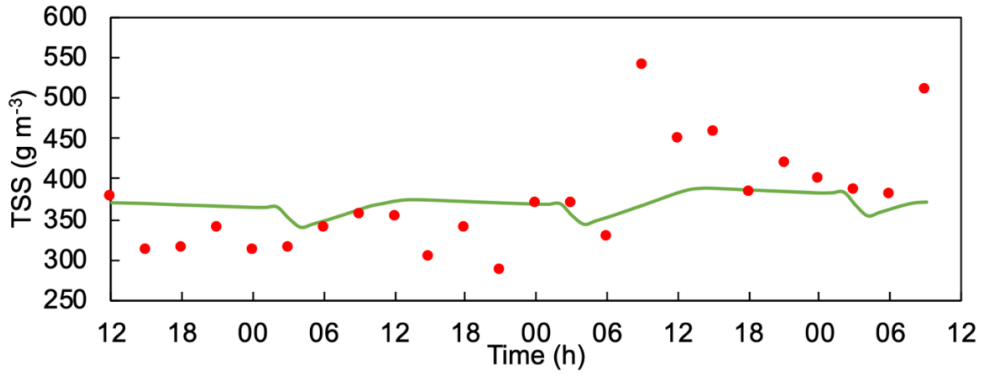

Fig. 4.2.2.5. Validation of TSS in HHT PBR. Simulated (green line) and experimental (red dots) data during winter measuring campaign.

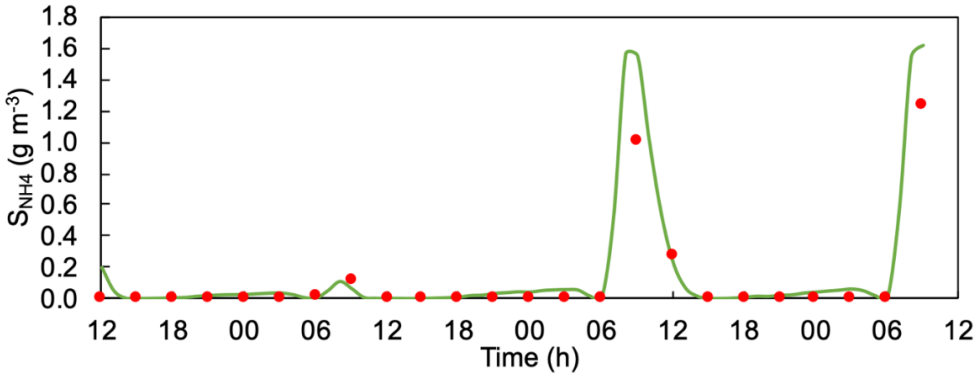

Fig. 4.2.2.6. Validation of ammonium nitrogen in HHT PBR. Simulated (green line) and experimental (red dots) data during winter measuring campaign.

4.2.3 Conclusions

The mechanistic BIO_ALGAE model for microalgae-based wastewater treatment systems was calibrated and validated based on measured data from two intensive sampling campaigns. Biological processes, chemical and physical parameters affecting simultaneously microalgae and bacteria were implemented in COMSOL Multiphysics™.

The microalgae and heterotrophic bacteria specific growth rate, the decay of heterotrophic bacteria, and parameters related to the mass transfer of oxygen, carbon dioxide and ammonia were selected for calibration of BIO_ALGAE model. Calibration and validation were conducted comparing simulated results and experimental data from HHT PBR fed with a mixture of agricultural run-off and domestic wastewater. Results of the calibration and validation indicated that the model was able to accurately reproduce the main parameters affecting microalgae growth (i.e. dissolved oxygen, total suspended solids, and ammonium nitrogen). Thus, the developed model demonstrated to be a useful tool to simulate the performance of the cultivation system treating wastewater. Based on the simulated data, it is possible to derive the relative proportion of microalgae and bacteria, and to make predictions on biomass production.

The next step in order to better understand microalgal-bacterial cultivation system would be to implement the influence of hydrodynamics on the process of cultivation.

4.3 Hydrodynamic conditions in HHT PBR

The aim of this part of the study was to analyze hydrodynamic conditions by CFD simulation in HHT PBR. The numerical model was calibrated and validated on the basis of experimental data, confirming its suitability for simulating the microalgae cultivation process and the need for further investigation. Based on this validated numerical model, the influence of PBR design and operating parameters on the hydrodynamics of the culture medium can be investigated with CFD simulations without any further complex experiments. This can help optimizing

microalgae production by changing operating parameters in accordance with hydrodynamics conditions.

4.3.1 Hydrodynamic conditions characterization

A set of experimental tracer tests were performed in the tubes of the PBR in order to determine the residence time distribution (RTD). The tests were performed in the tubes, instead of the whole PBR, aimed at estimating the mean residence time and main hydrodynamic characteristics in the irradiated area of the PBR. The RTD of a system or reactor can be obtained from tracer tests and is expressed by Eq. (4.1) assuming a constant flow (Levenspiel, 1999)

$$E(t) = \frac{C(t)}{\int_0^\infty C(t)dt} \tag{4.1}$$

where *E(t)* is the RTD (s^{-1}), *C* (mg L^{-1}) is the concentration of tracer in culture medium at any given time *t* (s). Subsequently, the mean residence time t_m (s) inside the PBR irradiated area can be calculated from the first moment of the function Eq. (4.2)

$$t_m = \int_0^\infty t \cdot E(t)dt \tag{4.2}$$

By substituting Eq. (4.1) into Eq. (4.2), and discretizing for given intervals of time, the mean residence time can be determined in discrete form as expressed in Eq. (4.3)

$$t_m = \frac{\sum t_i \cdot C_i \cdot \Delta t}{\sum C_i \cdot \Delta t} \tag{4.3}$$

where the t_i (s) is the discrete time, C_i (mg L^{-1}) is the concentration of tracer in discrete form, Δt (s) is the time difference. The variance of the RTD function in discrete form is

$$\sigma_t^2 = \frac{\sum (t_i - t_m)^2 \cdot C_i \cdot dt}{\sum C_i \cdot \Delta t} \tag{4.4}$$

From Eq. (4.3) and (4.4), the dimensionless variance σ^2 can be obtained

$$\sigma^2 = \frac{\sigma_t^2}{t_m^2} \tag{4.5}$$

This dimensionless variance σ^2 may be used to predict the mixing conditions in the tube. From the dimensionless variance, the dimensionless axial dispersion coefficient D_{ax} can be calculated, and it is assumed to be independent of tracer concentration and of the axial position in the tube (because the concentration is assumed to be radially uniform) (Rossi et al., 2017). Per definition, D_{ax} depends on tracer diffusion coefficient D_{diff} ($m^2\ s^{-1}$), mean culture medium velocity $\bar{u}$ (m s^{-1}) and length of the tube *L* (m) (Eq. (4.6))

$$D_{ax} = \frac{D_{diff}}{\bar{u} \cdot L} \tag{4.6}$$

The dispersion coefficient represents a very convenient tool to measure the spread of tracer in the tube and therefore the degree of mixing (Rossi et al., 2017). For the ideal plug flow D_{ax} approaches 0, while for perfect mixing ∞ (Levenspiel, 1999). The dispersion coefficient can be estimated from the dimensionless variance obtained in the RTD analysis.

For small extents of dispersion (D_{ax} < 0.01), i.e. small deviation from plug flow, Eq. (4.7) can be used (Levenspiel, 1999)

$$\sigma^2 = 2 \cdot D_{ax} \tag{4.7}$$

When the coefficient of dispersion is already estimated, the time normalized (dimensionless) RTD can be calculated from Eq. (4.8)

$$E_\theta = \frac{1}{\sqrt{4 \cdot \pi \cdot D_{ax}}} \cdot exp\left[-\frac{(1-\theta)^2}{4 \cdot D_{ax}}\right] \tag{4.8}$$

where θ is the normalized time (dimensionless) as expressed in Eq. (4.9)

$$\theta = \frac{t_i}{t_m} \tag{4.9}$$

Measurement of hydrodynamic characterization

The RTD in the horizontal tubes of the PBR was determined experimentally by the pulse-input tracer technique. The experiments were conducted in 8 tubes under the same operational conditions, i.e. the same rotational speed of the paddle wheels. The tests were performed from the inlet of the tubes in one open tank to the outlet in the other open tank. A concentrated solution of sodium chloride (NaCl, 50 g L^{-1}) was used as a tracer for the RTD tests. A pulse of 50 mL of the tracer solution was injected by means of a syringe at the inlet of each tube at time zero, and the electrical conductivity was continuously measured and recorded at the outlet of the tubes with a HACH CDC40103 probe connected to a HACH HQ40d conductivity meter (Figure 4.3.1.1a). Subsequently, measured conductivity values were converted to concentrations (conductivity standards provided by HACH) by assuming that 1 µS cm^{-1} is equivalent to 0.64 mg of NaCl per liter of water. The measurements were performed separately in the 8 tubes. After each measurement, the probe was consecutively moved to the next tube and the syringe was refilled with the same volume of tracer to perform the next test.

Additionally, two more tracer tests were performed in one tube under different operational conditions, modifying the difference in the water level in the open tanks. The rotational speed of the paddle wheels was modified in order to set different water levels in the tanks. These tests were used for the preliminary validation of the model.

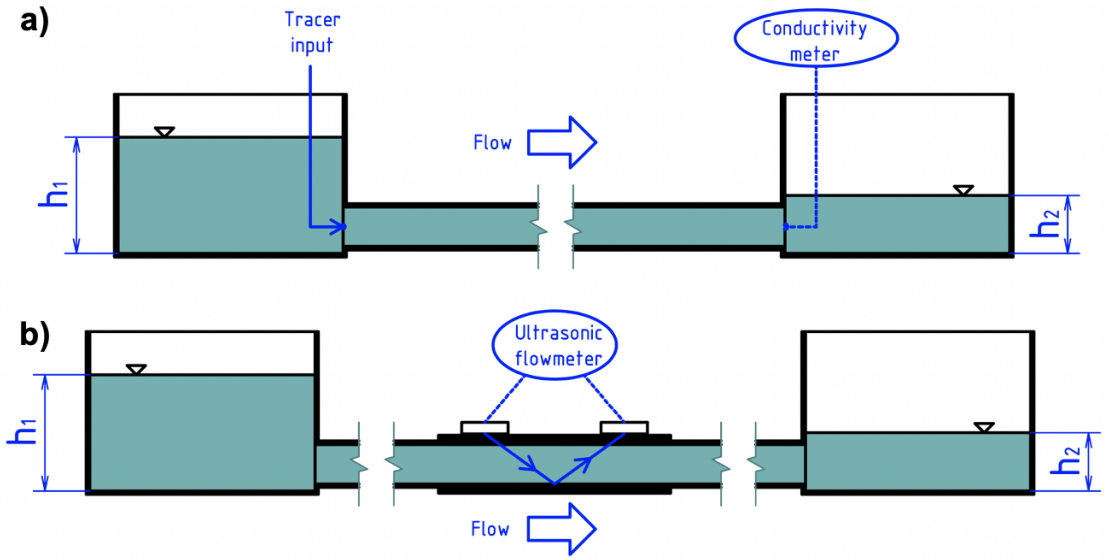

Fig. 4.3.1.1. Lateral view of the PBR, including the two open tanks and one tube, representing the: a) pulse input tracer technique; and b) ultrasonic flow meter technique.

The mean culture medium circulation velocity $\bar{u}$ (m s^{-1}) was determined from the ratio of circulation length L (m) to mean residence time t_m (s).

In addition, an ultrasonic flowmeter Flexim Fluxus F601 (accuracy 1.6 % of reading 0.01 m s^{-1}) was installed as shown in Figure 4.3.1.1b, in order to measure the actual velocity of the culture medium inside the tubes and to verify the accuracy of the pulse input tracer test. At a distance of 20 m from the exit tank, part of one tube of the PBR was replaced with a rigid PVC tube (about 3 meters). Ultrasonic transducers were clamped onto the external wall of the tube (length 2.5 m and diameter 0.11 m) and were never in direct contact with the culture medium flowing inside the tube. Ultrasonic signals were emitted by transducers installed on one side of the pipe. The signals were reflected on the opposite side of the rigid tube and finally received by a second transducer. The signals were emitted alternatively in and against the flow direction. The two ultrasonic transducers were connected to the transmitter of the flowmeter.

The RTD obtained experimentally in the horizontal tubes of the PBR are shown in Figure 4.3.1.2. Experimental tests were performed in the eight tubes, however, results corresponding to Tube 4 are not presented since measurements were not reliable due to a high biofilm concentration on the tube walls. The operating conditions of the PBR (i.e. the rotational speed of the paddle wheels) were set so the culture medium levels h_1 and h_2 in open tanks were 0.28 m and 0.24 m, respectively. The shape of the RTD in all the tubes present a sharp peak, resembling to plug flow with small axial dispersion. All the tubes showed similar behavior, with the peak occurring close to the normalized time θ=1. Note that the normalized time is obtained based on the measured mean residence time t_m (s).

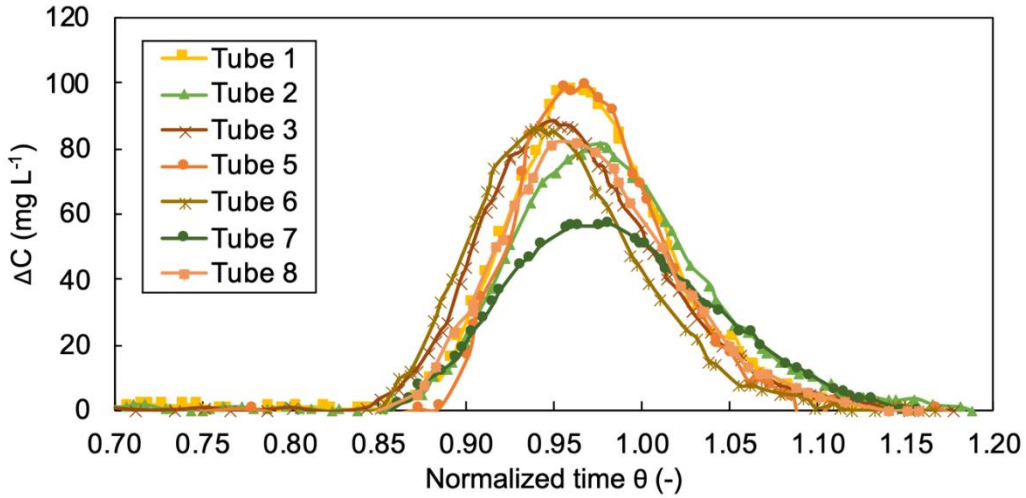

Fig. 4.3.1.2. RTD in the horizontal tubes of the PBR. The difference of concentration is ΔC and θ is the normalized time (dimensionless) $=t_i/t_m$.

The values of mean residence time t_m (s) and the variance calculated from Eq. (4.2) to Eq. (4.5), are presented in Table 4.3.1.1. The t_m ranged from 250 s in Tube 1 to 335 s in Tube 7, showing slightly higher values in the tubes located closer to the paddle wheel (6, 7 and 8). This suggests that the flow velocity in the tubes was partly influenced by the distance between each tube and the paddle wheel.

Table 4.3.1.1. Mixing characteristics in horizontal tubular photobioreactor.

Tube Nr.	t_m (s)	$\bar{u}$ (m s^{-1})	u_{max} (m s^{-1})	σ_t^2 (s^2)	σ^2 (-)	D_{diff} (m^2 s^{-1})	D_{ax} (-)
1	250	0.19	0.22	368.6	0.0059	0.0261	0.0029
2	274	0.17	0.20	422.8	0.0056	0.0226	0.0028
3	282	0.17	0.20	541.8	0.0068	0.0267	0.0034
4	N/A	N/A	N/A	N/A	N/A	N/A	N/A
5	254	0.18	0.21	282.5	0.0044	0.0190	0.0022
6	295	0.16	0.19	869.0	0.0100	0.0374	0.0050
7	335	0.14	0.17	954.6	0.0085	0.0280	0.0042
8	288	0.16	0.19	676.5	0.0314	0.0314	0.0041

Based on the mean residence time t_m (s) and the length of the transparent HHT PBR tube L=47 m, it was possible to determine the mean flow velocity $\bar{u}$ (m s^{-1}) in the tubes and the dimensionless dispersion coefficient D_{ax}, calculated from Eq. (4.6). The average flow velocity inside the tubes ranged from 0.14 to 0.19 m s^{-1}, in all cases higher than the recommended value of 0.1 m s^{-1} needed to prevent sedimentation of algal biomass (Chisti, 2016). These flow velocities generate a turbulent flow in the tubes, characterized by the Reynolds number ranging from 17,500 to 23,700. The dispersion coefficient can be used to quantify the extent

of the axial dispersion in the tubes. As already mentioned, it is not possible to directly measure the dispersion coefficient D_{ax}. However, using the fitting of measured data, it was possible to determine the dispersion coefficient D_{ax} for small extents of dispersion from Eq. (4.7) to (4.8). The results ranged between 0.0022 and 0.0050, in every case clearly below 0.01, thus validating the hypothesis of small dispersion used for the determination of the coefficient and confirming that the hydrodynamic behavior of the tubes was close to ideal plug flow. In addition, the highest extent of dispersion was observed in the tubes located closer to the paddle wheel (6, 7, and 8), which could be attributed to the lower flow velocity in those tubes. Anyway, the differences in flow velocity and axial dispersion between the different tubes were relatively low.

The difference in hydrodynamic conditions in the PBR tubes was influenced by the formation of biofilm on the inner wall of the tubes due to the organic matter present in the culture medium. Such biofilm can increase the pressure drop causing constant changes in the flow regime. In order to prevent the formation of biofilm, it is necessary to increase the flow rate velocity of the culture medium and thereby intensify the mixing and the effect of shear forces on the inner wall of the tubes, thus reducing the need for physical cleaning.

4.3.2 Numerical model setup

Two CFD geometries for PBR simulation were created in ANSYS FLUENT CFD 19.1. The 3D geometry was developed to simulate hydrodynamic conditions in open tanks and tubes. The 2D mesh was created only for the detailed description of hydrodynamics in tubes. In order to reduce cells and have still a good resolution, symmetry was anticipated and only half of the PBR tube was simulated in the 2D mesh.

Fluid dynamic model setup

The turbulent viscosity is a complex parameter to define, and several semi-empirical theories have been elaborated to determine its approximate value. According to the Boussinesq hypothesis, Reynolds stresses are proportional to fluid velocity gradients. This hypothesis is used in the k-ε standard and Re-Normalization Group (RNG) models, and its advantage is the relatively low computational requirement for turbulent viscosity determination. The standard k-ϵ model is more appropriate for models with high Reynolds numbers, while the RNG model provides an analytically derived differential formula for effective viscosity, which makes the RNG model more accurate and reliable for models with low Reynolds numbers.

From the analytical calculation of PBR operating conditions, it can be assumed that the flow regime is in the range of low turbulent Reynolds number Re (Eq. 4.25). Therefore, the RNG k-ϵ model was used to simulate the fluid dynamics behavior in HHT PBR. This model has demonstrated its applicability to the simulation of tubular and other photobioreactors in the turbulent flow regime (Bitog et al., 2011; Loyseau et al., 2018). The governing equations of the

turbulent kinetic energy k ($m^2\ s^{-2}$) and dissipation rate ε ($m^2\ s^{-3}$) are given by Eq. (4.10) and (4.11)

$$\frac{\partial}{\partial t}(\rho k) + \frac{\partial}{\partial x_i}(\rho k u_i) = \frac{\partial}{\partial x_j}\left[\alpha_k(\mu + \mu_t)\frac{\partial k}{\partial x_j}\right] + G_k + G_b - \rho\varepsilon \tag{4.10}$$

$$\frac{\partial}{\partial t}(\rho \varepsilon) + \frac{\partial}{\partial x_i}(\rho \varepsilon u_i) = \frac{\partial}{\partial x_j}\left[\alpha_\varepsilon(\mu + \mu_t)\frac{\partial \varepsilon}{\partial x_j}\right] + C_{1\varepsilon}\frac{\varepsilon}{k}G_k - C_{2\varepsilon}\rho\frac{\varepsilon^2}{k} \tag{4.11}$$

where G_k is the generation of turbulence kinetic energy due to the mean velocity gradients, G_b represents the generation of turbulence kinetic energy due to buoyancy. The model constants $C_{1\varepsilon}$=1.42, $C_{2\varepsilon}$=1.68, are analytically derived by RNG theory, α_k=α_ε=1.393 represent the inverse effective Prandtl numbers. Effective viscosity is represented by the sum of dynamic viscosity μ (Pa s) and turbulent viscosity μ_t (Pa s) given by Eq. (4.12)

$$\mu_t = \rho C_\mu \frac{k^2}{\varepsilon} \tag{4.12}$$

where constant C_μ=0.0845 is derived using RNG model theory (ANSYS Inc. (US), 2018). The calculations obtained using RNG methods should always be verified by experiments or at least by a qualitative comparison with literature results. The hydrodynamic conditions were numerically simulated with the software ANSYS FLUENT CFD 19.1.

Mesh generation

The 3D model consisted of 8 tubes connecting two tanks (one with high level and the other with low level) since the hydrodynamic conditions in the 8 tubes of the second half of the HHT PBR are identical. The grid contains approx. 2,565,305 elements with a 10 mm maximum size. Computations were performed until the calculation converged at a residue of 10^{-5} between two iterations. The mesh quality was checked using skewness reaching the value of 0.19. Because of the length of each tube, the flow in the HHT PBR can be regarded as a fully developed state, which can be employed for determining steady-state flow dynamics of the culture medium.

In order to examine more precisely the hydrodynamic conditions in a transparent tube, a second model with a 2D mesh for one tube was created as well. For a length of L=47 m and d=125 mm diameter, the grid contains approx. 1,375,358 elements with a 5 mm maximum size. The inflation function was applied in the area close to the tube wall with a minimum grid size of 0.1 mm. Computations were performed until the calculation converged at a residue of 10^{-5} between two iterations. The mesh quality was checked using skewness reaching the value of 0.11. For the detailed study of the flow in the tube, it is preferable to use a finer mesh. A large number of elements can thus be saved by switching from 3D to 2D model.

Boundary conditions

The microalgal culture medium at low concentrations shows clearly Newtonian behavior with viscosity values close to that of water (Martínez-Sanz et al., 2020; Souliès et al., 2016). Properties and physical parameters were set in the model by considering the culture medium as water (excluding microalgal biomass). For the first 3D overall PBR model, the inlet velocities were set according to the range of operating flow rate in the outlet cross-section of the paddle wheel, and resulted in velocities ranging between 0.385 and 0.606 m s^{-1}. The same conditions were set for outlet flow velocity. The outer walls and the internal structures of the tanks were set to no-slip boundary conditions to water, and roughness of 0.5 mm in transparent tubes was fixed. The roughness has been selected according to the biofilm formation on transparent HHT PBR tubes in non-sterile conditions (Callow, 2000).

To simulate hydrodynamic conditions in a 2D transparent tube model, the inlet and outlet were defined by the hydrostatic pressure derived from the water levels in tanks (Table 4.3.3.1). In order to simulate the effect of microalgae biofilm formation on hydrodynamic conditions, the roughness of 0.5 mm was set. Roughness selection connected with biofilm formation is described more in detail in chapter 4.3.4.

Particle tracking

The geometry of the modeled tube was modified due to the complexity of the calculation. The geometry of the HHT PBR tube was shortened to just one meter and a fully developed flow was defined for the inlet. The mesh consists of 1,375,358 elements with a 1 mm maximum size and the structure was modified to be significantly finer in the area around the transparent walls of the tube. Computations were performed until the calculation converged at a residue of 10^{-5} between two iterations. The mesh quality was checked using skewness reaching the value of 0.21. To simulate the hydrodynamic conditions in a modified 3D tube model, the inlet was defined by the inlet velocity according to the measured operating parameters in the HHT PBR. The particle tracking injection function was used to monitor the movement of microalgal cells in the culture medium during its flow in the tube. The parameters of selected particles (Table 4.3.2.1) were adjusted according to the properties of microalgal cells (Belohlav and Jirout, 2019). The single injection method was chosen for the entry of particles into the tube and the injection point was located at the lower part of the tube at a distance of 0.062 m from the tube axis. The injection point was chosen according to the possibility to simulate the movement of a particle that occurs in the area of the tube that is least irradiated by the light source (dark zone, which is the most unfavorable condition).

Table 4.3.2.1. Particle tracking simulation settings.

Parameter	Value
Particle density	1,010 kg m^{-3}
Particle diameter	5 µm
Particle injection point coordinates	X: 0 mm; Y: -62 mm

A model with a larger diameter of transparent tubes was also created to evaluate the hydrodynamic conditions during the scale-up of the cultivation system. In order to compare the hydrodynamic conditions in geometrically similar tubes to the original HHT PBR, a tube with a diameter of 200 mm was created. In order to make it easier to identify the dimensions, the diameter of the original HHT PBR tubes (125 mm) is marked d_1 (m), and geometrically similar tubes with a diameter of 200 mm are marked d_2 (m). Subsequently, the mesh was created also for tube d_2, which consists of 2,740,362 elements. Proportionally to tube d_1, the injection point was placed in the least irradiated area of the tube, which corresponds to a distance of 99 mm below the tube axis.

To simulate the intensity of the light radiation received by the microalgae cells from the incident light on the tube walls, it is important to monitor the distance of the cells from the irradiated wall of the tube. The cell position is thus defined as the vertical distance from the irradiated tube wall *H* (m), since it is assumed that the light source is located directly above the HHT PBR tubes. The scheme of the particle tracking system principle and the marked starting injection point is shown in Figure 4.3.2.1.

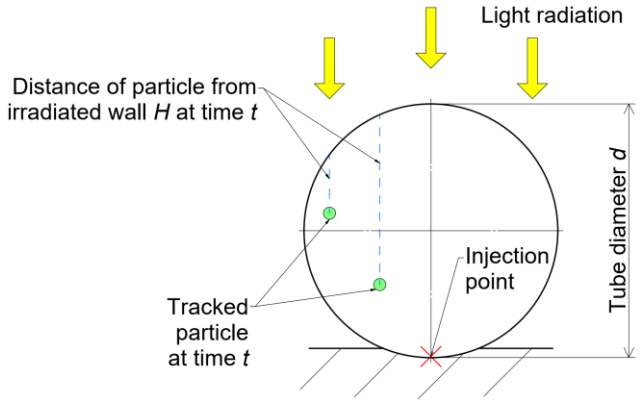

Fig. 4.3.2.1. Scheme of the particle tracking model principle, *H* represents the distance of the particle from the irradiated wall, *d* indicates the tube diameter.

4.3.3 Calibration and preliminary validation of CFD model

The CFD model was calibrated by comparing the simulated velocity profile inside the tubes with the velocity profiles obtained analytically based on the experimental results of the tracer tests. Model validation is required to verify the suitability of the numerical simulation for the other operating conditions of the PBR. From the measured values based on the *Re*, it was

possible to predict that the flow regime is in a turbulent range. Calibration of the CFD model and the subsequent preliminary validation of detailed hydrodynamic conditions was processed only for Tube 1 since the variation between the measured average flow velocities in all tubes was negligible (Table 4.3.3.1).

Several empirical velocity profiles exist for turbulent tube flow. Among those, the simplest and the best known is the power-law velocity profile expressed as

$$u_i = u_{max} \cdot \left(1 - \frac{r}{R}\right)^{1/n} \tag{4.13}$$

where R (m) is the tube radius, r (m) is the radial coordinate, u_{max} (m s^{-1}) is the centerline velocity, and n is the dimensionless constant whose value depends on the Reynolds number Re (Munson et al., 2009) as described in Eq. (4.14)

$$n = 1.03 \cdot ln(Re) - 3.6 \tag{4.14}$$

The centerline velocity can be experimentally determined from the residence time when the first change in the measured conductivity (converted to concentration of tracer) can be indicated. A closer examination shows that the power-law profile cannot be valid near the wall, since the velocity gradient is infinite there. In addition, Eq. (4.13) cannot be precisely valid near the centerline due to the first derivative of the velocity is not zero, therefore, the curve of velocity distribution is not smooth.

For a further description of the velocity distribution in the tube, it is possible to applicate the universal velocity profile (Bird et al., 2002). The viscous sublayer next to the transparent wall of the tube can be specified according to Eq. (4.15).

$$u_i = \frac{r \cdot u^{*2}}{\nu} \tag{4.15}$$

where ν (m^2 s^{-1}) is the kinematic viscosity and u^* (m s^{-1}) is expressed according to Eq. (4.16).

$$u^* = \sqrt{\frac{\tau_w}{\rho}} \tag{4.16}$$

where τ_w (Pa) is the shear stress on the transparent wall of the tube and ρ (kg m^{-3}) is the density. The validity of viscous sublayer expression is defined within the range of $0 < y^+ < 5$, where the dimensionless y^+ is defined

$$y^+ = \frac{r \cdot u^*}{\nu} \tag{4.17}$$

In the transition area, the velocity profile equation, which is valid within the range of $5 < y^+ < 30$, can be expressed

$$u_i = 5 \cdot ln(y^+) - 3.05 \tag{4.18}$$

For the values $y^+ > 30$, turbulent area can be specified

$$u_i = 2.5 \cdot \ln(y^+) + 5.5 \quad (4.19)$$

The universal velocity profile describes very well the velocity distribution in smooth tubes except for the area close to the centerline, where the velocity gradient from Eq. (4.19) is not zero.

If the height of the tube roughness k_s (m) exceeds the thickness of the viscous sublayer, the flow of the culture medium can be greatly affected. The velocity profile of hydraulically rough tubes can be expressed using the Eq. (4.20) (Bird et al., 2002)

$$u_i = u^* \cdot \left[2.5 \cdot \ln\left(\frac{r}{k_s}\right) + 8.5\right] \quad (4.20)$$

In this study, the power-law, the universal smooth tube, and the universal fully rough tube velocity profiles have been assessed and compared to the CFD simulations in order to calibrate the model. Once calibrated, the model has been used to simulate the velocity profile under different operational conditions, and results have been compared to those obtained in experimental tracer tests.

Calibration of the CFD 3D model and the subsequent validation of detailed hydrodynamic conditions was performed only for Tube 1, since the variation between the measured average flow velocities in all tubes was low (Table 4.3.1.1). Figure 4.3.3.1 shows the velocity profile simulated by the CFD model in a cross-section of Tube 1, together with the power-law, the universal smooth tube, and the universal fully rough tube velocity profiles based on the experimental data. The maximum centerline velocity u_{max} (m s^{-1}) used for the determination of analytical velocity profiles, was determined based on the first response to increasing conductivity (converted to concentration of tracer) during the measurement (Table 4.3.1.1). As shown in Figure 4.3.3.1, the analytical velocity profiles based on experimental data were in good agreement with CFD simulation. In particular, the universal velocity profile for hydraulically rough tubes (k_s was 0.5 mm, the same as in boundary conditions of the CFD model) describes the most accurately the distribution of the velocity inside the tube. In the microalgae cultivation process, it is also necessary to consider the effect of biofilm formation on the inner wall of the transparent tubes, due to its influence on the hydrodynamic conditions in the PBR. The thickness of biofilm depends on several factors and ranges from micrometers to millimeters (Katarzyna et al., 2015; Lan et al., 2017). The increase of the biofilm layer thickness can cause a rise in pressure loss in the tube and consequently lower flow velocity. Decreasing velocity then results in a drop in shear forces that are necessary to prevent further biofilm formation. If the biofilm layer reaches a certain thickness and stiffness, hydrodynamic conditions are not able to remove it or avoid its formation, and it is necessary to stop the operation of the PBR and mechanically remove the biofilm.

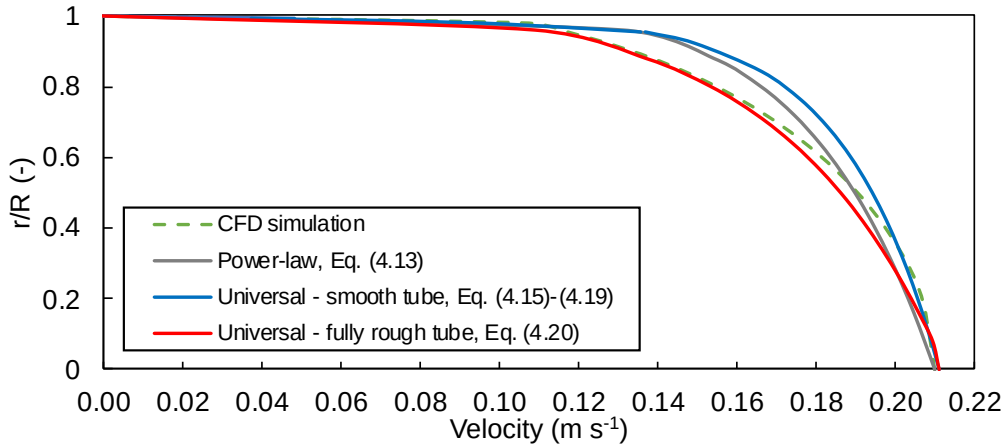

Fig. 4.3.3.1. Comparison of analytical calculation and numerical simulation of velocity profiles inside a tube of the PBR – calibration: Δh=0.04 m, Re=23,700; r indicates the radial coordinate and R is the inner radius of the tube.

Three different operational configurations were selected to validate the CFD simulation. The water level in the open tanks h_1 (m) and h_2 (m) have been changed by the variation of the paddle wheel rotational speed, resulting in three different configuration setups (A, B, C). For each operational configuration, RTD was determined by the pulse-input tracer measurement done in Tube 1. Additionally, the flow velocity was verified with an ultrasonic flowmeter. The water levels and main results of the tracer tests and the ultrasonic flowmeter measurements are shown in Table 4.3.3.1.

Table 4.3.3.1. Operational setup in HHT PBR.

Configuration	h_1 (m)	h_2 (m)	Δh (m)	t_m (s)	$\bar{u}_{tracer}$ (m s^{-1})	$\bar{u}_{flowmeter}$ (m s^{-1})	Re (-)
Calibration	0.28	0.24	0.04	247	0.19	N/A	23,700
A	0.35	0.29	0.06	186	0.25	0.249	31,200
B	0.36	0.26	0.10	145	0.32	0.319	39,900
C	0.39	0.26	0.13	128	0.37	0.371	46,200

The velocity profiles inside the tube in the three different conditions were simulated without changing any parameter in the CFD model. The results of the simulations were compared with the universal velocity profiles for rough tubes based on experimental data in Figure 4.3.3.2. CFD simulations were in good agreement with the analytical profiles. Thus, the numerical predictions were preliminarily validated by the experimental data, indicating that the established CFD simulation model can be adapted to simulate the fluid field in the HHT PBR. In order to fully validate the model, it would be useful to compare the experimental and simulated RTD curves.

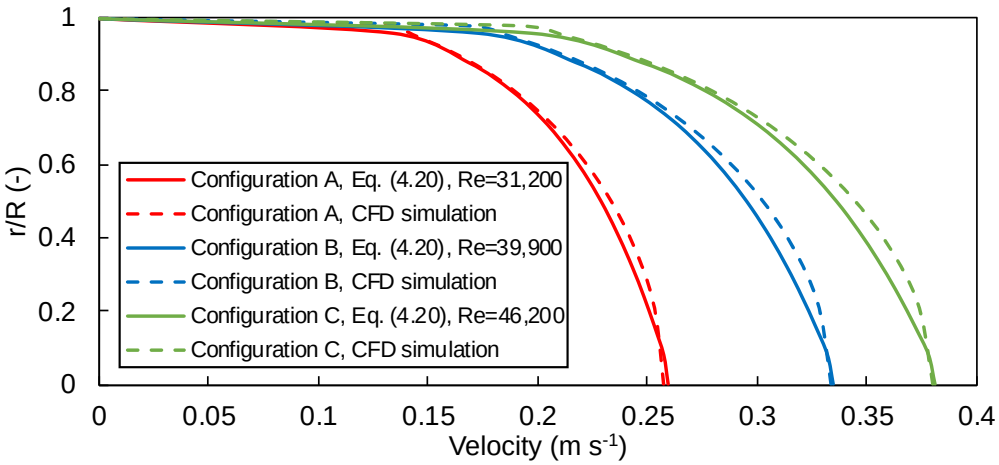

Fig. 4.3.3.2. Preliminary validation of the CFD model: comparison of simulations under the three different conditions considered and the universal velocity profiles for hydraulically rough tubes, *r* indicates the radial coordinate and *R* is the inner radius of the tube.

Mean velocities for different operating conditions can also be verified by an analytical calculation based on the pressure differential between the inlet and outlet of the transparent tube Δp_T (Pa). The pressure difference is defined by the different medium levels in the tanks Δh (m). The mean flow velocity $\bar{u}$ (m s^{-1}) is contained in two dimensionless criteria (friction coefficient λ, and Reynolds number *Re*), which are used to specify the pressure differential. Thus, the mean velocity cannot be directly determined. For this purpose, the dimensionless criteria that do not contain an unknown mean velocity can be expressed using Eq. (4.21)

$$Re \cdot \sqrt{\lambda} = \frac{d}{\mu} \cdot \sqrt{\frac{2 \cdot \Delta p_T \cdot \rho \cdot d}{L}} \tag{4.21}$$

where *d* (m) is the tube inner tube diameter, μ (Pa s) is the dynamic viscosity, ρ (kg m^{-3}) is the density, and *L* (m) is the length of the tube. For values of the dimensionless criteria from Eq. (4.21) greater than 1,138, the Colebrook equation can be used

$$\frac{1}{\sqrt{\lambda}} = -2 \cdot log\left(\frac{k^*}{3.71} + \frac{2.51}{Re \cdot \sqrt{\lambda}}\right) \tag{4.22}$$

where relative roughness *k** (-) can be specified using Eq. (4.23)

$$k^* = \frac{k_s}{d} \tag{4.23}$$

where k_s (m) is the roughness of the tube wall. The Reynolds number *Re* can be determined from Eq. (4.21) and Eq. (4.22), resulting in Eq. (4.24)

$$Re = \frac{1}{\sqrt{\lambda}} \cdot Re \cdot \sqrt{\lambda} \tag{4.24}$$

From the Reynolds number *Re* in Eq. (4.24) it is possible to derive the mean velocity $\bar{u}$ (m s^{-1}) in the tube (Munson et al., 2009)

$$\bar{u} = \frac{Re \cdot \mu}{d \cdot \rho} \tag{4.25}$$

The analytically calculated mean flow velocities for different configurations of operating conditions are shown in Table 4.3.3.2. The analytically calculated mean flow velocities correspond to the measured values (Table 4.3.3.1).

Table 4.3.3.2. Analytically calculated values of mean velocities in the tube of HHT PBR.

Configuration	h_1 (m)	h_2 (m)	Δh (m)	$\bar{u}$ (m s^{-1})
Calibration	0.28	0.24	0.04	0.21
A	0.35	0.29	0.06	0.26
B	0.36	0.26	0.10	0.34
C	0.39	0.26	0.13	0.39

4.3.4 Simulation of fluid dynamics

Velocity contours

This study was focused on the numerical investigation of overall hydrodynamic conditions in HHT PBR. The hydrodynamics in the open tanks of the PBR was analyzed using the validated 3D model. To this purpose, the hydrodynamic behavior of the PBR was simulated and compared with two different operating conditions. The streamlines in one open tank and the beginning of the eight tubes with a small difference in the water level (Δh=0.04 m; calibration configuration) and with a high difference in the water level (Δh=0.13 m; configuration C) are shown in Figure 4.3.4.1a and Figure 4.3.4.1b, respectively.

For small differences in culture medium levels (Figure 4.3.4.1a), low velocities were reached in a significant volume of the tank, in particular in the zone further from the paddle wheels, where the velocity reached values lower than 0.1 m s^{-1}. The volume of the open tank consisted of 47 % of the medium flowing with a velocity lower than 0.1 m s^{-1}. This low velocity can cause microalgae sedimentation and accumulation in the open tanks (Chisti, 2016). The increase in the difference in the water level could reduce the extent of this zone. With a difference of water level of 0.13 m (Figure 4.3.4.1b), the velocity in the zone further from the paddle wheels increased, significantly reducing the volume with the low velocity of 23 % of total open tank volume. However, flow velocity was still low (lower than 0.1 m s^{-1}) in some specific volumes of the open tank. This suggests that sedimentation and accumulation of microalgae in the tanks cannot be completely avoided by changing the operating conditions. These results also suggest that the shape of the open tanks could be improved in order to further reduce the

extent of dead volumes, for instance substituting the corner located opposite to the paddle wheel and tubes with a chamfer or round shape.

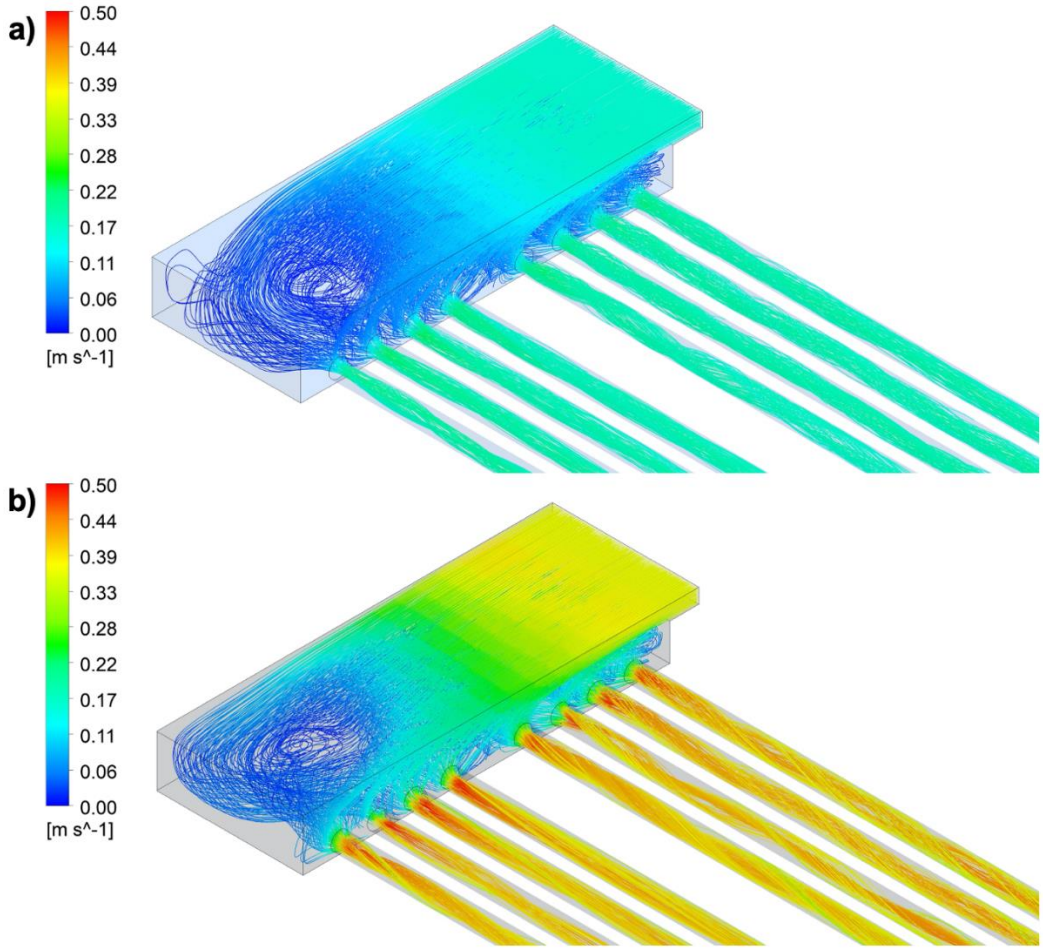

Fig. 4.3.4.1. Contour plot of the velocity streamlines in the HHT PBR open tank and tubes: a) calibration, Δh=0.04 m, b) configuration C, Δh=0.13 m.

Shear stress distribution

Pressure drop in PBR tubes may increase as the biofilm is formed and grows on the inner wall of the tubes. An increasing pressure drop could cause a rising water level in the inflow open tank, without increasing the velocity in the tubes and tanks. Therefore, it is always necessary to control biofilm growth inside the tubes, as well as the water levels in the tanks by adjusting the rotational speed of the paddle wheels. Moreover, the shear force close to the inner wall of the tube is a very important parameter for HHT PBR operation due to its role in avoiding biofilm formation and/or excessive growth. In other types of PBRs, such as air lift reactors, the low fluid-induced shear stress can be increased by applying aeration, as reported by Ding et al., (2021) in a laboratory scale experiment. In HHT PBR, the shear stress in the tubes can be increased by increasing the water level difference Δh in the open tanks.

The distribution of total shear stress in the tube in turbulent flow consists of a laminar τ_{lam} (Pa) and a turbulent shear stress τ_{tur} (Pa). The total shear stress can be expressed using Eq. (4.26)

$$\tau = \tau_{lam} + \tau_{tur} \tag{4.26}$$

In turbulent and transition areas, the effect of turbulent shear stress on the total stress distribution is dominant. However, the laminar shear stress is more important in the viscous sublayer near the wall of the tube. The laminar shear stress can be easily defined by the dynamic viscosity μ (Pa s) of the flowing medium (Eq. (4.27))

$$\tau_{lam} = \mu \cdot \frac{du}{dr} \tag{4.27}$$

One of the first attempts of semi-empirical analysis of turbulent flow was the concept developed by Prandtl in 1925 based on mixing length l_m (m) (Bird et al., 2002). Prandtl defined the turbulent viscosity μ_t (Pa s) based on the mixing length

$$\mu_t = \rho \cdot l_m^2 \cdot \left|\frac{du}{dr}\right| \tag{4.28}$$

where ρ (kg m^{-3}) is the density of the flowing medium. However, the mixing length parameter is not also easy to determine. Further considerations indicate that l_m is not constant throughout the flow field and additional assumptions are needed, according to the mixing length variation throughout the flow. Boussinesq hypothesis (chapter 4.3.2) defines the shear stress in turbulent flow τ_{tur} (Pa) in terms of the turbulent viscosity according to Eq. (4.29)

$$\tau_{tur} = \mu_t \cdot \frac{du}{dr} \tag{4.29}$$

The use of CFD allows the numerical solution of turbulent viscosity according to the Boussinesq hypothesis. The RNG k-ε model provides an analytically-derived differential formula for viscosity, which makes the model more accurate and reliable for a wider class of flows. The RNG model considers the effects of swirl or rotation by modifying the turbulent viscosity appropriately. In this study, the turbulent shear stress in the tubes of the PBR was estimated by the Boussinesq hypothesis, according to Eq. (4.29), using the turbulent viscosity determined by the CFD model. Subsequently, the total shear stress distribution was estimated as well. The CFD simulation of shear stress distribution for various operational conditions (detailed in Table 4.3.3.1) is shown in Figure 4.3.4.2.

The shear stress distribution can also be determined by the pressure differential in the tube Δp_T (Pa), which is defined by the medium level difference Δh (m) in the open tanks. Equations (4.27) and (4.28) are valid for laminar and turbulent flow as well (Munson et al., 2009)

$$\tau = \frac{2 \cdot \tau_w \cdot r}{d} \tag{4.30}$$

where r (m) is the radial coordinate, and τ_w (Pa) is the shear stress on the tube wall.

The wall shear stress τ_w (Pa) can be determined from Eq. (4.31)

$$\tau_w = \frac{\Delta p_T \cdot r}{2 \cdot L} \tag{4.31}$$

where *L* (m) is the length of the tube.

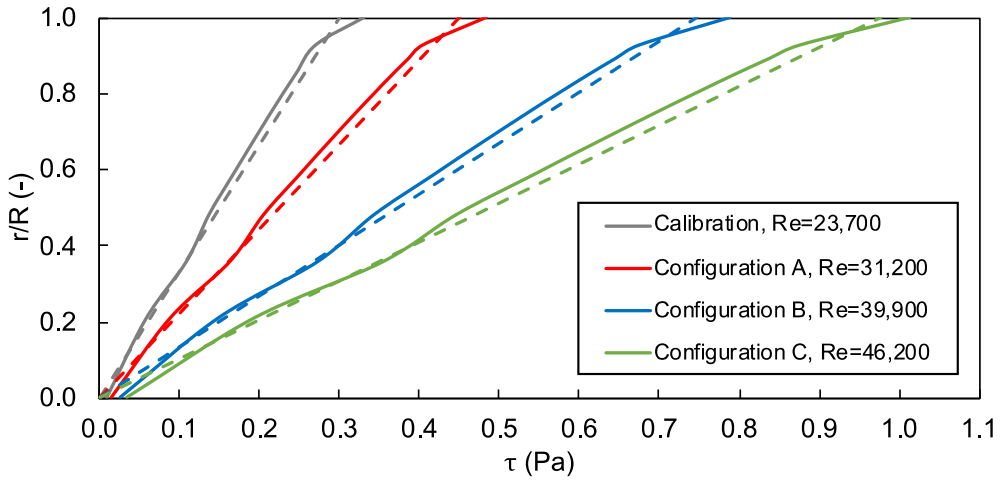

Fig. 4.3.4.2. Total shear stress distribution inside HHT PBR tube, the solid lines represent the distribution from the CFD simulation, the dashed lines represent the distribution determined from the pressure differential, *r* indicates the radial coordinate and *R* is the inner radius of the tube.

There was an evident increase in wall shear stress in accordance with the increasing velocity of the culture medium. In turbulent and transition areas, the effect of turbulent shear stress on the overall stress distribution is dominant. The laminar shear stress is more important in the viscous sublayer near the wall of the tube (Bird et al., 2002). Shear stress achieved in the wall ranged from 0.3 Pa for the lowest velocity to 1.0 Pa for the largest one. The shear stress values on the wall were higher than the critical value of the shear stress at which microalgae is fixed on the transparent walls in closed systems working in controlled laboratory conditions. At values lower than 0.2 Pa, a biofilm layer is formed in a closed cultivation system. However, in order to disrupt the integrity of the already formed biofilm, it is necessary to reach values of shear stress on the wall higher than 6 Pa (Belohlav et al., 2020; Zakova et al., 2019). It can be assumed that in the PBR processing wastewater in non-sterile conditions, the critical values of wall shear stress will be even higher than in the systems working in laboratory conditions. Therefore, these results suggest that the biofilm could not be removed by the shear forces once it is formed in the HHT PBR. Physical cleaning of the tubes should be periodically performed. However, the shear force obtained with the highest velocities seems to be able to prevent or reduce the formation of biofilm, thus reducing the need for cleaning or increasing the time interval between consecutive cleanings. It is also important to consider that some of the microalgae strains can be inhibited by high shear stress, while others are not sensitive to

values up to 80 Pa (Michels et al., 2016). Biofilm formation is also affected by the species of the microalgae present in the PBR. During the winter season, the HHT PBR was dominated by filamentous microalgae that were easier trapped on the tube wall. On the contrary, in the summer season, when the temperature and sunlight radiation intensity was higher, smaller microalgae were dominating the culture medium, and the consequent formation of biofilm was significantly slower. Further study should focus on finding a critical value of wall shear stress that will reduce the formation of biofilm on transparent walls or disrupt the stability of the resulting biofilm.

In general, the CFD simulation can be used for further investigation of design parameters and the operating conditions and the model can be used for further scale-up of HHT PBR and design modification.

4.3.5 Particle tracking

The particle tracking simulation was performed for three operating configurations (Table 4.3.5.1) corresponding to the different rotational speeds of the HHT PBR paddle wheel. Three operating modes were selected to simulate particle tracking, which describes the minimum and maximum operating conditions (calibration and configuration C). Configuration A, which corresponds to the flow rate most often used during the cultivation, was included for comparison as well.

Table. 4.3.5.1. Mean flow velocities for geometrically similar tubes.

Configuration	Reynolds number	Mean velocity in tube (m s^{-1})	
		d_1 = 125 mm	d_2 = 200 mm
Calibration	23,700	0.19	0.12
A	31,200	0.25	0.16
C	46,200	0.37	0.23

Using the developed CFD model, the movement of particles was monitored depending on the operating conditions of HHT PBR. The movement of the particles during their flow through the tube is shown in Figure 4.3.5.1. From the comparison, the dispersion of motion with increasing flow velocity in the tube was evident.

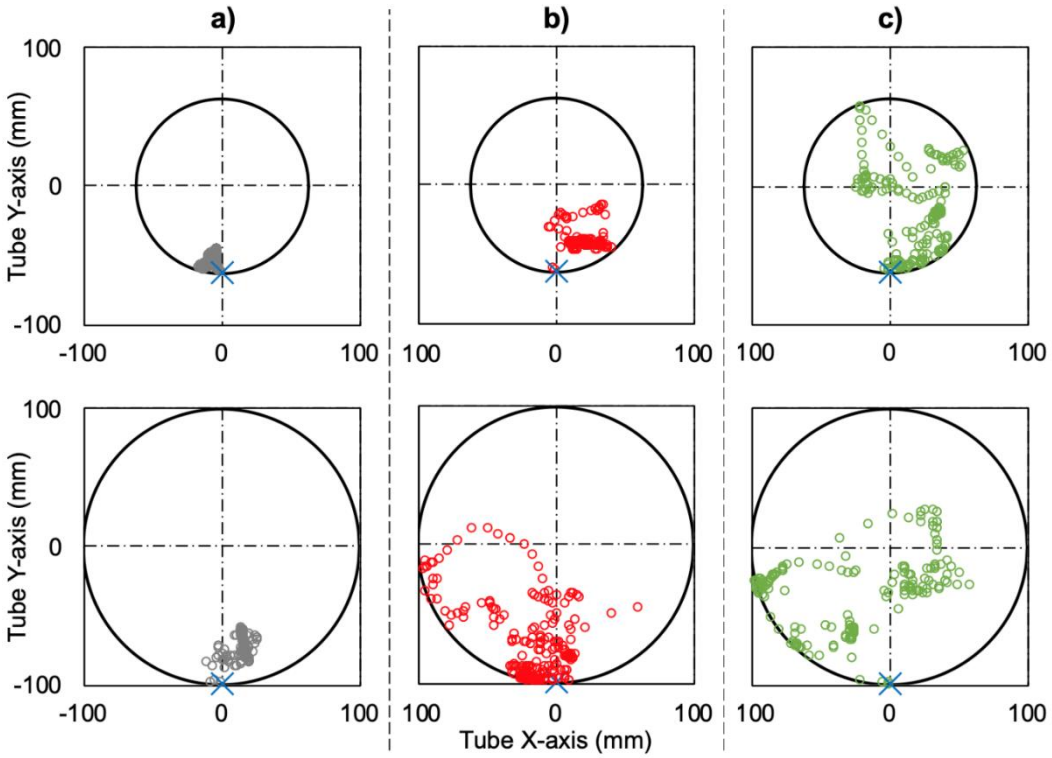

Fig. 4.3.5.1. Particle tracking in tube d_1=125 mm (top) and d_2=200 mm (bottom). Cross-sectional view – a) calibration, *Re*=23,700, b) configuration A, *Re*=31,200, c) configuration C, *Re*=46,200. The circles represent the position of one particle as it flows through the tube. Blue cross indicates injection point.

In order to verify the applicability of the model to geometrically similar tubes, it is necessary to create a new model with a different geometry. The hydrodynamic model of the tube with a diameter of d_1=125 mm, which corresponds to the original dimensions of the HHT PBR (detailed in chapter 4.1), was successfully validated based on the experimental measurements (chapter 4.3.3). To compare the hydrodynamic conditions in geometrically similar tubes, the same CFD model for a tube with a diameter of d_2=200 mm was created. Settings and basic parameters of both models are described in chapter 4.3.2. The operating conditions in tube d_2 were set according to *Re* corresponded to the operating configurations in tube d_1. Specifically, the flow rate in tube d_2 corresponds to the same value of *Re* as for tube d_1. The selected flow velocities in both tubes are shown in Table 4.3.5.1. Based on the developed model, it was possible to compare the particle tracking at the same values of *Re* for both tube geometries. The movement of particles in the cross-section of the tubes is shown in Figure 4.3.5.1. It was obvious that increasing flow rate causes increasing dispersion of particles and the mixing of the culture medium was more intensive for both tube geometries, however, the trajectories in geometrically similar tubes were different for the same *Re* values.

It is important to provide sufficient solar radiation for all microalgal cells in order the ensure effective cultivation. Therefore, the movement of the particle and its distance from the

irradiated surface of the tube was monitored (Figure 4.3.2.1). In HHT PBR, only the upper part of the tube is irradiated. If the culture medium is insufficiently mixed, the particles moving in the lower part of the tube will not be irradiated and the incident radiation is scattered by the layer of culture medium and the other cells in the culture medium. The distance of the particle from the irradiated wall *H* (m) during the flow through the tube is shown in Figure 4.3.5.2. From the comparison, it can be seen that at lower flow velocities, the particles were still moving close to the initial position. As the flow rate increases, the particles more often get closer to the irradiated area of the tube.

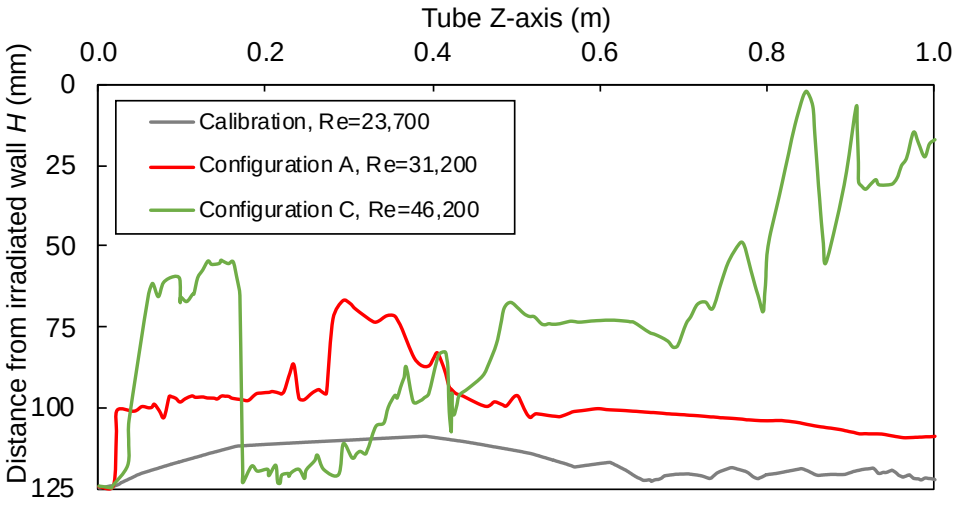

Fig. 4.3.5.2. Distance of the particle from irradiated wall in HHT PBR tube.

To compare the distances of the cells from the irradiated wall for geometrically similar tubes, the depth was related to the diameter of the tubes *d* (m). The dimensionless distance from the irradiated wall *H/d* is shown in Figure 4.3.5.3. A mean value of the dimensionless distance from the irradiated wall (dashed line) was generated for each configuration as well. It can be seen from the comparison that the dimensionless distance from the irradiated wall was comparable for geometrically similar tubes at the same flow regime. The hydrodynamic conditions based on the original CFD model for the tubes d_1 are therefore also applicable to geometrically similar systems with a different scale. Therefore, it is not necessary to create a new CFD model of hydrodynamic conditions during the scale-up process.

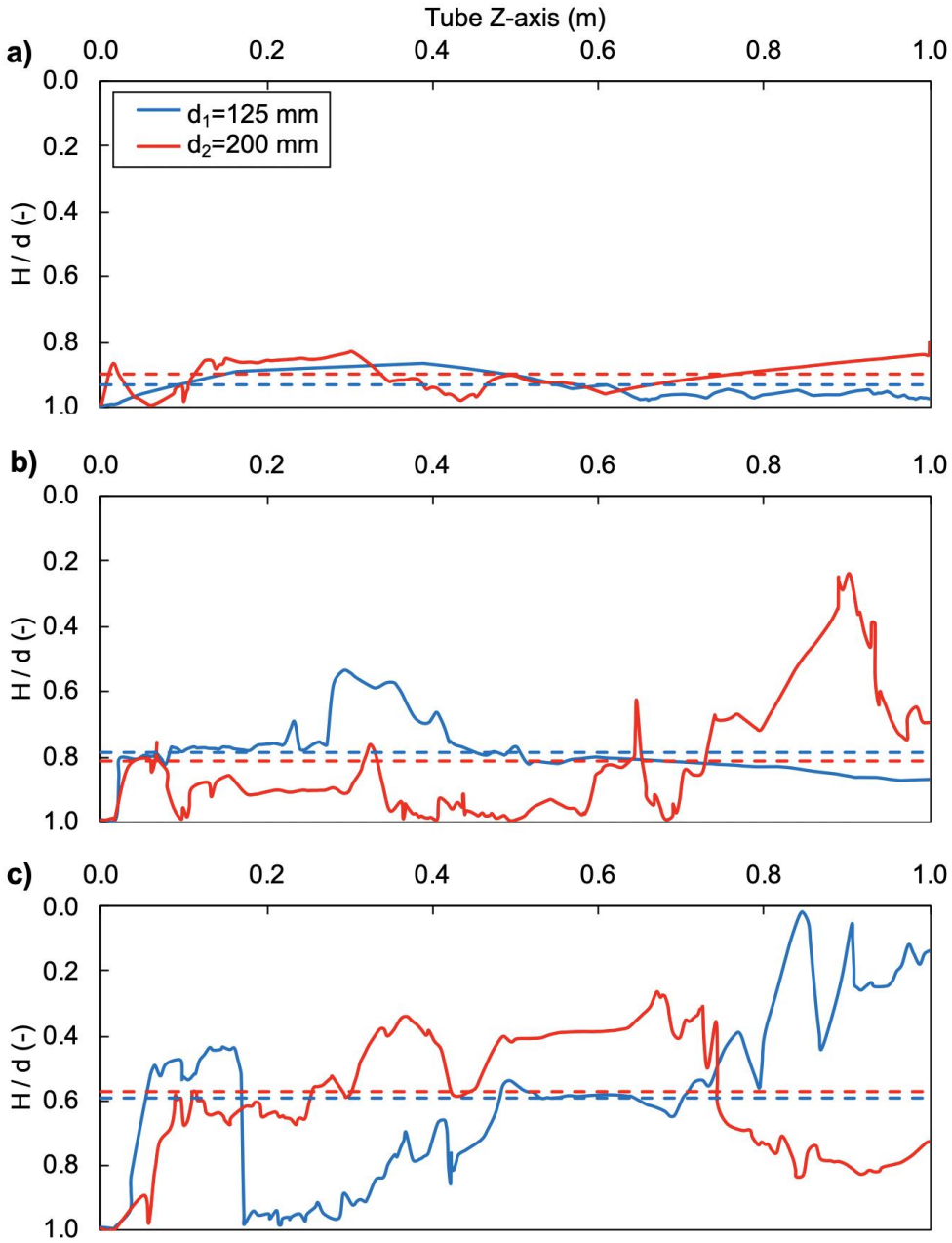

Fig. 4.3.5.3. Dimensionless distance of microalgae cell from the irradiated wall of HHT PBR tube - a) calibration, *Re*=23,700, b) configuration A, *Re*=31,200, c) configuration C, *Re*=46,200. Dashed lines represent the mean values, *H* indicates the distance from the irradiated wall and *d* is the tube diameter.

4.3.6 Conclusions

In order to study the hydrodynamic conditions in HHT PBR, the mean flow velocity in the transparent tubes was measured. The RTD was measured by means of the pulse-input tracer technique, and at the same time, by the ultrasonic flow meter as well. Based on experimental measurements, a numerical model simulating hydrodynamic conditions in transparent HHT PBR tubes was validated. The velocity distribution in the transparent tube was analytically determined from the measured data. The calculated velocity distribution was then compared with the velocity distribution generated by a numerical model for different operating flow rates, showing a good agreement. Therefore, the numerical model can be further used to simulate the other hydrodynamic parameters.

When the flow rate of the culture medium in the HHT PBR increased, the dead zones in the retention tanks were eliminated. However, even at the highest flow rate, which corresponds to a value of *Re*=46,200 in transparent tubes, the formation of dead zones was not completely avoided. From a comparison of the shear stress distribution in a transparent tube for different flow velocities, an increase in the wall shear stress with increasing flow velocity was evident. At a mean flow velocity of 0.19 m s^{-1}, the wall shear stress reaches 0.3 Pa. When the mean flow velocity was increased to 0.37 m s^{-1}, the wall shear stress reaches a value of over 1 Pa. Shear forces are important especially in terms of biofilm formation on transparent surfaces. The influence of shear force on the wall on biofilm formation is discussed in chapter 7.3.2.

Using the particle tracking model, it was possible to simulate the movement of microalgae cells in transparent tubes depending on different operating configurations. To verify the possibility of using a hydrodynamic model for geometrically similar systems, a model with an inner diameter of d_2=200 mm tubes was developed as well. As the flow rate of the culture medium in the transparent HHT PBR tubes increases, also the particle distribution increases. While maintaining the same flow regime in geometrically similar tubes, the dimensionless average distance of the microalgal cells from the irradiated wall was comparable. Therefore, during the integration of hydrodynamic conditions into a cultivation mechanistic model (chapter 6), there is no need to create a new CFD model for the geometrically similar design of the HHT PBR.

The aim of the next work was the implementation of the created numerical hydrodynamic model into a calibrated mechanistic model simulating the cultivation process. Using an integrated model, it will be possible to explore the effect of hydrodynamic conditions on the cultivation process. The created model could also be used for scale-up or modification of the geometry of the cultivation system.

5

Multi-physical model integrating the hydrodynamics and PBR performance

This chapter is based on articles:

Belohlav, V., Jirout, T., Kratky, L., Uggetti, E., Díez-Montero, R., García, J. (in preparation). Integration of hydrodynamics in cultivation model of hybrid horizontal tubular photobioreactor.

Belohlav, V., Jirout, T., Kratky, L. (2021). Integration of hydrodynamics into a biokinetic model for the simulation of microalgae cultivation in a photobioreactor. In European Biomass Conference and Exhibition Proceedings; ETA – Florence, Proceedings Pre-proof.

The aim of this part of the study was to integrate the influence of hydrodynamic conditions into a mechanistic BIO_ALGAE model simulating the cultivation process. For this purpose, a CFD model describing hydrodynamic conditions in a hybrid horizontal tubular photobioreactor was created, calibrated and validated (chapter 4). Using this model, it is possible to investigate the mixing of the culture medium and its effect on the movement of microalgal cells. By integrating hydrodynamic conditions into a BIO_ALGAE model, it is possible to investigate the influence of operating conditions on the distribution of light in the culture medium and the production of microalgae. The integrated multi-physical model was calibrated and validated based on the experimental data.

5.1 Model of light attenuation

The original BIO_ALGAE model does not consider the intensity of culture medium mixing as it flows through the transparent tubes. However, in cultivation systems that work with a wide layer of culture medium (raceway pond, column PBR), the intensity of mixing can affect the efficiency of the whole process of microalgae cultivation. In systems where no mixing of culture medium occurs, the microalgae can grow only in a part of the entire volume of the culture medium that is irradiated. Systems with intensive mixing and a large layer of culture medium can thus achieve higher productions than systems that work with a smaller layer of unmixed culture medium (Belohlav et al., 2018). For the integrated multi-physical cultivation model, the depth of the culture medium z (m) in Lambert-Beer's law (Eq. 2.12) was replaced by the mean distance of the particle from the irradiated wall H (m), which depends on the hydrodynamic conditions in HHT PBR (Figure 4.3.5.3). Accordingly, the average intensity of light radiation I_{av} (W m^{-2}) acting on microalgal cells in the tube is defined

$$I_{av} = \frac{I_o \cdot \left(1 - e^{(-K_I \cdot X_C \cdot H)}\right)}{K_I \cdot X_C \cdot H} \tag{5.1}$$

where I_o (W m^{-2}) is the incident light intensity, K_I (m^2 g^{-1}) is the extinction coefficient, X_C (g m^{-3}) is the sum of particulate components (microalgae biomass and bacteria). The integrated multi-physical cultivation model also includes the average depth of the culture medium in the retention tanks z_{tank} (m). The average value of z_{tank} is specified based on the level difference on both sides of the tank h_1 and h_2 (Table 4.3.3.1).

5.2 Multi-physics modeling methodology

The overall modeling methodology is shown in Figure 5.2.1. The hydrodynamic CFD model is used to simulate the particle trajectories for which the distance of the particle from the irradiated wall can be generated. Generated data can be subsequently passed to the attenuation model (Eq. 5.1) integrated into BIO_ALGAE model in order to predict the production of microalgal biomass.

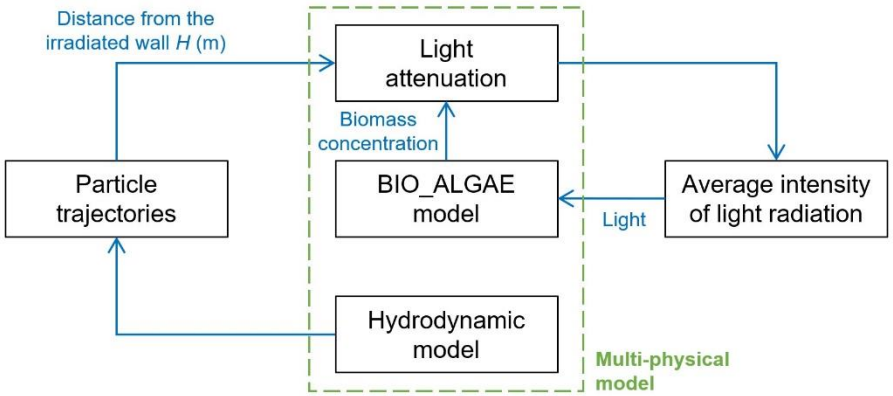

Fig. 5.2.1. Coupling multi-physics methodology of BIO_ALGAE model, hydrodynamics and light attenuation in HHT PBR.

5.3 Model calibration and validation

The model was calibrated using measured data from the winter campaign, which are described more in detail in chapter 4.3.1. The velocity of the culture medium in transparent tubes was set to be 0.25 m s^{-1} during the measuring campaigns, which correspond to configuration A (Table 4.3.3.1). The mean distance of the particle from the irradiated wall *H* and the average depth of the culture medium in the retention tanks z_{tank} for the various operating configurations are shown in Table 5.3.1.

Table 5.3.1. Parameters of integrated cultivation model.

Configuration	$\bar{u}$ (m s^{-1})	*Re* (-)	*H* (m)	z_{tank} (m)
Calibration	0.19	23,700	0.116	0.260
A	0.25	31,200	0.099	0.320
C	0.37	46,200	0.074	0.325

The average values of the influent parameters were determined according to Henze et al. (2015), where the ratios of parameters were defined based on the measured influent value of chemical oxygen demand COD (gO_2 m^{-3}). The measured values of the culture medium temperature in HHT PBR (Figure 4.2.1.2) and the intensity of solar radiation (Figure 4.2.1.3) were used in the model as well. The simulation was repeated several times after the time corresponding to the length of the measurement campaign. The calculation was repeated until all parameters in the model had stabilized. The total calculation thus simulated the cultivation process in the order of tens of days.

The model was calibrated using the mentioned calibration parameters: μ_{ALG}, μ_H, $k_{death,H}$, k_La_{O2}, k_La_{CO2}, and k_La_{NH3}. The resulting values of these parameters are shown in Table 5.3.2. Compared to the original calibration parameters of the BIO_ALGAE model (detailed in

Table 4.2.2.3), only a slight change in volumetric mass transfer coefficient for oxygen k_La_{O2} occurred. Influence on the similarity of calibration parameters is described in detail in chapter 6.

Table 5.3.2. Calibrated parameters.

Parameter	Description	Value (d^{-1})
μ_{ALG}	Maximum specific growth rate of microalgae	1.7
μ_H	Maximum specific growth rate of heterotrophic bacteria	1.3
$k_{death,H}$	Inactivation constant of heterotrophic bacteria	0.3
k_La_{O2}	Volumetric mass transfer coefficient for oxygen	3.7
k_La_{CO2}	Volumetric mass transfer coefficient for carbon dioxide	3.0
k_La_{NH3}	Volumetric mass transfer coefficient for ammonia	0.7

The numerical model was calibrated by comparing the generated curves from the model with the experimental data. The following parameters were used for calibration: dissolved oxygen S_{O2} ($gO_2\ m^{-3}$), total suspended solids TSS ($gCOD\ m^{-3}$), and ammonium nitrogen S_{NH4} (gNH_4^+-$N\ m^{-3}$). The resulting curves of the calibrated model are shown in Figure 5.3.1. Calibration was performed to minimize the RMSE. The RMSE of the calibrated model for each component was $RMSE_{SO2} = 1.36\ gO_2\ m^{-3}$, $RMSE_{TSS} = 15.81\ gTSS\ m^{-3}$ and $RMSE_{NH4} = 0.06\ gNH_4$-$N\ m^{-3}$. The higher value of $RMSE_{TSS}$ is due to the model considering respiration at the end of the night, resulting in a steep drop in biomass. The decrease in experimentally measured TSS during the night cycle is due to low oxygen production in the culture medium, which keeps the biomass buoyant.

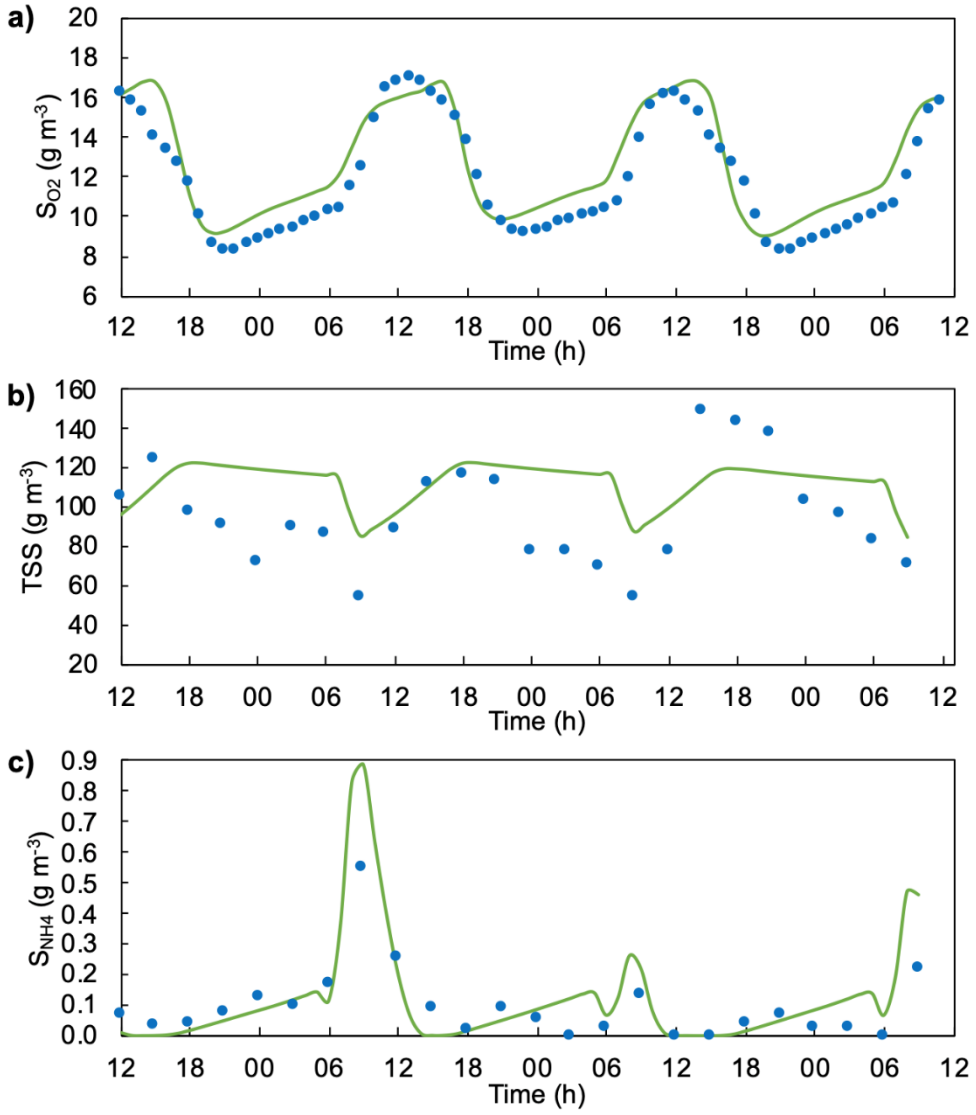

Fig. 5.3.1. Calibration of the integrated cultivation model of HHT PBR – a) dissolved oxygen, b) total suspended solids and c) ammonium nitrogen. Simulated (green line) and experimental (blue dots) data during the winter measuring campaign.

The model was validated according to experimental data from the spring campaign (chapter 4.2.1). The influent parameters, initial conditions, culture medium temperature (Figure 4.2.1.2), and solar radiation (Figure 4.2.1.3) were slightly different in comparison with winter values. Experimental data matched well with simulated data. The global error of the simulations was slightly higher in comparison with calibration. Validation of dissolved oxygen is shown in Figure 5.3.2a with $RMSE_{SO2}$ = 2.40 gO_2 m^{-3}. Validation of TSS and ammonium nitrogen are shown in Figure 5.3.2b and Figure 5.3.2c. The RMSE value of each component was $RMSE_{TSS}$ = 33.24 gTSS m^{-3} and $RMSE_{NH4}$ = 0.10 gNH_4-N m^{-3}. TSS values were influenced by influent parameters in addition to respiration and oxygen production during the night. The model is not sensitive enough to capture such a step change and showed only a gradual increase.

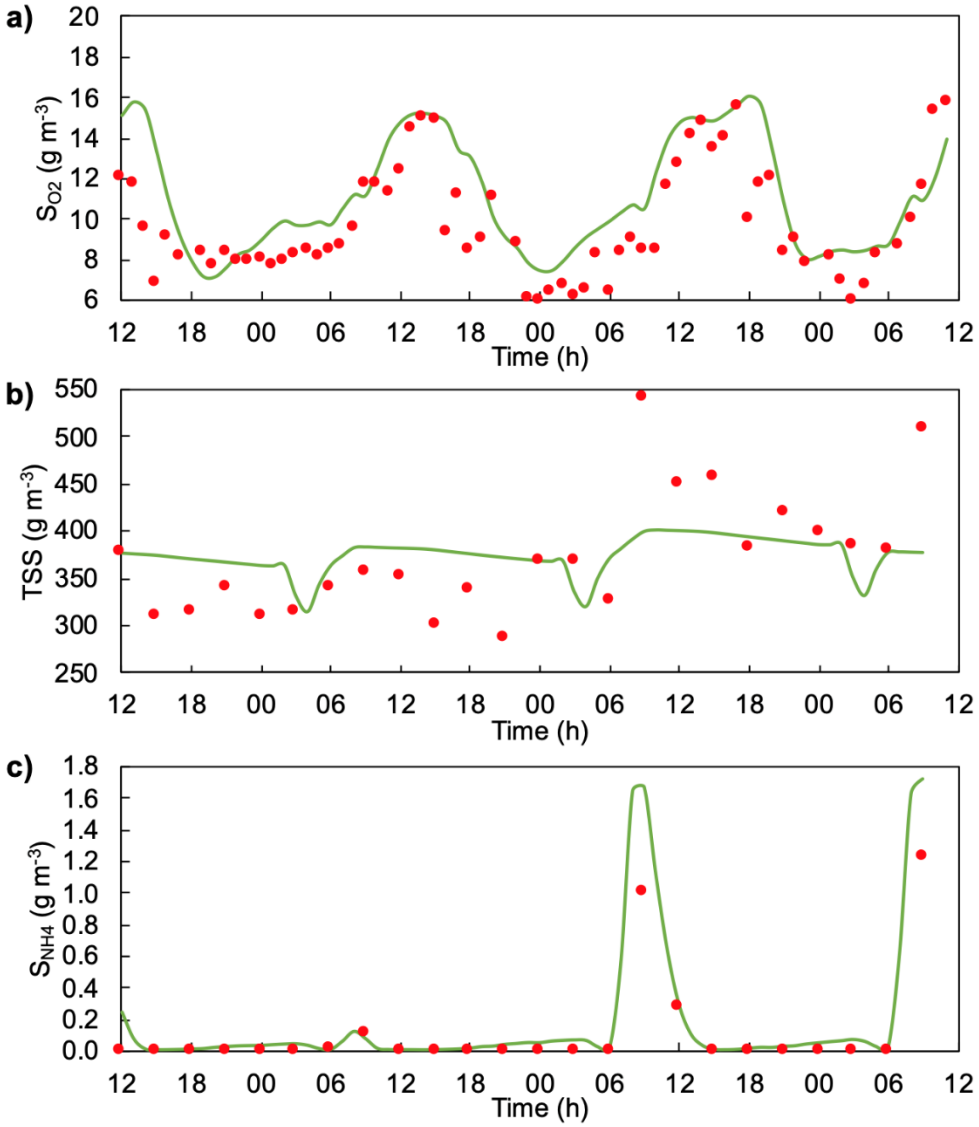

Fig. 5.3.2. Validation of the integrated cultivation model of HHT PBR – a) dissolved oxygen, b) total suspended solids and c) ammonium nitrogen. Simulated (green line) and experimental (red dots) data during the winter measuring campaign.

5.4 Conclusions

The created multi-physical model considers the effect of the distance of the microalgae cell from the irradiated wall of HHT PBR, which is significantly influenced by the mixing conditions of the culture medium. The developed multi-physical model was calibrated and validated based on the data from winter and spring intensive experimental campaigns. Using a validated integrated model, it is possible to monitor the influence of hydrodynamic conditions on the irradiation of the culture medium in HHT PBR and microalgae production as well.

6

Hydrodynamics influence on microalgae production and light regime

This chapter is based on articles:

Belohlav, V., Jirout, T., Kratky, L., Uggetti, E., Díez-Montero, R., García, J. (in preparation). Integration of hydrodynamics in cultivation model of hybrid horizontal tubular photobioreactor.

Belohlav, V., Jirout, T., Kratky, L., Uggetti, E., Díez-Montero, R., García, J. (in preparation). Mutual hydrodynamics and light regime influence on microalgae biomass production in a hybrid horizontal tubular photobioreactor.

The aim of this chapter was to study the influence of hydrodynamic conditions in HHT PBR on microalgae production. Specifically, this work was carried out to investigate the intensification of the mixing of the culture medium and its subsequent effect on the production of microalgae. Indeed, the CFD hydrodynamic model can simulate the distribution of the microalgae cells in the culture medium during its flow through a transparent tube. By using this model, it is also possible to study more in detail the effect of hydrodynamics on cell irradiation and their movement between the light and dark zones. By integrating microalgae cell tracking into the BIO_ALGAE model, the effect of different operating conditions on microalgae biomass production ware investigated as well.

6.1 Hydrodynamics influence on microalgae production

The effect of flow rate on microalgae concentration in culture medium X_{ALG} (g L^{-1}) was not significant, as can be seen in Figure 6.1.1.

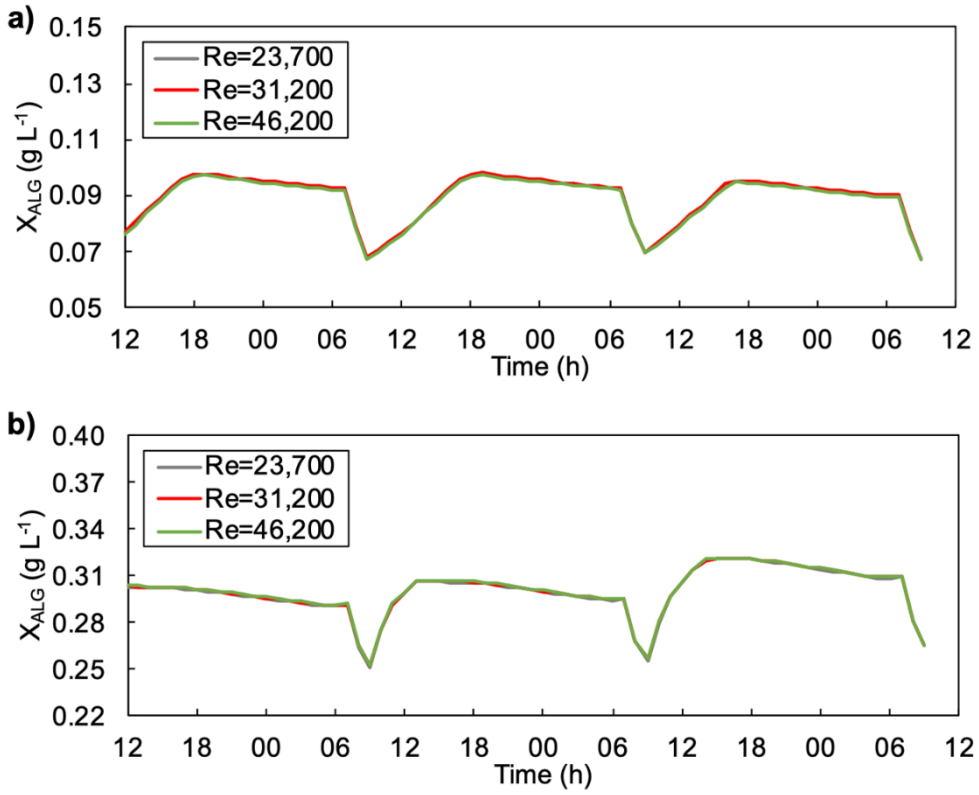

Fig. 6.1.1. Microalgae production – a) winter campaign, b) spring campaign.

With an increasing flow rate, only a negligible change occurs in X_{ALG} in HHT PBR. The flow regime changes from the *Re*=23,700 to 31,200 leads to 0.21 and 0.12 % increase in X_{ALG} during winter and spring campaigns, respectively. For the flow regime *Re*=46,200, there was an increase of 0.21 % compared to *Re*=23,700 during the spring campaign. However, during a winter campaign concentration actually decrease by 0.54 %. The decrease in the production of microalgae was influenced by the retention tanks, which can no longer be completely

irradiated, and dark zones were formed due to the higher microalgae concentration in the culture medium. The effect of light penetration into the culture medium is described more in detail in chapter 6.2. A slight increase in X_{ALG} was affected by the generally low production of microalgae. The concentration of microalgae in the culture medium reaching 0.1 g L^{-1} during the winter season and 0.3 g L^{-1} during the spring season. In this case, the culture medium has a low concentration and the light radiation was not limited in the penetration of the culture medium layer. As described in chapter 4.2.1, microalgae production (X_{ALG}) in HHT PBR was limited by a lack of nutrients during both measurement campaigns. More precisely, it was a lack of phosphorus, which was deficient throughout the whole year in influent wastewater. Similar cultivation systems usually reach microalgae concentrations over 1 g L^{-1} (Olivieri et al., 2014).

It is possible to adjust the nutrient content of the influent wastewater in order to increase the X_{ALG} reaching the value of 1 g L^{-1}. In this case, a comparison of microalgae concentration in culture medium X_{ALG} for three operating configurations is shown in Figure 6.1.2. According to the change of flow regime *Re*=23,700 to 31,200, microalgae production can increase by 0.7 %. In terms of HHT PBR performance, it means an increase in biomass production of 16 g day^{-1} from the base 2,145 g day^{-1}. For the flow regime *Re*=46,200, the production increased by 2.0 % in comparison to *Re*=23,700, which means an increase in biomass production to 43 g day^{-1}.

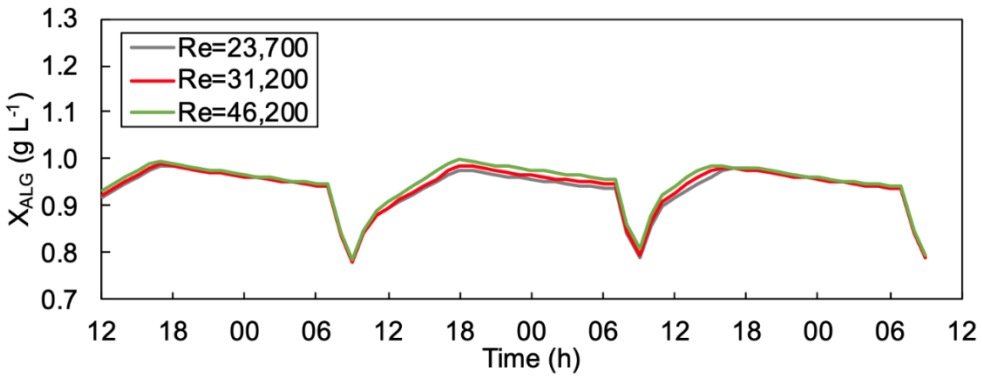

Fig. 6.1.2. Microalgae production in HHT PBR with increased nutrient content in influent wastewater.

Hydrodynamic conditions at higher flow rates of the culture medium were simulated using a validated multi-physical model. The hydrodynamic conditions corresponding to the various operating modes of the HHT PBR were described in chapter 4. According to experimental measurements, measured flow velocities in transparent tubes were in the range from 0.19 m s^{-1} to 0.37 m s^{-1}, which corresponds to *Re*=23,700 and *Re*=46,200, respectively. The CFD model has also been developed for these operating conditions, which described the motion of particles simulating microalgal cells (chapter 4.3.5). The dependence of the

dimensionless distance from the irradiated wall *H/d* on Reynolds number *Re* was almost linear in this range. In order to be able to use the validated model also for higher flow rates of the culture medium in transparent tubes, the CFD hydrodynamic model was created also for a flow rate of 1 m s^{-1} and 2.5 m s^{-1}, which corresponds to *Re*=124,800 and *Re*=311,900, respectively. According to the created CFD model of hydrodynamic conditions, the dimensionless distance of microalgal cells from the irradiated area corresponds to *H/d*=0.35 at *Re*=124,800 and *H/d*=0.25 at *Re*=311,900. From the dependence of *H/d* on *Re* (Figure 6.1.3), it is possible to observe that at values of *Re* higher than 50,000 the dependence becomes non-linear.

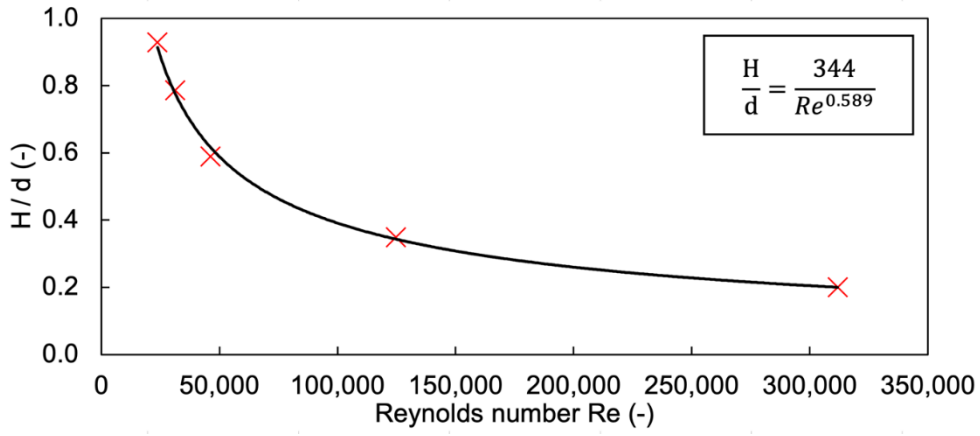

Fig. 6.1.3. The dependence of the dimensionless distance from the irradiated wall on Reynolds number in transparent tube, *H* indicates the distance from the irradiated wall and *d* is the tube diameter.

However, the higher wall shear stress values, which are associated with increasing flow rates, can also damage the microalgae cells. Acién Fernández et al. (2001) defined the maximum flow rate according to the diameter of the PBR tube. For a tube diameter of 125 mm, the maximum speed corresponds to 1.4 m s^{-1}. From Figure 6.1.3, it is possible to derive a dimensionless distance *H/d* at a velocity of 1.4 m s^{-1}, which corresponds to the *Re*=174,700. The dimensionless distance of the microalgae cell from the transparent wall *H/d* was 0.28 for *Re*=174,700.

Using the created multi-physical model, the cultivation process was simulated for operating conditions that ensure intensive mixing of the culture medium in transparent HHT PBR tubes. Using the validated model, the production of biomass X_{ALG} (g L^{-1}) was simulated under operating conditions that correspond to the flow regime in transparent tubes *Re*=174,700. According to Figure 6.1.3, the theoretical distance of the microalgae cell from the irradiated wall *H* was 0.035 m. In Figure 6.1.4, a significant increase in the production of microalgae in comparison with the base flow regime (*Re*=23,700) is shown. For the flow regime in the transparent tube of *Re*=174,700, the biomass production increase by 4.6 % compared to base *Re*=23,700, which results in an increase in biomass production by 99 g day^{-1} from the base

2,145 g day^{-1}. It has to be considered that with increasing *Re*, the pressure drop will also increase, which is reflected in the operating costs.

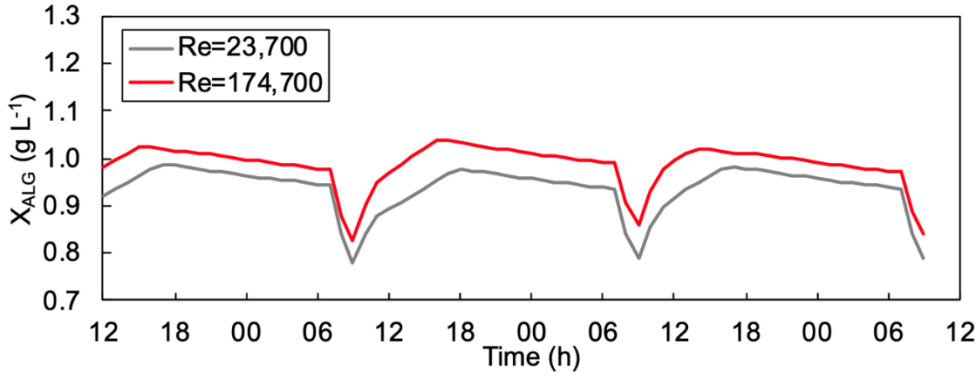

Fig. 6.1.4. Microalgae production for various operating conditions corresponding to flow regime in transparent tubes *Re*=23,700 (shadow line) and *Re*=174,700 (red line).

6.2 Hydrodynamics influence on light regime

Using Eq. (5.1), it is possible to compare the effect of microalgae concentration on the average intensity of light radiation I_{av} acting on microalgal cells. For comparison, the average daily value of incident light intensity I_o recorded during the spring measurement campaign was used (431 W m^{-2}). The effect of microalgae concentration on I_{av} is shown in Figure 6.2.1.

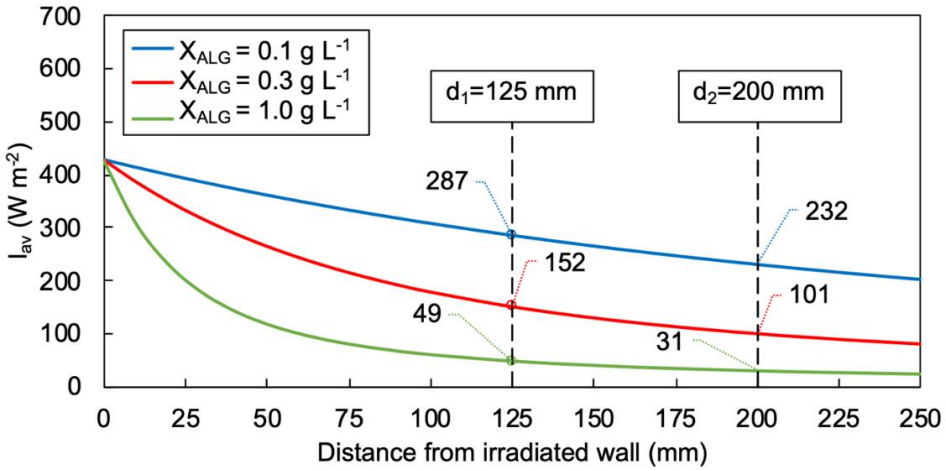

Fig. 6.2.1. Influence of microalgae concentration on average intensity of light radiation in culture medium.

When the X_{ALG} in HHT PBR reached 0.1 and 0.3 g L^{-1}, the I_{av} was reduced by 33 % and 65 % at the farthest point from the irradiated wall of the HHT PBR tube d_1=125 mm. The light radiation in the tube d_2=200 mm was reduced by 46 % for concentration 0.1 g L^{-1} and 77 % for concentration 0.3 g L^{-1}. However, when the X_{ALG} reaches 1 g L^{-1}, there was a significant reduction of I_{av} by 89 % in d_1 and 93 % in d_2. Therefore, the mixing of culture medium would

have a more intensive effect in systems working with significantly greater thickness of the culture medium, such as raceway pond or column PBRs. These systems usually work with a wide layer (around 30 cm), which can be difficult to irradiate even with low concentrations of microalgae in the culture medium.

By using the validated integrated model, it is possible to monitor the influence of hydrodynamic conditions on the irradiation of the culture medium in HHT PBR. The flow rate and the associated mixing of the culture medium in the transparent tubes have a significant effect on the average intensity of light radiation I_{av} acting on microalgal cells. A comparison of I_{av} for different configurations of operating conditions is shown in Figure 6.2.2.

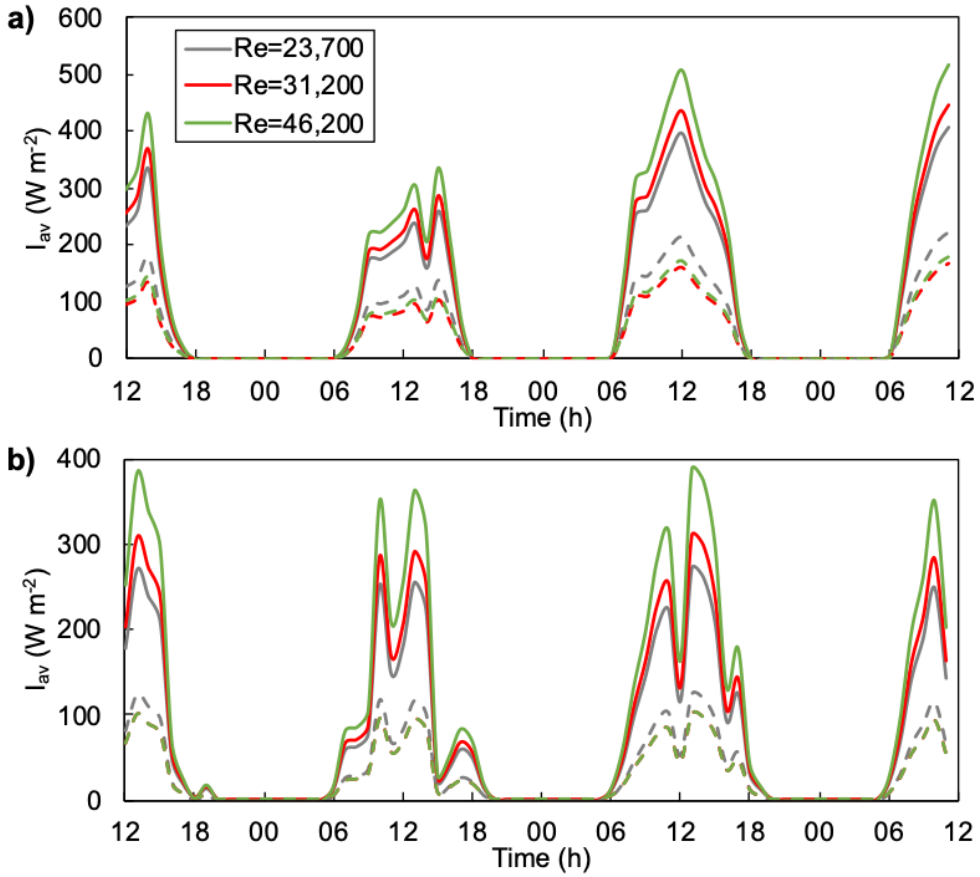

Fig. 6.2.2. Average intensity of light radiation – a) winter campaign data and b) spring campaign data. The full lines represent the light radiation in tubes and dashed curves represent light radiation in retention tanks.

An increase of I_{av} due to the increasing flow rate of the culture medium in the transparent tube was evident (green lines vs. red and gray lines). However, the culture medium was also partially irradiated in retention tanks (dashed lines). Compared to tubes, the intensity of I_{av} in tanks was lower. Nevertheless, in tanks, a partial difference in I_{av} between operating conditions was observed. This was due to the different culture medium levels in the two parts of the tanks, which were affected by the rotational speeds of the paddle wheel (higher rotation speeds

correspond to higher culture levels and lower I_{av}). As the average depth of the culture medium in the retention tanks z_{tank} increases with increasing flow rate, the I_{av} decreases conversely to the tubes. A comparison of I_{av} in the winter and spring measurement campaigns shows that in spring the I_{av} values were lower than in the winter campaign, although the incident light intensity I_o was higher during the spring campaign. This was due to the higher concentration of microalgae and bacteria in the culture medium in spring (TSS), which can be observed from Figure 5.2.1b and Figure 5.2.2b.

Since the transparent HHT PBR tubes were placed on the ground, only the upper part of the tubes could be irradiated. Therefore, if the culture medium in the tube is not sufficiently mixed, the particles located in the lower part of the tube do not receive the required amount of light radiation. The dark zones are formed in the tubes, which reduces the efficiency of the cultivation. In order to quantify the light regime in the HHT PBR tube, it is necessary to define the light and dark zones. The area of the tube where the average light intensity is lower than the critical value of the saturation light intensity is defined as the dark zone. Conversely, in the light zone, the average light intensity is higher. The saturation light intensity for *Chlorella* is reported to range from 67.25 to 96.84 μmol m^{-2} s^{-1} (Cheng et al., 2016; Huang et al., 2014). The critical saturation light intensity for cyanobacteria is lower and reaches values around 50 μmol m^{-2} s^{-1} (Tilzer, 1987). To evaluate the light regime under different operating conditions of HHT PBR, it is possible to use the light fraction ε_L indicating the fraction of the time in the light zone in a light/dark (L/D) cycle. The light fraction is defined by Eq. (6.1)

$$\varepsilon_L = \frac{t_i}{t_L + t_D} \tag{6.1}$$

where t_L (s) is the retention time of microalgae cell in the light zone, and t_D (s) is the time when the cell is in the dark zone.

The transition boundary between the light and dark zones can be defined by the critical saturation intensity of the light, which was selected to be 70 μmol m^{-2} s^{-1} (Huang et al., 2014; Tilzer, 1987). The light regime was calculated using Eq. (5.1) for the concentration of microalgae in the culture medium 1 g L^{-1}, and the intensity of incident light corresponding to the spring average daily measured value of 431 W m^{-2} (Figure 4.2.1.3). The transition boundary between the light and dark zones for both tubes d_1 and d_2 are shown in Figure 6.2.3. A tube with a diameter of d_1=125 mm consists of 83 % of a light zone and 17 % of a dark zone. In a tube d_2=200 mm, the total tube volume consists of 55 % of a light zone, and the dark zone reaches 45 %. For both tubes, the dimensionless distance of the transition boundary between the light and dark zones was defined as well. The dimensionless distance of the transition boundary H/d in tube d_1 corresponds to the value of 0.72 and in tube d_2 to the value of 0.45. Comparing the transition boundary with the distance of the particles from the irradiated wall (Figure 4.3.5.3), it is possible to define the light fraction ε_L.

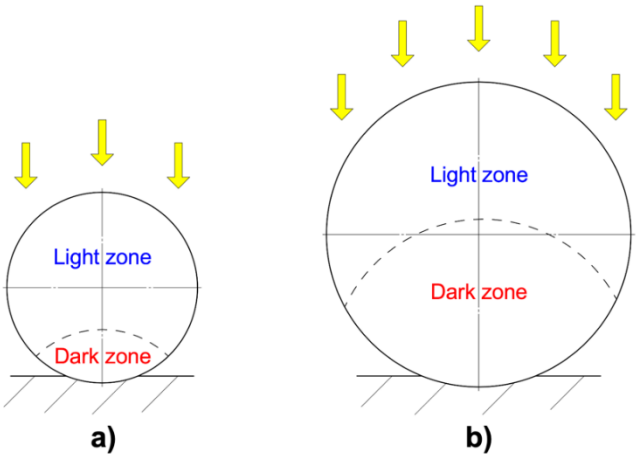

Fig. 6.2.3. Transition boundary between the light and dark zone - a) tube d_1=125 mm and b) tube d_2=200 mm. Dashed line indicates the transition boundary.

As the velocity in the tube increases, the particles more often enter the light zone of the tube. Conversely, in the case of the lowest flow velocity (*Re*=23,700), the particles in both tubes do not get out of the dark zone during their entire flow (Figure 4.3.5.3a). For the flow regime *Re*=31,200 (Figure 4.3.5.3b), the light fraction ε_L was 0.128 and 0.075 for the tubes d_1 and d_2, respectively. At a higher velocity of the culture medium, corresponding to the value *Re*=46,200 (Figure 4.3.5.3c), the light fraction in tube d_1 was 0.678, and in tube d_2 was 0.369.

6.3 Conclusions

The increasing flow rate results in a more intensive mixing of the culture medium. The developed integrated multi-physical model showed that in systems working with a large layer of culture medium or a high concentration of microalgae, the intensification of mixing increases the production of microalgae. The aim was therefore to bring the hydrodynamic conditions in the culture system as close as possible to the state where the entire volume of the culture medium will be ideally mixed. This state can be achieved by increasing the flow rate in the tubes. However, increasing the flow rate is limited by the critical condition when the microalgae cells can be damaged and growth is limited due to the high value of shear stress. Another way to intensify the mixing of the culture medium is to use static mixers, which can be installed directly in the tubes of PBR. Based on the geometry of the static mixer, the flow in the tube is divided into several separate streams that intersect with each other. However, concerning the structure and properties of microalgae, it is also important to take into account the possibility of trapping microalgae on the walls of the static mixer, which could cause its clogging and subsequent contamination of the processed batch. With the installation of a static mixer in a PBR tube, the pressure drop also increases, which will affect operating costs. The aim of further work is to verify the possibility of using static mixers in cultivation systems.

7

Hydrodynamics of flat panel PBR

This chapter is based on articles:

Belohlav, V., Zakova, T., Jirout, T., Kratky, L. (2020). Effect of hydrodynamics on the formation and removal of microalgal biofilm in photobioreactors. *Biosystems Engineering*, 200, 315–327.

Belohlav, V., Jirout, T., Kratky, L., Uggetti, E., Díez-Montero, R. (2019). Numerical analysis of hydrodynamic conditions in pilot flat-panel photobioreactor: operating and design parameters influence on the microalgae cultivation. In European Biomass Conference and Exhibition Proceedings; ETA - Florence, pp 255–260.

Belohlav, V., Jirout, T. (2019). Design methodology of industrial equipment for microalgae biomass primary harvesting and dewatering. *Chemical Engineering Transactions*, 76, 919–924.

Simulations of the integrated model showed the positive effect of mixing intensification on increasing microalgal biomass production. By increasing the flow rate of the culture medium, the mixing can be intensified. However, as the flow rate increases, microalgal cells may be damaged. It is also possible to use the static mixers in order to intensify the mixing of the culture medium in the irradiated area of the PBR. Another important parameter in scaling-up of the cultivation system is also the formation of a biofilm on transparent walls, which prevents the light irradiation of the culture medium.

Hydrodynamics in flat panel photobioreactor (FP PBR) is more complex than in HHT PBR. In the flat panel PBR, it is possible to change the configurations of the inflow and outflow of the culture medium from the PBR chamber. By changing the inflow and outflow configuration, it is thus possible to change the hydrodynamics of the culture medium in the irradiated area of the PBR. For each inlet and outlet configuration, the effect of flow rate on mixing and homogenization was investigated. By comparing the created hydrodynamic model with experimental measurements, the influence of hydrodynamics on the prevention of biofilm formation was specified as well. By using the created hydrodynamic model, it is possible to optimize the operating and design parameters of the flat panel PBR.

7.1 Photobioreactor design and system operation

The FP PBR was installed in the laboratories of the Department of Process Engineering at the Czech Technical University in Prague (Figure 7.1.1). The laboratories are completely enclosed, so it is possible to control the influence of the environment on the cultivation system. The volume of the culture medium in the FP PBR chamber is 75 L. The height of the chamber is 2.0 m and the width is 0.7 m. Transparent polymethylmethacrylate (PMMA) plates are placed on both sides of the chamber. The irradiated area of FP PBR is 2.8 m^2. The chamber is irradiated on one side using LED light strips, which are distributed over the entire surface of the plate. The intensity of light radiation can be regulated. The distance between the transparent plates is 0.05 m. Stainless profiles are also placed on the transparent plates, which prevent the plates from bending due to the effect of hydrostatic pressure in the FP PBR chamber. Inlet and outlet ports are located on the chamber and it is possible to change the inflow and outflow of the culture medium from the upper part to the bottom of the FP PBR chamber (Figure 7.1.2). Two necks are located on either side of the lower part of the chamber. One neck is located in the middle of the upper part. The element for the distribution of aeration gas in the culture medium is installed at the bottom of the chamber. Furthermore, the chamber is equipped with several necks for connecting measuring devices monitoring the cultivation process. The 3D scheme of the FP PBR is shown in Figure 7.1.2.

Fig. 7.1.1. Flat panel system installed in Department of Process Engineering laboratory.

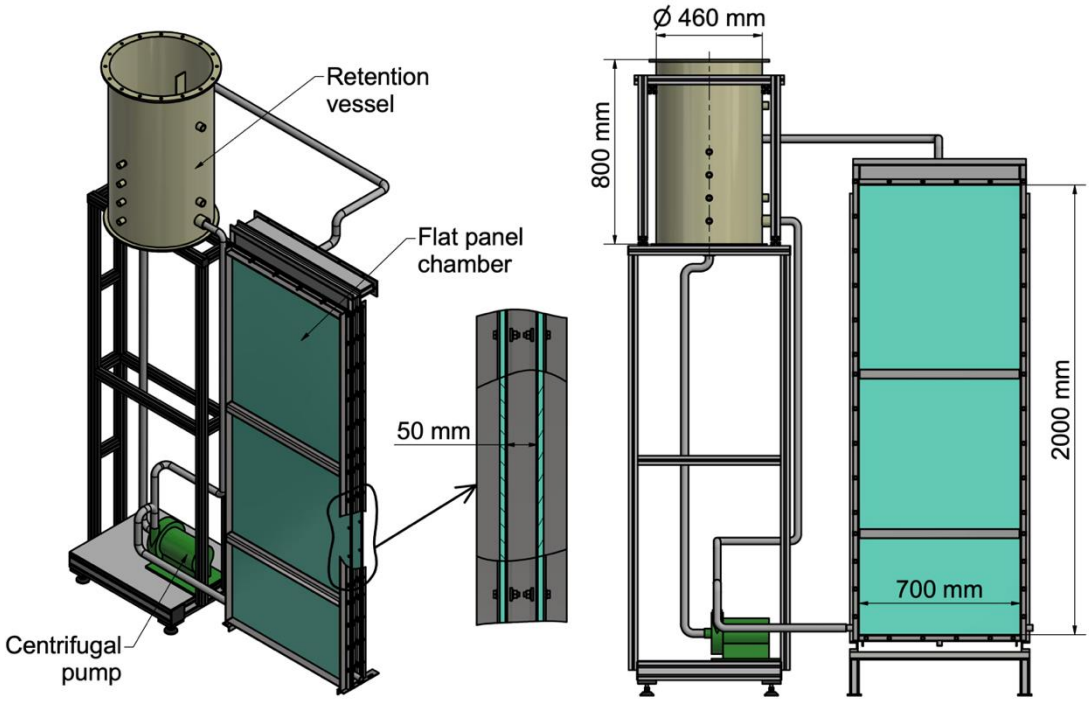

Fig. 7.1.2. 3D drawing of flat panel system.

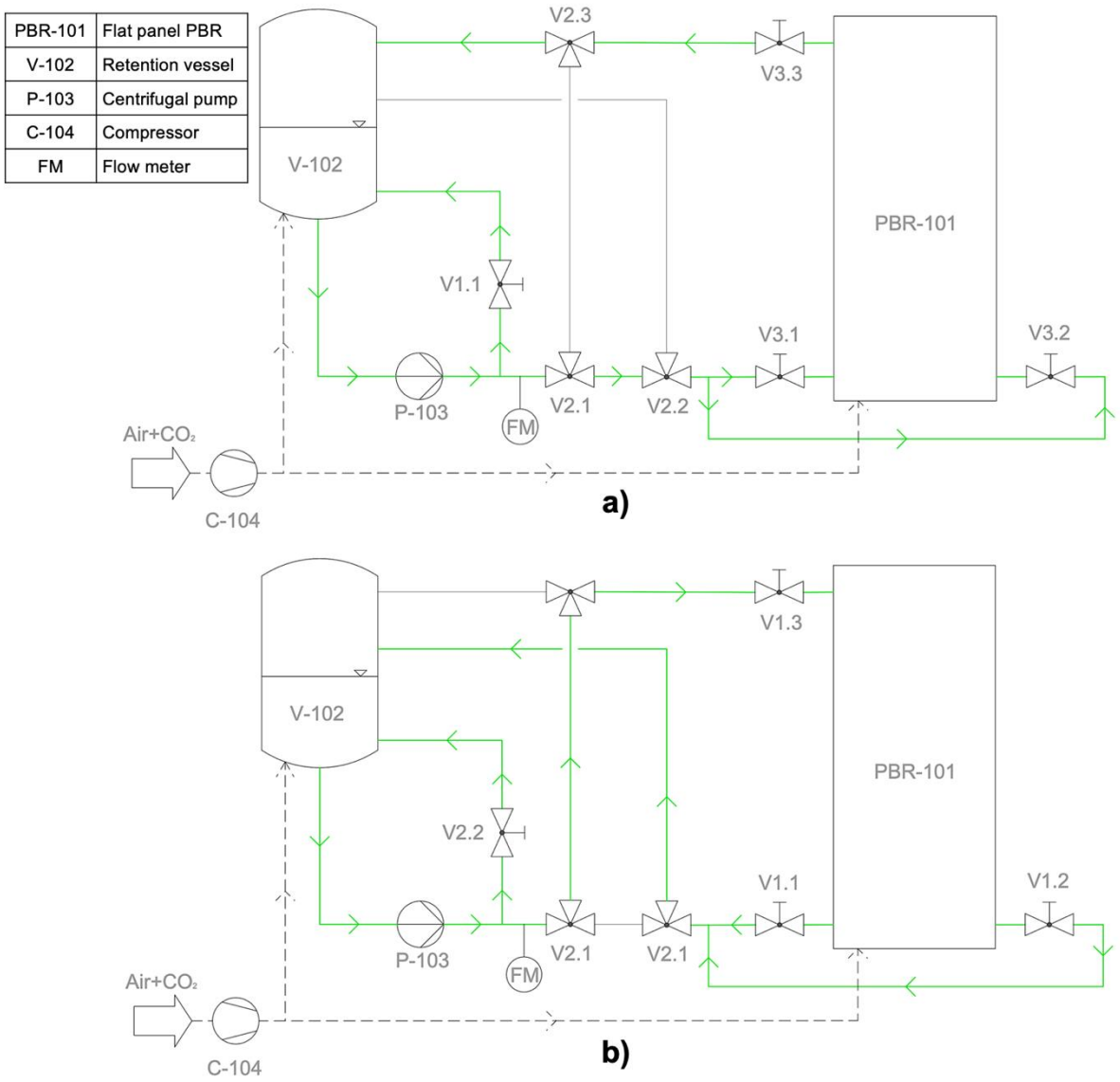

Fig. 7.1.3. Scheme of FP PBR system – a) bottom inlet configuration, b) top inlet configuration.

The FP PBR consists of two operating systems (Figure 7.1.3): retention vessel (V-102) and transparent PBR chamber (PBR-101). Nutrients are added to the culture medium from the retention vessel and the produced oxygen is desorbed in the retention vessel. The vessel is also equipped with a system for thermal regulation Lauda RE 104 (Lauda-Königshofen, Germany), and aeration of the culture medium. The total volume of the vessel is 100 L. However, the volume of the culture medium in the retention vessel is minimized to approximately 45 L during the cultivation process. The chamber is equipped with a system for air distribution C-104 (Aircraft Airstar 503/50, BOW Inc., Brno, Czech Republic). Retention vessel and FP PBR are connected by a centrifugal pump P-103 (Ebara CDXM/A 70/05, EBARA pumps S.p.A., Gambellara, Italy) ensuring the flow of culture medium. The system can be operated in several setting modes. The flow rate of the culture medium can be regulated by a valve placed in the outlet of the pump (V1.1) and controlled according to the electromagnetic

flowmeter FM (Krohne Optiflux 1050, KROHNE Messtechnik GmbH, Duisburg, Germany). Positions of inlets and outlets can be varied according to the setting of valves (V2.1, V2.2, and V.2.3), which are placed between the retention vessel and the FP PBR chamber. Two bottom necks (V3.1, V3.2) and one top neck (V3.3) were used for the measurement of hydrodynamic conditions in FP PBR. A pH and temperature probes Greisinger GMH3551 (GHM Messtechnik GmbH, Germany) are placed in the retention vessel and in the top and bottom part of the FP PBR chamber. In addition, an oximeter Greisinger GMH3651 (GHM Messtechnik GmbH, Germany) is installed in the top part of the chamber. The remaining parameters are monitored by taking samples and analyzing them in the laboratory.

Microalgae species *Chlorella vulgaris* was used for the cultivation with an initial inoculum concentration of 3 g L^{-1} and a volume of 4 L. The total volume of culture medium in the system was 120 L. Nutrients were added into the system prior to the inoculum injection. The composition and quantity of nutrients (Table 7.1.1) were selected according to Douskova et al. (2009).

Table 7.1.1. Quantity of nutrients in 4 L of the inoculum culture medium for microalgae cultivation.

Nutrients	Quantity (mg)
$(NH_2)_2CO$	66,000
KH_2PO_4	14,232
$MgSO_4 \cdot 7H_2O$	12,240
$C_{10}H_{12}O8N_2NaFe$	2,376
$CaCl_2$	5,280
H_3BO_3	50
$CuSO_4 \cdot 5\ H_2O$	57
$MnCl_2 \cdot 4H_2O$	198
$CoSO_4 \cdot 7H_2O$	37
$ZnSO_4 \cdot 7H_2O$	161
$(NH_4)_6Mo_7O_{24} \cdot 4H_2O$	10
$(NH_4)\ VO_3$	1

7.2 Calibration and validation of CFD model

7.2.1 Numerical model setup

Fluid dynamic model setup

The Reynolds number was used to determine whether the fluid was in a laminar or turbulent flow. From the analytical calculation of PBR operating conditions, it can be assumed that the flow regime was in the range of a low turbulent Reynolds number. Therefore, the Re-Normalization Group (RNG) k-ϵ model was used to simulate the fluid dynamics behavior in FP PBR (governing equations: Eq. (4.10) to Eq. (4.12)). However, calculations obtained using RNG methods should always be verified by experiments or at least by a qualitative comparison with literature results. The hydrodynamic conditions were numerically simulated with the software ANSYS FLUENT CFD 19.1.

Mesh generation and boundary conditions

The 3D mesh for the FP PBR CFD simulation was created in ANSYS. The geometry was created only for the FP PBR chamber with inlet and outlet neck. The grid contains approx. 2,110,674 elements with a 10 mm maximum size. The inflation function was applied in the area close to the wall of the model with a maximum size of 0.1 mm. Computations were performed until the calculation converged at a residue of 10^{-5} between two iterations. The mesh quality was checked using skewness reaching the value of 0.26. To simulate the hydrodynamic conditions in a 3D PBR model, the inlet was defined by the inlet velocity, and the same conditions were defined for the outlet as well. The inlet and outlet velocities were set according to the flow rate of the culture medium during the experimental measurements (chapter 7.2.2). The microalgal culture medium at low concentrations shows clearly Newtonian behavior with viscosity values close to that of water (Martínez-Sanz et al., 2020; Souliès et al., 2016). Properties and physical parameters were set in the model by considering the culture medium as water. The outer walls and the internal structures of the chamber were set to no-slip boundary conditions to water.

7.2.2 Model calibration and preliminary validation

The time of homogenization and flow in the FP PBR chamber was measured using a pulse-input tracer method (phenolphthalein reacted with sodium hydroxide). The tracer was applied to the retention vessel and consequently, the streamlines in the FP PBR chamber were visually monitored. At the same time, the homogenization time was measured when the tracer was completely dispersed. The homogenization time was then compared to the hydraulic retention time (HRT) in the FP PBR chamber.

The CFD model was created for three setting configurations of the inlet and outlet of the culture medium. Two configurations working based on the scheme with bottom inlets, which is shown in Figure 7.1.3a. The first configuration considers the inflow of the culture medium through the one bottom neck and the outflow through one top neck (Figure 7.2.2.1a). In the second configuration, the bottom inlet was divided into two opposite necks (Figure 7.2.2.1b). The scheme of the FP PBR system for the third configuration is shown in Figure 7.1.3b. For the third configuration, the valves were set so the inflow of medium is situated through the top inlet neck and the outflow through the two bottom outlet necks (Figure 7.2.2.1c).

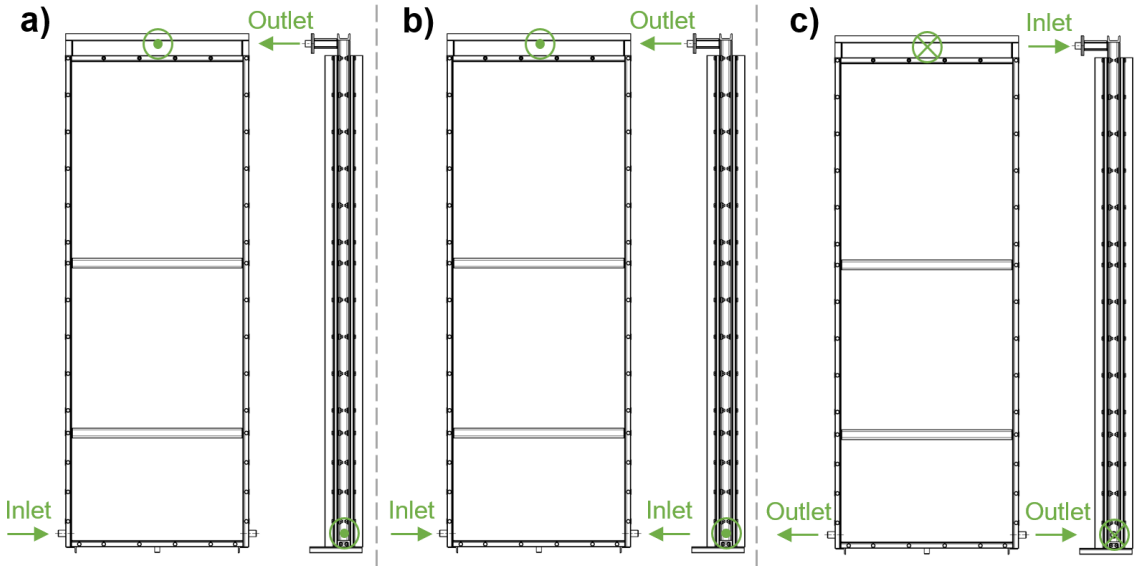

Fig. 7.2.2.1. Scheme of setting modes in FP PBR – a) single bottom inlet and top outlet, b) double bottom inlet and top outlet, c) top inlet and double bottom outlet.

An experiment with a flow rate of 45 L min^{-1} was created to calibrate the CFD model. The comparison of tracer measurement and trajectory contours for each setting mode is shown in Figure 7.2.2.2. The contours illustrate the movement of the culture medium in the FP PBR chamber.

Fig. 7.2.2.2. Calibration of CFD model. Comparison of tracer experimental measurement method (on the bottom) and numerical simulation of streamlines (on the top) – flow rate: 45 L min^{-1}. a) single bottom inlet and top outlet, b) double bottom inlet and top outlet, c) top inlet and double bottom outlet.

Validation of the developed CFD model is needed in order to determine its usability for the simulation of various conditions of FP PBR. The flow rate distribution of the culture medium was therefore compared to experimental measurements. In a real FP PBR, the streamlines were monitored for the flow rate of 63 L min^{-1} and subsequently compared to the CFD model (Figure 7.2.2.3). Based on the measurement, it can be determined that the measured and simulated streamlines were in good agreement and the CFD model can be used to simulate various operating conditions in FP PBR. In order to fully validate the model, it would be useful to compare the experimental and simulated RTD curves.

Fig. 7.2.2.3. Preliminary validation of CFD model. Comparison of tracer experimental measurement method (on the bottom) and numerical simulation of streamlines (on the top) – flow rate: 63 L min^{-1}. a) single bottom inlet and top outlet, b) double bottom inlet and top outlet, c) top inlet and double bottom outlet.

7.3 Hydrodynamic conditions in FP PBR

7.3.1 Velocity distribution and flow regime

The model of velocity distribution in the FP PBR chamber was developed to simulate three setting modes of inlet and outlet configurations (detailed in Figure 7.2.2.1). The velocity and trajectory contours for each setting mode are shown in Figure 7.3.1.1 corresponding to a flow rate of 45 L min^{-1}, and Figure 7.3.1.2 corresponding to a flow rate of 63 L min^{-1}, respectively. The contours illustrate the movement of the culture medium in the FP PBR chamber.

From the comparison of the culture medium velocity distribution in the FP PBR chamber, it is possible to observe different behavior for different operating modes. The configuration with single bottom inlet (Figure 7.3.1.1a, Figure 7.3.1.2a) reaches the highest flow velocities in the chamber. However, the flow in the chamber forms a circulation loop, which can result in the formation of dead zones in the central part of the chamber. In the case of the configuration with a double bottom inlet (Figure 7.3.1.1b, Figure 7.3.1.2b), the flow rate was still high. The inflows of the culture medium were directed against each other, which results in a mutual dispersion of the flow, which ensures a more uniform flow in the central part of the FP PBR chamber. In the case of the top inlet configuration (Figure 7.3.1.1c, Figure 7.3.1.2c), the culture medium in the chamber reaches the lowest velocities. However, the flow was the most uniform in the central part of the chamber.

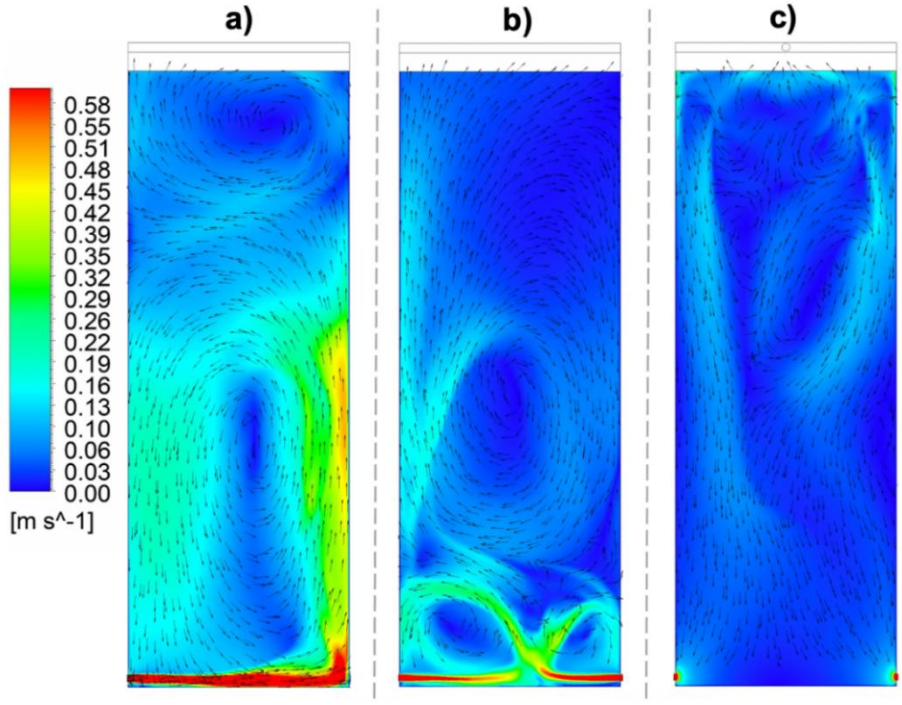

Fig. 7.3.1.1. Velocity distribution in FP PBR chamber – flow rate: 45 L min^{-1}. a) single bottom inlet and top outlet, b) double bottom inlet and top outlet, c) top inlet and double bottom outlet.

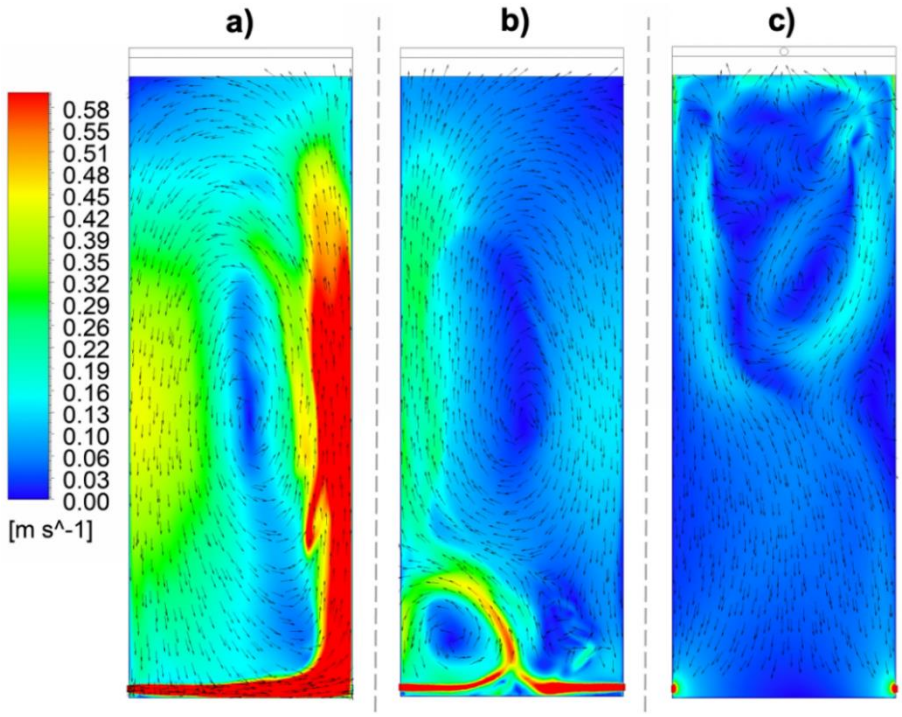

Fig. 7.3.1.2. Velocity distribution in FP PBR chamber – flow rate: 63 L min^{-1}. a) single bottom inlet and top outlet, b) double bottom inlet and top outlet, c) top inlet and double bottom outlet.

The time when the tracer was completely dispersed was also determined for each configuration. Table 7.3.1.1 shows the homogenization times and the hydraulic retention time (HRT) for each culture medium flow rate. The tracer measurements were triplicated for each setting mode and flow rate as well. From a comparison of the homogenization time and the HRT, it was evident that the homogenization time was significantly higher for the top inlet configuration than in the case of both bottom inlet configurations. Therefore, low intensity mixing occurs during the top inlet configuration. The single bottom inlet configuration achieves the highest velocities in the chamber; however, the homogenization time was comparable to HRT at a flow rate of 45 L min^{-1}, and even higher at a flow rate of 63 L min^{-1}. In the configuration with a double bottom inlet, the most intensive mixing occurs, since the homogenization time was lower than the HRT for both flow rates. From the comparison, the configurations with two bottom inlets seem to be the most suitable for further examination of hydrodynamic conditions.

Table 7.3.1.1. Homogenization time and HRT in FP PBR chamber.

Inflow	Homogenization time (s)			HRT (s)
(L min^{-1})	Top inlet	Single bottom inlet	Double bottom inlet	
45	143	97	78	97
63	126	75	64	69

The Reynolds number was used to determine whether the fluid was in a laminar or turbulent flow. In general, the Reynolds number is the ratio of inertial forces to viscous forces. To evaluate the rate of turbulence development in the PBR chamber, the local values of turbulent Reynolds number Re_t (-) distribution were generated for all operating modes (Figure 7.3.1.3). The Reynolds number Re (-) for the flow in a rectangular channel can be calculated

$$Re = \frac{d_h \cdot u \cdot \rho}{\mu} \tag{7.1}$$

where d_h (m) is the hydraulic diameter, u (m s^{-1}) is the mean flow velocity, ρ (kg m^{-3}) is the density, and μ (Pa s) is the dynamic viscosity. However, the local values of turbulent Reynolds number Re_t are defined

$$Re_t = \frac{b \cdot \rho \cdot \sqrt{k}}{\mu} \tag{7.2}$$

where k (m^2 s^{-2}) is the turbulent kinetic energy. The numerical model uses for the determination of Re_t the distance to the nearest wall b (m) instead of hydraulic dimension d_h (m) in Re for the flow in a rectangular channel. For flow rates of 45 and 63 L min^{-1}, the Re in a rectangular channel corresponds to values of 2,000 and 2,800, respectively. In a horizontal cross-section with a distance of 0.25 m from the bottom inlet, the mean value of Re_t is 1,420 and 2,250 for the flow rates of 45 and 63 L min^{-1}. Therefore, from the comparison of Re and Re_t in Figure 7.3.1.3, it is evident that the values are comparable.

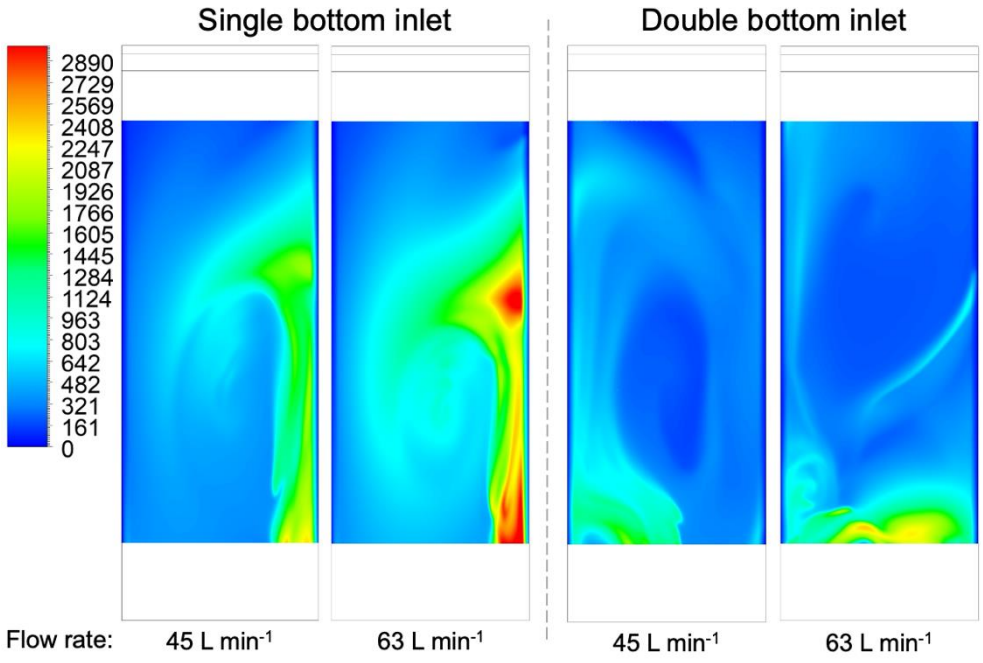

Fig. 7.3.1.3. Turbulent Reynolds number distribution in FP PBR chamber. Note that inflow and outflow zones are not plotted since the Re_t reaching orders of magnitude higher values then in the central zone.

7.3.2 Biofilm formation

Biofilm removal has an important role in closed cultivation systems. Biofilm is visible as a thin viscous layer of sediments, and its thickness can reach hundreds of micrometers (Figure 7.3.2.1). Biofilm formation reduces light intensity entering into the system (Zippel and Neu, 2005). Its presence also leads to the loss of cell pigmentation, contamination by microbes and bacteria, and encrustation of the PBR surface (Zeriouh et al., 2017). Since light irradiation is one of the crucial processing parameters for the growth of microalgae, the removal of biofilm on the transparent wall of the PBR is a very important step to ensure sufficient and effective performance of the process of cultivation (Cicci et al., 2014).

Fig. 7.3.2.1. Microalgae biofilm fixed in FP PBR chamber.

To avoid the formation of microalgae on the transparent walls of the closed cultivation systems, it is important to ensure acceptable hydrodynamic conditions. The effect of shear force on the wall, respectively, the wall shear stress τ_w (Pa s) can disrupt the stability of the microalgae biofilm. Therefore, it is important to define the critical value of the wall shear stress, which can prevent the formation of biofilm and therefore subsequently provide the efficient operation of the cultivation system. Based on a specified critical value, the operating conditions of a cultivation process can be adjusted to prevent biofilm formation.

The biofilm fixed on a transparent plate of FP PBR at a flow rate of 45 L min^{-1} is shown in Figure 7.3.2.2a. Microalgae formed a thin layer of biofilm on the transparent plates, which prevent the irradiation of the culture medium. However, the biofilm formation does not occur in locations with high flow velocities. A simulation of wall shear stress distribution on the transparent plates was developed for the same flow rate (Figure 7.3.2.2b). Based on the comparison that can be observed in Figure 7.3.2.2, the area where the biofilm was not formed can be determined by the model. The critical cross-sections were chosen in the defined area

of the PBR chamber in order to determine the critical shear stress value on the wall. According to the formed biofilm, cross-sections were selected in four vertical Y-axis distances from the bottom inlet of the FP PBR chamber: 0.25, 0.75, 1, and 1.5 m. Selected cross-sections are shown in Figure 7.3.2.2b. The distribution of wall shear stress along the horizontal X-axis is shown in Figure 7.3.2.2c.

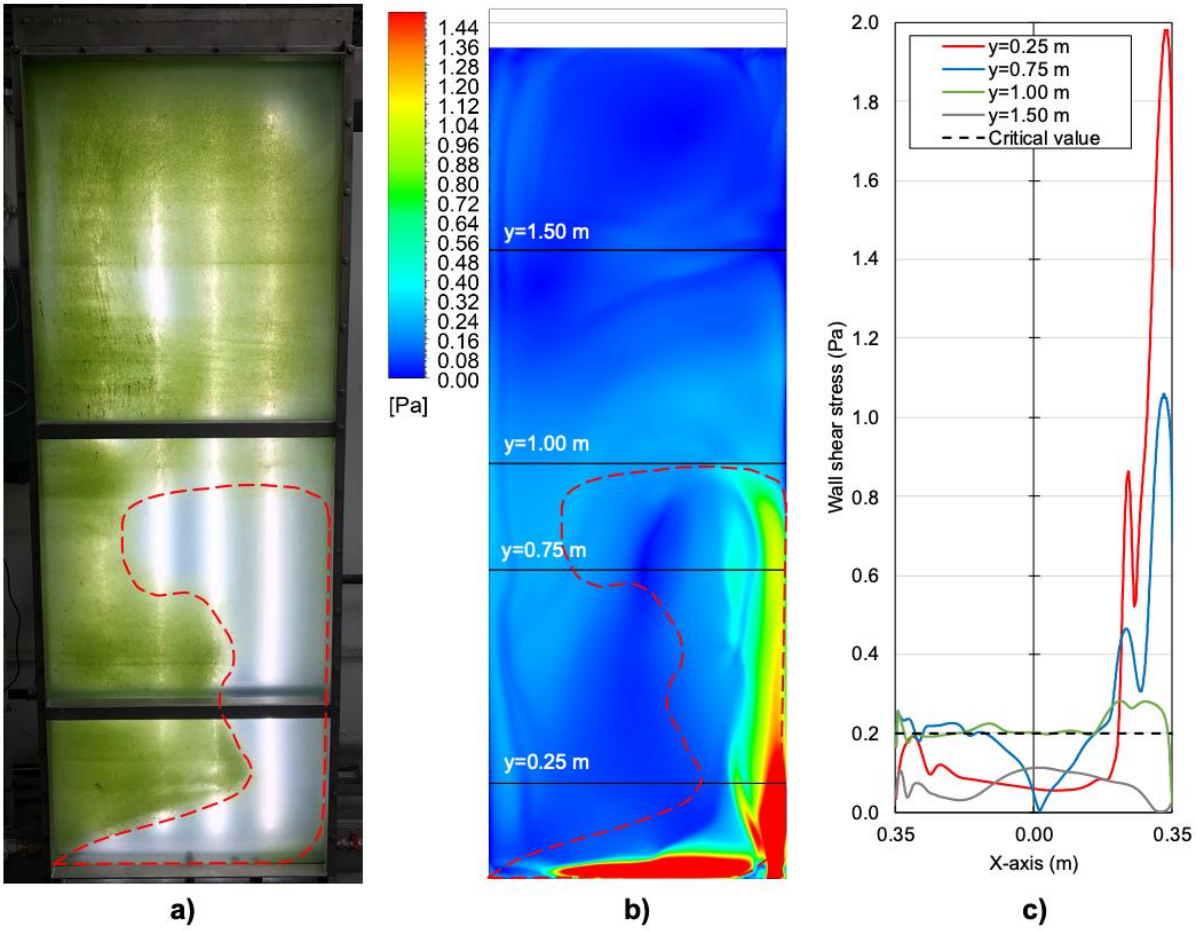

Fig. 7.3.2.2. Comparison of experimental microalgae biofilm formation and CFD simulation of wall shear stress distribution in FP PBR chamber, flow rate: 45 L min^{-1} – a) fixed biofilm on transparent plate, b) wall shear stress distribution, c) distribution of wall shear stress along the selected cross-sections.

According to the comparison of wall shear stress distribution on the transparent walls (Figure 7.3.2.2c) and the formed biofilm (Figure 7.3.2.2a), it is possible to determine the critical wall shear stress value. At wall shear stress values τ_w higher than 0.2 Pa, the biofilm formation does not occur. In order to avoid biofilm formation, it is necessary to minimize the locations in the FP PBR plates, where the shear stress value on the wall will be lower than the critical value. Using the developed CFD model, it is possible to predict the biofilm formation based on the different operating and design parameters. Using this method, the areas where the biofilm formation could potentially occur can be localized and subsequently eliminated. From the wall

shear stress distribution in Figure 7.3.2.2b, the area with wall shear stress below critical value accounts for 70 % of the total FP PBR transparent plate area.

7.3.3 Wall shear stress

Using the validated CFD model for the single bottom inlet configuration, the wall shear stress distribution was also created for the culture medium flow rate of 63 L min^{-1} (Figure 7.3.3.1). The wall shear stress distribution at 63 L min^{-1} is shown in Figure 7.3.3.1a and the cross-section shear stress distribution is shown in Figure 7.3.3.1b. It is evident that as the flow rate of the culture medium increases, the shear stress value approaches the critical value τ_w of 0.2 Pa. However, the velocity distribution in Figure 7.3.3.1b showed that the culture medium forms a circulation loop in the FP PBR chamber. Thus, the biofilm formation can be eliminated in specified cross-sections, but the dead zones can form directly in the center of the circulation loop.

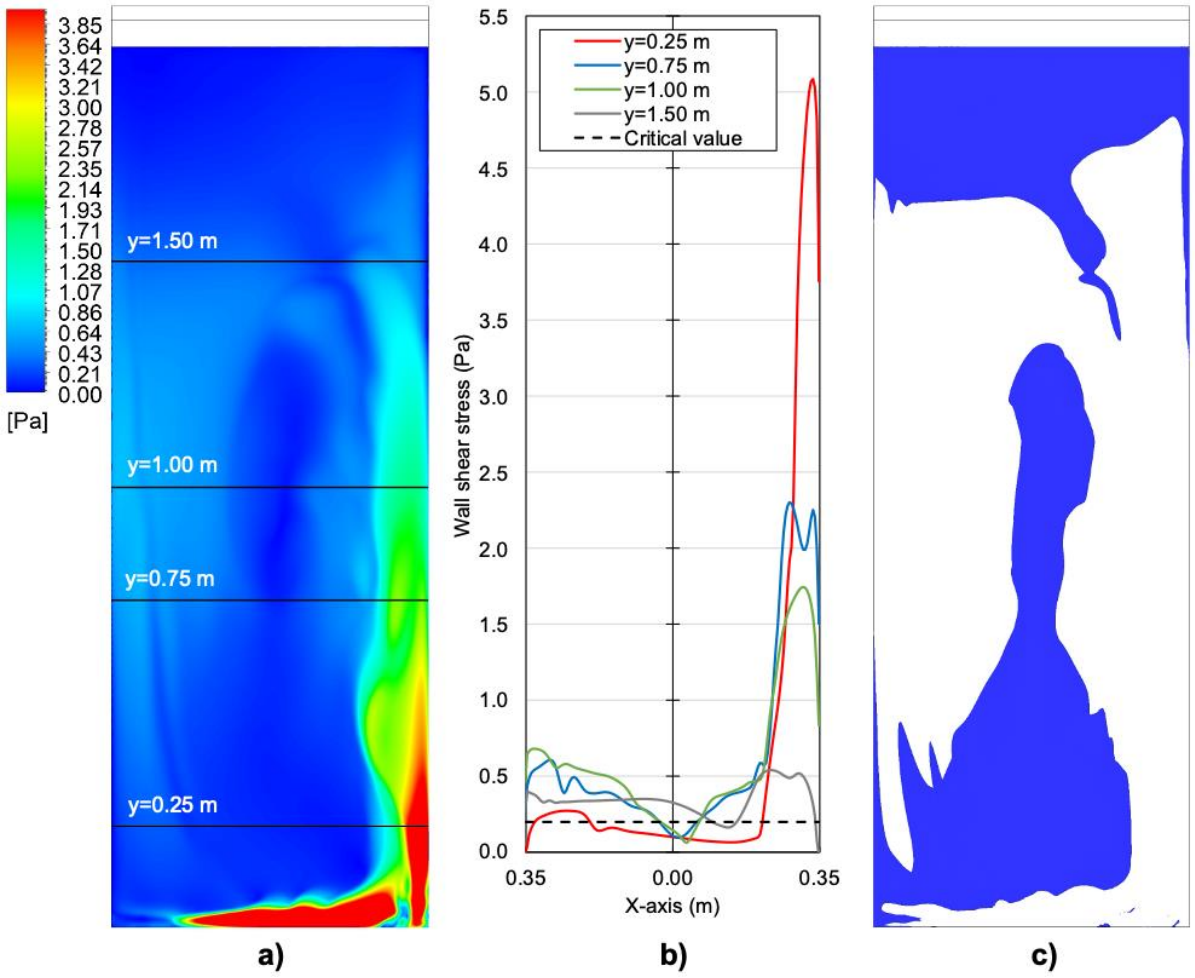

Fig. 7.3.3.1. Wall shear stress distribution in FP PBR chamber with single bottom inflow, flow rate: 63 L min^{-1} – a) wall shear stress distribution, b) distribution of wall shear stress along the selected cross-sections, c) wall shear stress below the critical wall shear stress value of 0.2 Pa (in blue).

The shear stress distribution below the critical value is shown in Figure 7.3.3.1c. The comparison demonstrates the development of wall shear stress on the transparent wall of PBR according to the increasing culture medium flow rate. At a flow rate of 45 L min^{-1}, the shear stress below the critical value of 0.2 Pa formed 70 % of the total transparent area of the FP PBR wall. This ratio was also confirmed by experimental measurement, which can be seen in Figure 7.3.2.2a. By increasing the flow rate to 63 L min^{-1}, the area was reduced to 33 %. However, at the top of the PBR chamber, the wall shear stress was still below the critical value. Also, the circulating loop begins to form in the central part of the chamber. This loop causes non-intensive mixing of culture medium at the center of the FP PBR chamber and wall shear stress on the wall was low as well. Therefore, another operating or design settings of the cultivation system need to be applied in order to eliminate this area.

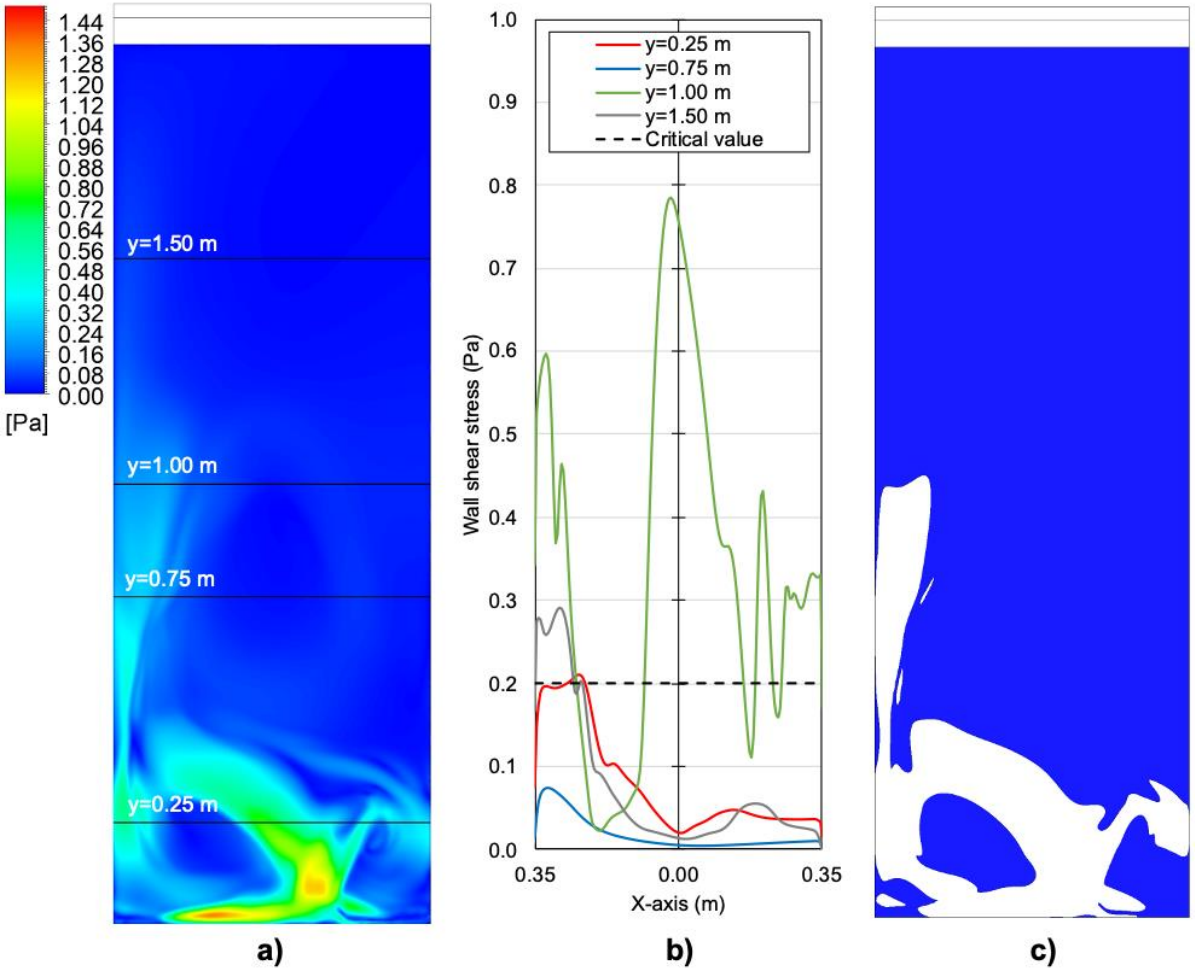

Fig. 7.3.3.2. Wall shear stress distribution in FP PBR chamber with double bottom inflow, flow rate: 45 L min^{-1} – a) wall shear stress distribution, b) distribution of wall shear stress along the selected cross-sections, c) wall shear stress below the critical wall shear stress value of 0.2 Pa (in blue).

The simulation of wall shear stress was also created for the double bottom inlet configuration. The shear stress distribution on the wall for a flow rate of 45 L min^{-1} is shown in Figure 7.3.3.2.

Due to the mutual dispersion of the inflow streams, the circulation loop in the central part of the chamber was partially eliminated. Due to lower flow velocities compared to the configuration with a single bottom inlet, the values of shear stress on the wall do not reach such high values (Figure 7.3.3.2a and Figure 7.3.3.2b). At a flow rate of 45 L min^{-1}, the shear stress below the critical value of 0.2 Pa was present in 86 % of the total transparent area of the FP PBR wall.

The wall shear stress distribution for a flow rate of 63 L min^{-1} and double bottom inflow is shown in Figure 7.3.3.3. At a flow rate of 63 L min^{-1}, the shear stress below the critical value of 0.2 Pa forms 82 % of the total transparent area of the FP PBR wall. Thus, increasing the flow rate in a double bottom inlet configuration did not cause a significant increase in shear stress on the wall. The decrease in the area with shear stress lower than the critical value (from 86 % to 82 %) was significantly lower than in the case of a single bottom inlet configuration (from 70 % to 33 %).

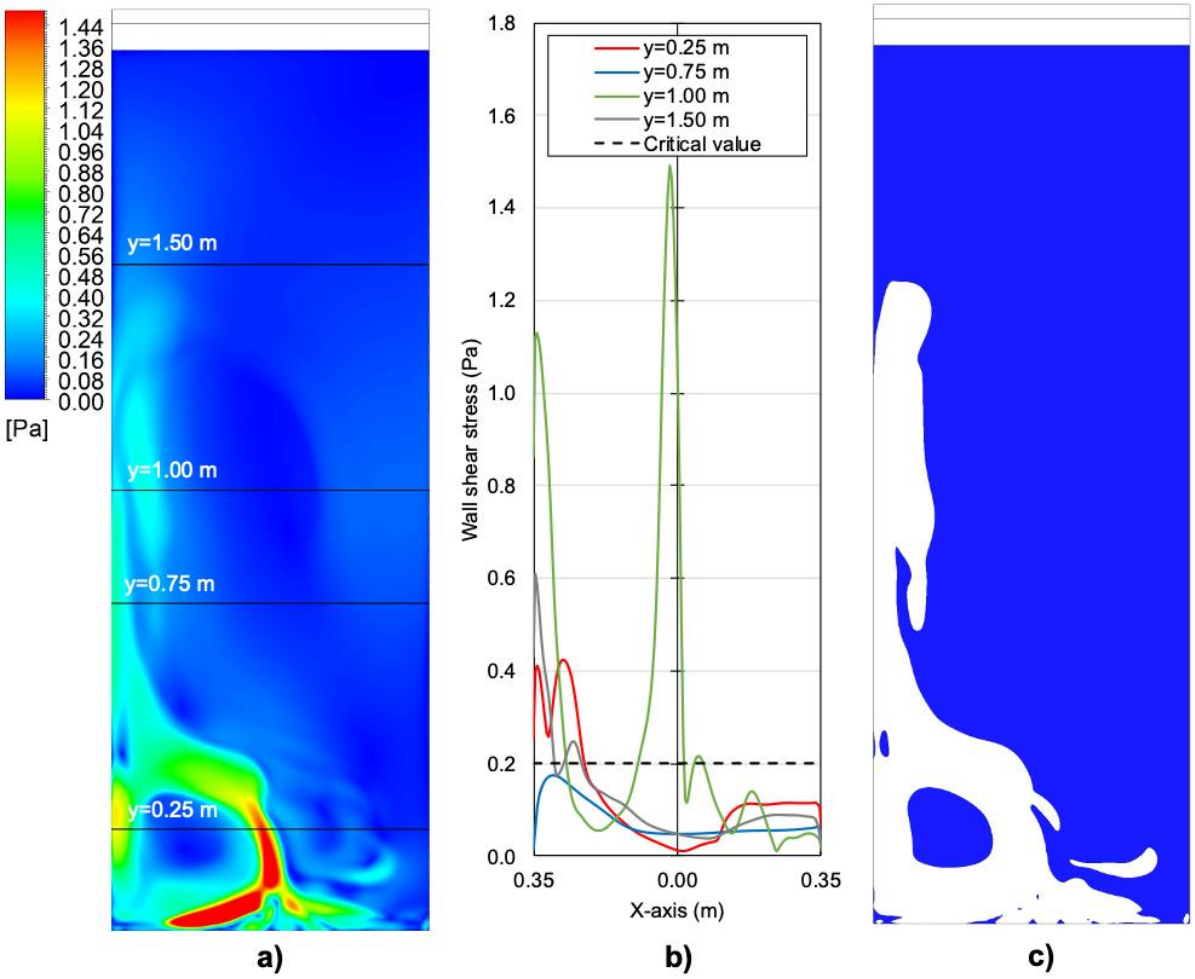

Fig. 7.3.3.3. Wall shear stress distribution in FP PBR chamber with double bottom inflow, flow rate: 63 L min^{-1} – a) wall shear stress distribution, b) distribution of wall shear stress along the selected cross-sections, c) wall shear stress below the critical wall shear stress value of 0.2 Pa (in blue).

7.3.4 Conclusions

The homogenization time was significantly higher for the top inlet configuration (143 and 126 s for 45 and 63 L min^{-1} inflow) than in the case of both bottom inlet configurations. The single bottom inlet configuration achieves the highest velocities in the chamber; however, the homogenization time (97 and 75 s) was comparable to HRT at a flow rate of 45 L min^{-1} (97 s), and even higher at a flow rate of 63 L min^{-1} (69 s). In the configuration with a double bottom inlet, the most intensive mixing occurs since the homogenization time (78 and 64 s) was lower than the HRT for both flow rates (97 and 69 s). From the comparison, the configurations with bottom inlets seem to be the most suitable for microalgae cultivation.

The biofilm formation was monitored on transparent FP PBR plates during microalgae cultivation. Using the validated CFD model, the wall shear stress distribution was created, and consequently, the critical wall shear stress value preventing biofilm formation was defined. The critical wall shear stress value was 0.2 Pa. The model of wall shear stress distribution was developed for the selected flow rates of the culture medium. It is possible to reduce the area with the wall shear stress below the critical value by increasing the flow rates of the culture medium in the system. At a flow rate of 45 L min^{-1}, the area with the wall shear stress below critical value forms 70 % and 86 % of the total transparent area of FP PBR for single and double bottom inlet, respectively. At a flow rate of 63 L min^{-1}, the area was reduced to 33 % in single bottom inlet configuration, and 82 % in double bottom inlet configuration. According to the results, a configuration with a single bottom inlet seems to be more suitable for the separation of fixed biofilm on transparent walls of the FP PBR.

However, as the flow rate in the configuration with a single bottom inlet increases, a circulation loop was formed in the FP PBR chamber. The circulation loop forms dead zones in the center of the chamber, which can subsequently form the biofilm. Due to the mutual dispersion of the inflow streams in the double bottom inlet configuration, the circulation loop in the central part of the chamber was partially eliminated. However, due to lower flow velocities compared to the configuration with a single bottom inlet, the values of shear stress on the wall do not reach such high values. It is possible to reduce the formation of dead zones by design modification of the chamber, position modification of inlet and outlet, or by installing a static mixer in the FP PBR chamber. The validated hydrodynamic model can be used to study the velocity and shear stress distribution in the FP PBR. It is possible to specify the proportion of the area on which the biofilm will be formed for the selected values of the critical wall shear stress. According to the time-averaged flow values of the RANS CFD model, it is necessary to consider the possible deviation of the wall shear stress critical value. Therefore, to compare the hydrodynamic conditions in the FP PBR, further refinement of the critical wall shear stress value was reported in Belohlav et al., (2020).

8

Homogenization and mixing of flow in flat panel PBR

This chapter is based on the article:

Belohlav, V., Jirout, T., Kratky, L. (2021). Optimization of hydrodynamics by installation of static mixer in flat panel photobioreactor. *Chemical Engineering Transactions*, 86, 139-144.

A utility model (U1 34 865 CZ) was registered for the developed design of the static mixer. An application for a European patent was submitted.

By changing the configuration of the inlet and outlet of the FP PBR chamber, it is possible to significantly influence the hydrodynamic conditions. In the previous chapter, it was described that in the bottom inlet configurations, the most intensive mixing occurs. Intensification of mixing affects the shear forces on the transparent walls that can eliminate the formation of biofilm. However, the disadvantage here remains due to the inhomogeneity of the flow along the FP PBR chamber and the different residence times of the culture medium in the irradiated area. The aim of this work was to design a static mixer that could be installed in the FP PBR chamber. The static mixer should ensure the distribution of the medium flow throughout the cross-section of the chamber, ensure homogenous residence time of the culture medium in the irradiated area, and further intensify the mixing of the culture medium. Moreover, microalgae cells should not be fixed on the walls of the static mixer, which could cause the contamination of the cells in the culture medium. The design of the static mixer should be adapted to the requirements of 3D printing technology. In the following chapter, the numerical model simulating hydrodynamic conditions in FP PBR with a static mixer was described. The applicability of the numerical model was calibrated and validated based on the experimental tracer tracking method.

8.1 Static mixer

The aim of the static mixer design was to intensify the mixing and to homogenize the flow of the culture medium. The design of the static mixer was inspired by the geometry of conventional Sulzer SMX and SMV static mixers, which can be installed in tubes of circular cross-section. SMX and SMV static mixers are applicable for low turbulence flow regimes and gas-liquid mixtures. These static mixers are applicable over a wide range of operating parameters (Paul et al., 2004). The geometry of the static mixer has been designed in order to divide the inflow stream of the medium into several individual streams that will mix with each other. The geometry was further adapted to create flooding behind the blades of the static mixer. The formation of floods behind the blades should result in the formation of eddies and the mixing of the processed medium. The static mixer consists of a pair of blades. The blades perpendicular to the transparent walls of the FP PBR direct the flow of the culture medium to the side of the PBR chamber. By changing the flow direction, the stream of the culture medium can be mixed by the stream directed by the blade inclined to the transparent walls of FP PBR. Reduction of flow cross-section should result in a local increase in flow rate velocity. The concept of a static mixer was designed according to the principle of 3D printing technology. The entire static mixer consists of seven segments, which were placed along the width of the FP PBR chamber. The dimensional scheme and 3D model of one static mixer segment are shown in Figure 8.1.1. The geometry and application of the static mixer is protected as a utility

model (U1 34 865 CZ, registered Feb 23, 2021) and an application for a European patent was submitted as well.

The segments of the static mixer were placed in the FP FPB chamber and glued with silicone to the transparent wall of the FP PBR. The static mixer was located at a distance of 0.46 m from the bottom inlets. The printed segment of the static mixer and the complete static mixer in the FP PBR chamber is shown in Figure 8.1.2. and Figure 8.1.3.

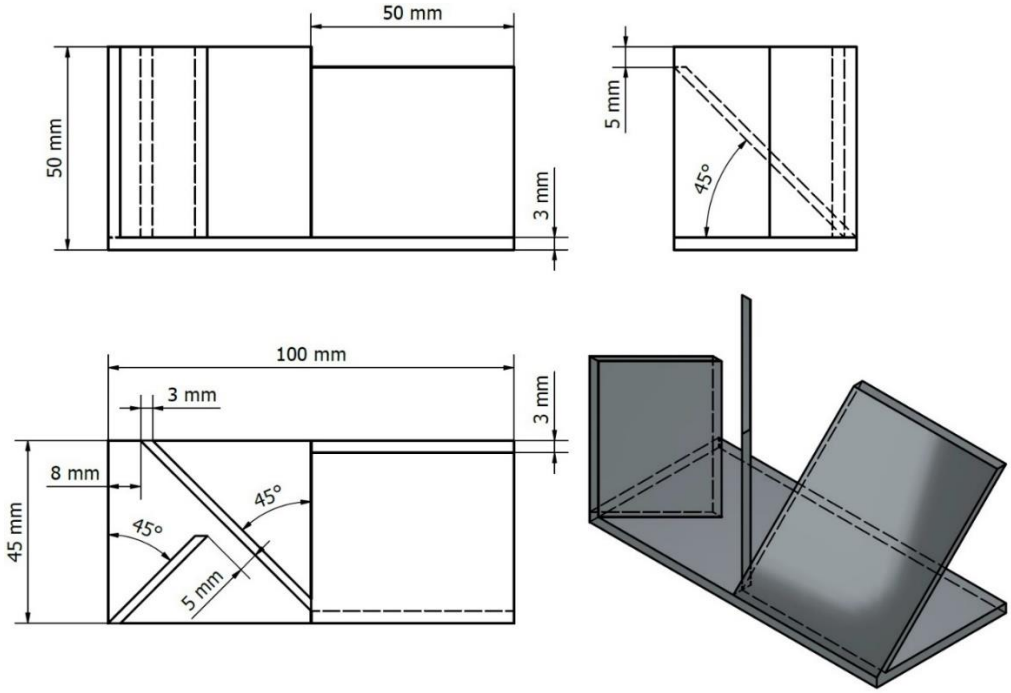

Fig. 8.1.1. Dimensional scheme and 3D model of static mixer element.

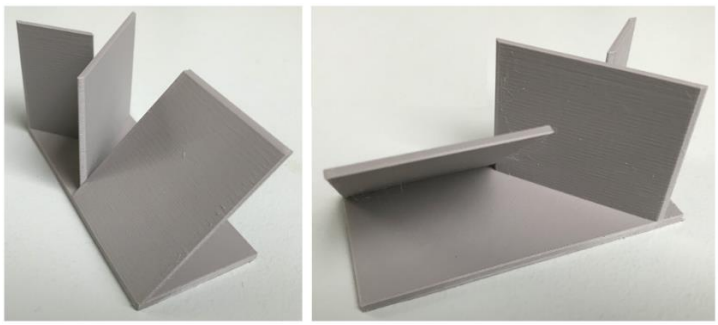

Fig. 8.1.2. 3D printed static mixer element.

Fig. 8.1.3. Static mixer in FP PBR chamber.

8.2 Calibration and validation of CFD model

8.2.1 Numerical model setup

The geometry of the chamber with the static mixer mostly corresponds to the model for the empty chamber, which was described in chapter 7.2.1. The geometry and mesh were created in the ANSYS system. The structure of the mesh in the inlet and outlet part of the chamber corresponds to the empty chamber. In the part of the static mixer, the mesh was refined in order to simulate the flow in this area. The total mesh contains 6,676,576 elements with a 2 mm maximum size. The inflation function was applied in the area close to the wall of the model with a maximum size of 0.1 mm. Computations were performed until the calculation converged at a residue of 10^{-5} between two iterations. The mesh quality was checked using skewness reaching the value of 0.23. The RNG k-ϵ model was used for the simulation. To simulate the hydrodynamic conditions in the FP PBR model, the inlet was defined by the inlet velocity, and the same conditions were defined for the outlet as well. The flow velocities in the inlet and outlet were selected comparable to the flow simulation in an empty chamber. Specifically, the inlet and outlet velocities were set according to the flow rate of the culture medium during the experimental measurements (chapter 7.2.2). Properties and physical parameters were set in the model by considering the culture medium as water. The outer walls and the internal structures of the chamber were set to no-slip boundary conditions to water.

In order to be able to study in detail the influence of the static mixer on the hydrodynamic conditions in the FP PBR chamber, a special model with a uniform inflow to the static mixer was created. The inlet was created at a sufficient distance in front of the static mixer so that the medium flow was fully developed. A second static mixer was also added to the model. The geometry of the static mixer blades perpendicular to the transparent walls of the FP PBR was inverted relative to each other in two serially installed static mixers (Figure 8.3.4.1). According to this, it is possible to observe the effect on the stabilization of the flow in the chamber. The distance between the two static mixers was 200 mm. The section behind the second static mixer was designed so that the hydrodynamic conditions behind the static mixer could be observed. The inlet was defined by the inlet velocities that were derived for the selected medium flow rates. In order to be able to consider a uniform inflow of medium to the static mixer, a rectangular cross-section was chosen as the inlet. The selected medium flow rates of 45 L min^{-1} and 63 L min^{-1} thus correspond to an inlet mean velocity of 0.02 m s^{-1} and 0.03 m s^{-1}. The same velocity was used for the outlet in the outlet rectangular cross-section. The grid of the mesh for the set of two static mixers in the chamber contains 2,817,622 elements with a 2 mm maximum size. The inflation function was applied in the area close to the wall of the model with a maximum size of 0.1 mm. Computations were performed until the

calculation converged at a residue of 10^{-5} between two iterations. The mesh quality was checked using skewness reaching the value of 0.22.

8.2.2 Model calibration and preliminary validation

The homogenization time and flow in the FP PBR chamber with a static mixer were measured using the same pulse input tracer method as for the measurement with an empty FP PBR chamber (chapter 7.2.2). The tracer was applied to the retention vessel and consequently, the streamlines in the FP PBR chamber were monitored. At the same time, the homogenization time was measured when the tracer was completely dispersed. The homogenization time was then compared to the HRT in the FP PBR chamber.

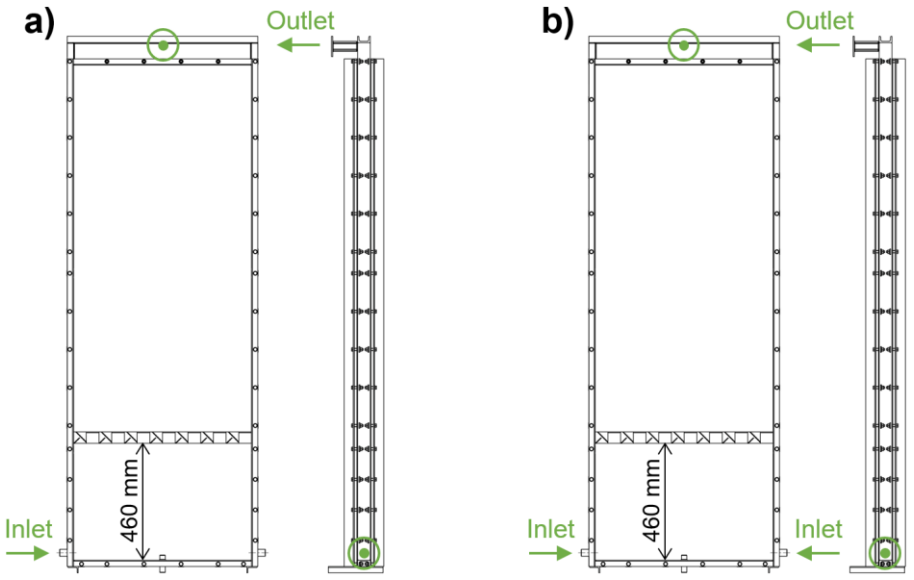

Fig. 8.2.2.1. Scheme of setting modes in FP PBR with static mixer – a) single bottom inlet and top outlet, b) double bottom inlet and top outlet.

The CFD model was created for two setting configurations with bottom inlets, which work based on the scheme shown in Figure 7.1.3a. The first configuration considers the inflow of the culture medium through the one bottom neck and the outflow through one top neck (Figure 8.2.2.1a). In the second configuration, the bottom inlet was divided into two opposite necks (Figure 8.2.2.1b). A model for a flow rate of 45 L min^{-1} was created to calibrate the CFD model. The comparison of tracer measurement and trajectory contours for each setting mode are shown in Figure 8.2.2.2. The contours illustrate the movement of the culture medium in the FP PBR chamber with the static mixer. Validation of the developed CFD model is needed in order to determine its usability for the simulation of various conditions of FP PBR with the static mixer. The flow rate distribution of the culture medium was therefore compared to experimental measurements. The streamlines were monitored for the flow rate of 63 L min^{-1} and subsequently compared to the CFD model (Figure 8.2.2.3). Based on the measurement, it can be determined that the measured and simulated streamlines were in good agreement and the

CFD model can be used to simulate various operating conditions in FP PBR with an installed static mixer. In order to fully validate the model, it would be useful to compare the experimental and simulated RTD curves.

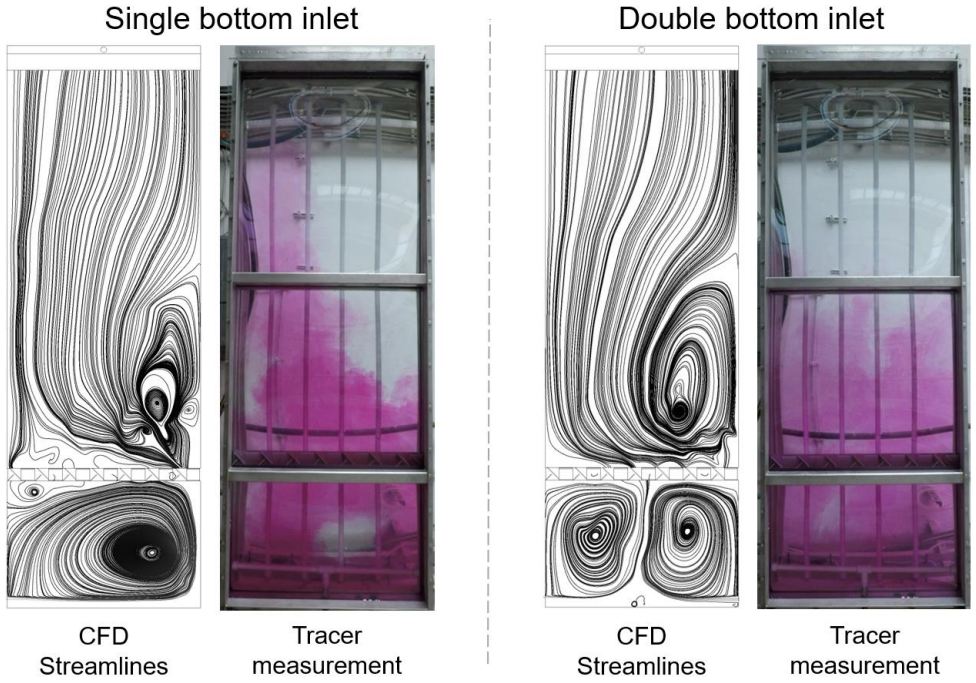

Fig. 8.2.2.2. Calibration of CFD model of FP PBR chamber with static mixer. Comparison of numerical simulation of streamlines and tracer experimental measurement method (27 s from tracer entering the chamber) – flow rate: 45 L min^{-1}.

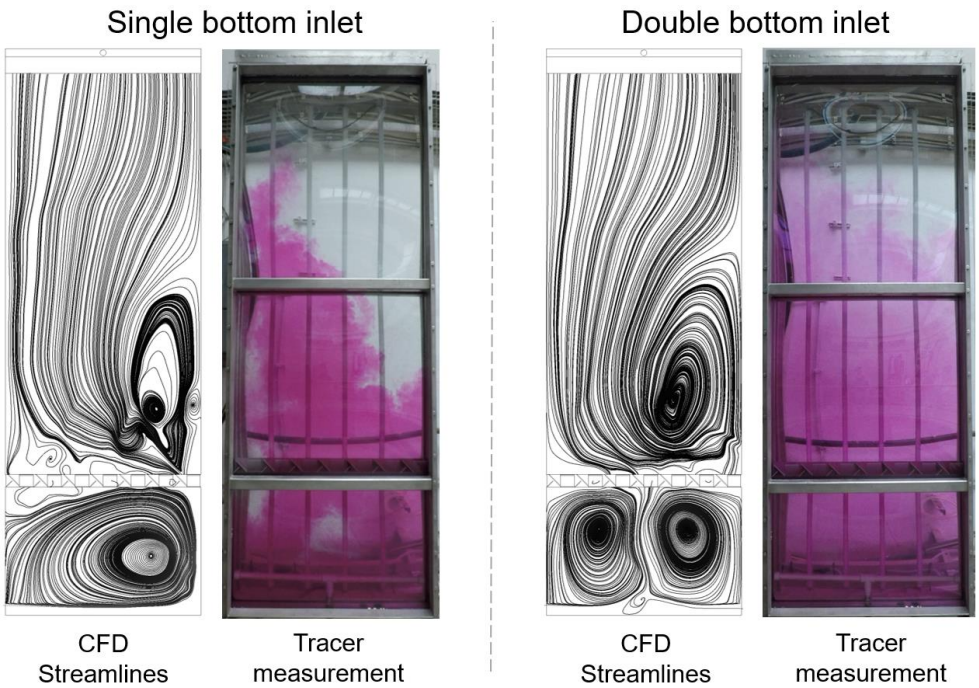

Fig. 8.2.2.3. Preliminary validation of CFD model of FP PBR chamber with static mixer. Comparison of numerical simulation of streamlines and tracer experimental measurement method (18 s from tracer entering the chamber) – flow rate: 63 L min^{-1}.

8.3 Hydrodynamic conditions in FP PBR with static mixer

8.3.1 Velocity distribution and flow regime

The model of velocity distribution in the FP PBR chamber with the static mixer was developed to simulate two setting modes according to different inlet configurations. The velocity and trajectory contours for each setting mode are shown in Figure 8.3.1.1. The contours illustrate the movement of the culture medium in the FP PBR chamber.

The single bottom inlet configuration (Figure 8.3.1.1) creates a circulation loop in the lower part of the chamber below the static mixer, which prevents the medium from flowing homogeneously through the segments of the static mixer. On the left side of the static mixer, there was a minimum flow of medium and, conversely, most of the medium was directed to the right side of the mixer. This causes a local increase in flow rate on the right side of the static mixer. Due to the inflow located on one side of the static mixer, a circulation loop was formed in the upper part of the FP PBR chamber as well as in the bottom part. The medium stream was then returned to the static mixer on the right side of the chamber. A dead zone was formed on the right side of the chamber above the static mixer, where the mixing intensity was very low. The formation of dead zones was also noticeable from experimental measurements (Figure 8.2.2.2 and Figure 8.2.2.3 for single bottom inlet configuration). At a flow rate of 45 L min^{-1}, the majority of the medium above the static mixer flows on the left side of the chamber. As the flow rate increases to 63 L min^{-1}, more intensive mixing above the static mixer occurs, which results in a partial disturbance of the dead zone. However, the flow was not homogeneous in the cross-section of the FP PBR chamber and the residence time of the culture medium in the chamber was unstable.

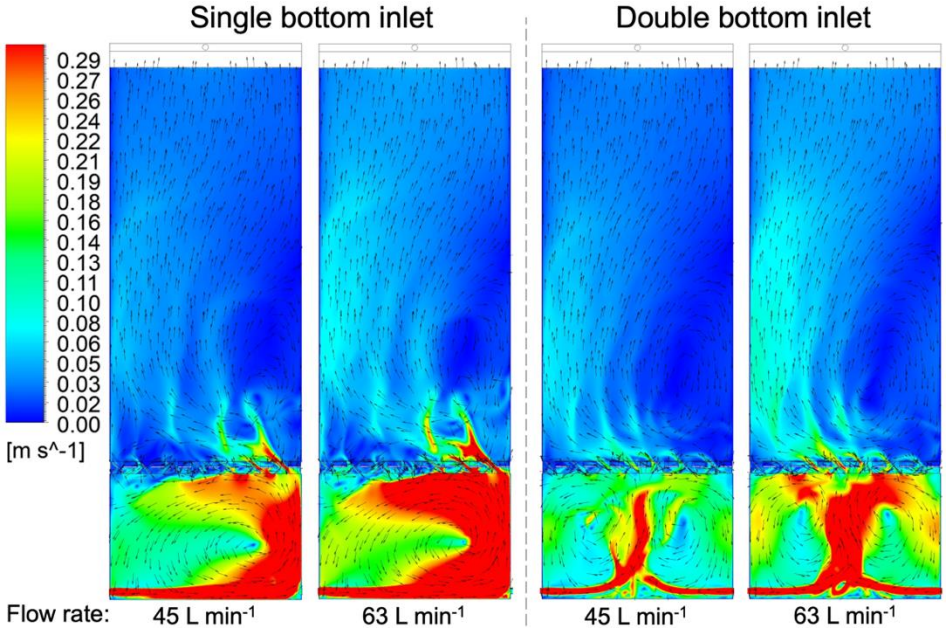

Fig. 8.3.1.1. Velocity distribution in FP PBR chamber with static mixer.

The double bottom inlet configuration ensures a more uniform flow of medium to the center of the static mixer. The flow above the static mixer was significantly more stable and homogeneous. The flow distribution for the double bottom inlet in Figure 8.2.2.2 and Figure 8.2.2.3 shows a significantly more homogeneous flow distribution in the FP PBR chamber compared to the single bottom inlet configuration. In Figure 8.3.1.1 it can be observed that also in the case of the double bottom inlet configuration, the medium reaches higher velocities in the left part of the chamber. However, the formation of dead zones in the right part of the chamber was not so noticeable in comparison with the single bottom inlet configuration. The flow in the left part was caused by the inclination of the blades of the static mixer, which are perpendicular to the transparent surface of the FP PBR (Figure 8.1.2 and Figure 8.1.3). When the medium flows out of the static mixer, the flow was directed to the left side of the chamber. By installing another static mixer with the inverted rotation of the blades, it would be possible to eliminate the flow on the side of the chamber and further intensify the process of mixing the culture medium. Compared to an empty chamber of FP PBR, the use of a static mixer generally stabilizes the flow in the PBR chamber, which was more homogeneous throughout its cross-section. Moreover, as the flow rate increases, no circulation loop was formed in the center of the chamber.

The time when the tracer was completely dispersed was also determined. Table 8.3.1.1 and Table 8.3.1.2 show the homogenization times and the HRT for each culture medium flow rate and for the configurations with and without the static mixer. All tracer measurements were triplicated.

Table 8.3.1.1. Single bottom inlet configuration - comparison of homogenization time and HRT in empty FP PBR chamber and FP PBR chamber with static mixer.

Inflow (L min^{-1})	HRT (s)	FP PBR chamber	Homogenization time (s)
45	97	Empty	97
		Static mixer	113
63	69	Empty	75
		Static mixer	78

At a flow rate of 45 L min^{-1} and 63 L min^{-1}, the homogenization time in configuration with static mixer was 16 s and 3 s longer than in the configuration with an empty chamber. From Figure 8.3.1.1, it can be observed that the uneven inflow to the static mixer has the greatest effect on homogenization. The most intensive mixing occurs in the part of the chamber below the static mixer, where a circulation loop was formed. Part of the flowing medium passes through the right side of the static mixer into the upper part of the chamber. However, due to the uneven inflow to the static mixer, dead zones were formed in the right part of the chamber,

where the mixing intensity was very low. At a flow rate of 63 L min^{-1}, the dead zones still remain in the right part of the chamber above the static mixer, which prolongs the homogenization time. However, the difference in homogenization time was reduced by 3 s compared to the configuration with FP PBR empty chamber, where the dead zones were formed in the central part of the chamber (Figure 7.3.3.1).

Table 8.3.1.2. Double bottom inlet configuration - comparison of homogenization time and HRT in empty FP PBR chamber and FP PBR chamber with static mixer.

Inflow (L min^{-1})	HRT (s)	FP PBR chamber	Homogenization time (s)
45	97	Empty	78
		Static mixer	65
63	69	Empty	64
		Static mixer	42

However, for the double bottom inlet configuration, there was a significant change when comparing an empty chamber and a chamber with a static mixer. Using the static mixer, the homogenization time was reduced by 13 s and 22 s at a flow rate of 45 L min^{-1} and 63 L min^{-1}, respectively. Thanks to a more homogenous inlet to the static mixer, the culture medium was mixed and the flow behind the static mixer was stabilized (Figure 8.3.1.1). The medium flow was significantly more homogeneous in the cross-section of the entire chamber than in the variant without a static mixer. From the velocity profile in the empty FP PBR chamber (Figure 7.3.1.1 and Figure 7.3.1.2), it can be seen that without the static mixer, the flow velocity varies on the sides of the chamber and the dead zones were formed in the central part. From the point of view of flow uniformity, the use of a static mixer in the case of a double bottom inlet configuration was clearly more suitable, reducing significantly the homogenization time in the FP PBR chamber. By comparing the distribution of the turbulent Reynolds number Re_t in the empty chamber (Figure 7.3.1.3) and the chamber with the static mixer (Figure 8.3.1.2), it can be seen that higher Re_t values can be achieved locally in the empty chamber. This was influenced by a better flow distribution over the entire cross-section of the FP PBR chamber with the static mixer.

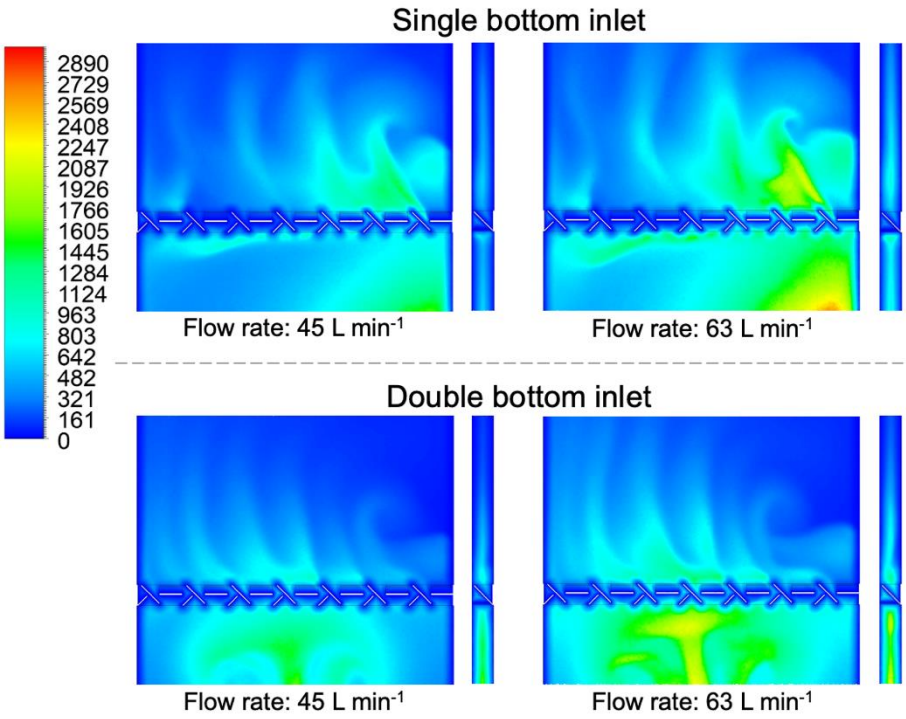

Fig. 8.3.1.2. Turbulent Reynolds number distribution in FP PBR chamber with static mixer. Front view and side view on the static mixer area.

To compare the average value of Re_t in the entire cross-section of the rectangular chamber, the cross-section in the middle of the height of the FP PBR chamber was selected. This height corresponds to a distance of 1 m from the lower part of the FP PBR chamber. From the Re_t distribution for the single bottom inlet configuration, a significant difference can be observed between the empty chamber and the chamber with the static mixer (Figure 8.3.1.3).

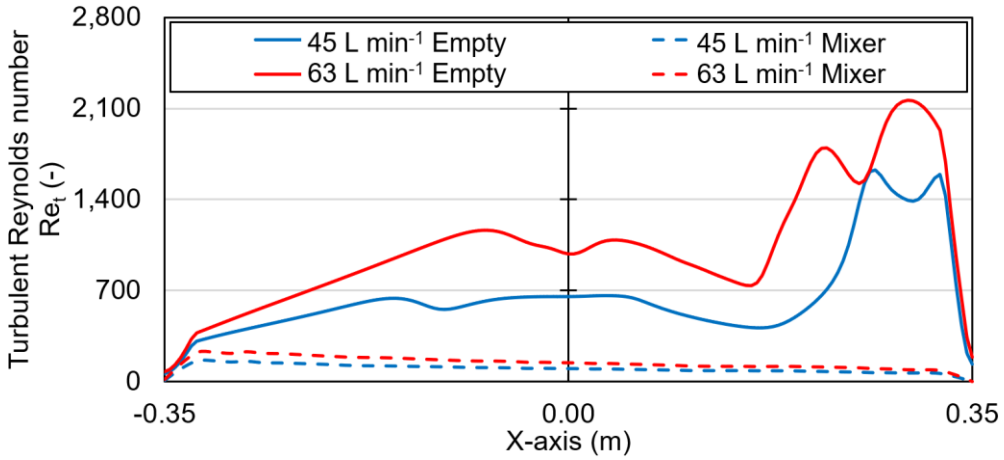

Fig. 8.3.1.3. Configuration with single bottom inlet - turbulent Reynolds number distribution along the X-axis in a distance of 1 m from bottom of FP PBR chamber.

From the curve of distribution along the X-axis, it can be observed that in the chamber with the static mixer, the flow was significantly more stable and homogenous over the entire width of the FP PBR chamber. The average Re_t values at the flow rate of 45 L min^{-1} and 63 L min^{-1}

reach only 98 and 143, respectively. In the empty chamber, the Re_t values reach 652 at a flow rate of 45 L min^{-1} and 1040 at a flow rate of 63 L min^{-1}.

In general, in the double bottom inlet configuration, lower values were achieved at a distance of 1 m from the bottom of the FP PBR chamber compared to the single bottom inlet configuration. However, due to the more stable flow in the chamber, it is also possible to observe a more stable distribution of Re_t in the cross-section of the chamber (Figure 8.3.1.4). In the double bottom inlet configuration, the Re_t values for the empty chamber and for the chamber with the static mixer were more balanced. The Re_t average values in the empty chamber at a flow rate of 45 L min^{-1} and 63 L min^{-1} reach the values of 294 and 259, respectively. When using a static mixer in the FP PBR chamber, the Re_t values reach 96 at a flow rate of 45 L min^{-1}, and 146 at a flow rate of 63 L min^{-1}. Also in the case of a double bottom inlet configuration, it is possible to observe a more stable flow in the cross-section of the chamber using a static mixer in the FP PBR chamber.

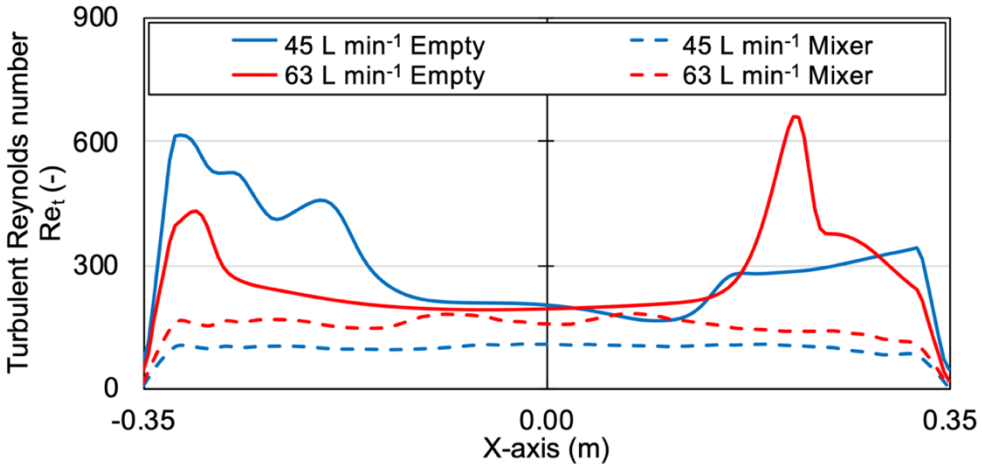

Fig. 8.3.1.4. Configuration with single bottom inlet - turbulent Reynolds number distribution along the X-axis in a distance of 1 m from bottom of FP PBR chamber.

8.3.2 Wall shear stress

Using a validated FP PBR model with a static mixer, the wall shear stress distribution on the transparent walls was simulated (Figure 8.3.2.1). It can be seen from the comparison that the highest values of wall shear stress were reached in the area below the static mixer. This was due to the locally higher flow velocities from inlets, which are evident from Figure 8.3.1.1. In the upper part of the chamber above the static mixer, the values of wall shear stress on the wall were significantly lower. In the comparison with the empty FP PBR chamber (Figure 7.3.3.2 to Figure 7.3.3.3), the values of wall shear stress on the transparent walls were generally lower. Nevertheless, in the case of the FP PBR chamber with a static mixer, the flow was stable and more homogeneous in the cross-section of the chamber.

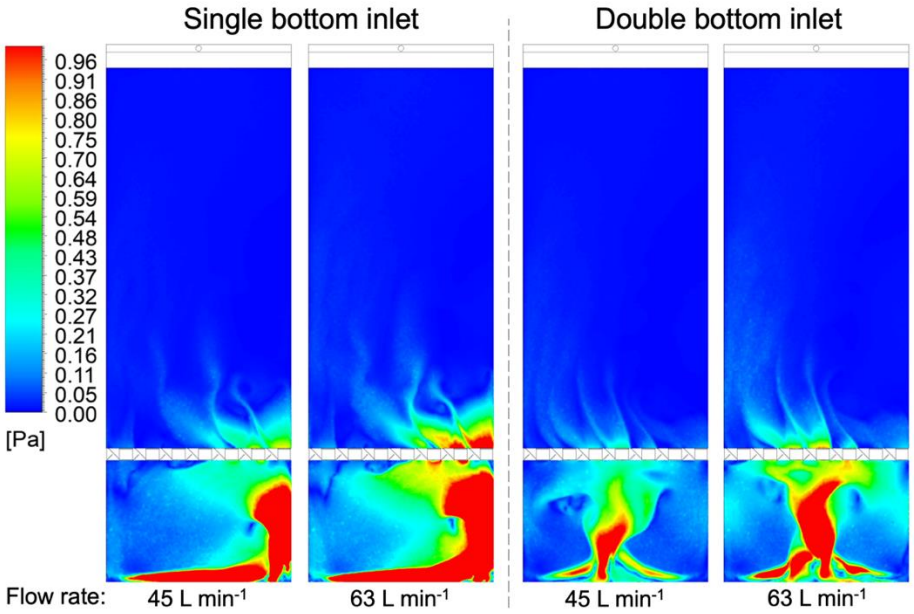

Fig. 8.3.2.1. Wall shear stress distribution in FP PBR chamber with static mixer.

The configuration of FP PBR with a static mixer is more suitable from the point of view of uniformity of HRT of the processed culture medium in the irradiated area of the FP PBR. However, on the contrary from the point of view of the effect of the wall shear forces on the stability of the formed biofilm seems to be a more suitable configuration with an empty chamber. For the configuration with an empty FP PBR chamber, the critical value of the wall shear stress was determined. Formation of biofilm was avoided if the wall shear stress was higher than the critical value. This critical wall shear stress corresponds to a value of 0.2 Pa. Using a validated model with a static mixer, a model of the distribution of wall shear stress below the critical value was created (Figure 8.3.2.2).

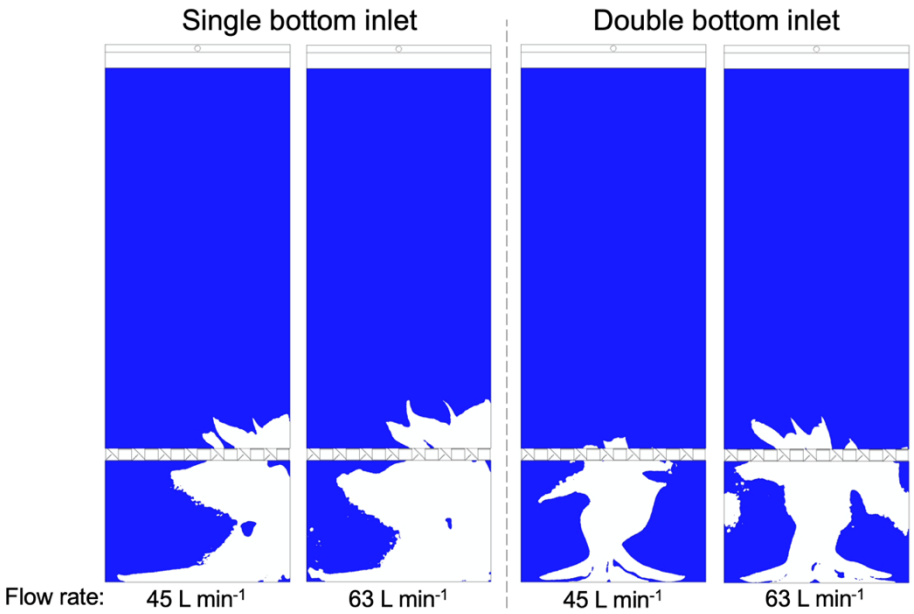

Fig. 8.3.2.2. Distribution of wall shear stress on the transparent wall of FP PBR below the critical wall shear stress value of 0.2 Pa (in blue).

The comparison showed that in the entire upper part above the static mixer, the wall shear stress on the transparent wall does not exceed a critical value. Thus, it can be assumed that microalgae cells will be fixed on transparent walls and biofilm will grow.

8.3.3 Pressure drop

The increase in pressure drop is directly related to the increase in operating costs. When installing a static mixer in the FP PBR chamber, an increase in pressure drop can be expected. The designed geometry of the static mixer should thus increase the overall pressure drop as little as possible. The pressure drop in the FP PBR chamber was measured using differential pressure sensors JSP DMD 331 (JSP Industrial Controls, Czech Republic). The sensors were placed on the inlet and outlet of the chamber and the pressure difference on the sensors was measured using a transducer. The pressure drop Δp (Pa) in the FP PBR chamber was measured for different flow rates of the culture medium. The measurements were performed for an empty chamber configuration and for a configuration with a static mixer so the pressure drop of the designed static mixer could be determined as well. From the created CFD models for both configurations, the pressure values in the inlet and outlet were also generated. The measured values and values from the CFD simulation are shown in Table 8.3.3.1.

Table 8.3.3.1. Measured and simulated pressure drop in FP PBR chamber.

Configuration	Pressure drop Δp (kPa)			
	Experimental		CFD	
	45 L min^{-1}	63 L min^{-1}	45 L min^{-1}	63 L min^{-1}
Empty PBR chamber	4.4	7.7	3.2	6.8
PBR chamber with static mixer	5.3	8.7	3.6	7.2

From the measured values it is possible to determine the pressure drop of the static mixer. The difference between the pressure drop in the empty chamber and the pressure drop in the chamber with the static mixer shows that at a flow rate of 45 L min^{-1} the pressure drop of the static mixer reaches 0.9 kPa and at a flow rate of 63 L min^{-1} the pressure drop was 1 kPa. The pressure drop of the static mixer generated from the CFD simulation was approximately 0.4 kPa for both flow rates. From practical experience, the RNG k-ϵ model generally underestimates the pressure drop values compared to experiments. A simplified analytical calculation of the pressure drop in an empty FP PBR chamber can be used for comparison. The pressure drop is dominated by the loss at the inlet to the chamber, which is caused by the sudden expansion of the flow cross-sectional area, and the loss at the outlet from the chamber, which is caused by the contraction of the flow cross-sectional area. The frictional pressure drop through the rectangular cross-section chamber is negligible compared to the local losses at

the inlet and outlet and thus is not be considered in the calculation. The inlet and outlet pressure drop Δp (Pa) can be determined from Eq. (8.1)

$$\Delta p = \xi \cdot \frac{u^2}{2} \cdot \rho \tag{8.1}$$

where ξ (-) is the local loss coefficient, u (m s^{-1}) is the mean velocity relative to the free rectangular cross-section of the chamber, and ρ (kg m^{-3}) is the density of the medium. The loss coefficient at the chamber inlet ξ_{in} (-) can be determined using the approximation

$$\xi_{in} = \left(1 - \frac{A_1}{A_2}\right)^2 \tag{8.2}$$

where A_1 (m) is the cross-sectional area of the inlet nozzle, and A_2 (m) is the cross-sectional area of the FP PBR chamber. The loss coefficient at the chamber outlet ξ_{out} (-) can be determined from Eq. (8.3)

$$\xi_{out} = \left(1 - \frac{A_2}{A_3}\right) \tag{8.3}$$

where A_3 (m) is the cross-sectional area of the outlet nozzle (Munson et al., 2009). At a flow rate of 45 L min^{-1}, the analytically calculated pressure drop in the empty chamber of the FP PBR is 1.71 kPa and at a flow rate of 63 L min^{-1} the pressure drop is 3.35 kPa. The analytical calculation values are lower than the CFD and experimental values (Table 8.3.3.1). The analytical calculation assumes a uniform expansion or contraction, however, in a real situation, there is a change in flow direction after entering the chamber. Similarly, the outflow from the chamber is not uniform as well. The flow in the chamber is not fully developed either, which is not considered in the above analytical calculation.

At a flow rate of 45 L min^{-1} the *Re* in a rectangular chamber reaches the value of 2,000 and at a flow rate of 63 L min^{-1} reaches the value of 2,800, which is not a significant difference from the critical value of 1,100 (Zhang, 2017) defining the transition between the laminar and turbulent flow regimes in a rectangular channel. Thus, it cannot be assumed that the dimensionless friction coefficient λ (-) is independent of *Re*. These statements are confirmed by the dependence of λ on the *Re* for conventional static mixers in circular cross-section tubes. In the region of the critical Reynolds number, the dependence of λ for conventional static mixers can be described by a power dependence determined from Eq. (8.4)

$$\lambda = \frac{B}{Re^{\beta}} \tag{8.4}$$

where B is the constant and β is a power constant of value less than one (Theron and Sauze, 2011). The exponential dependence close to the critical Reynolds number region for typical representatives of conventional static mixers, such as Kenics, Helax, and Sulzer SMX, is shown in Figure 8.3.3.1 (Kabátek et al., 1989; Li et al., 1997).

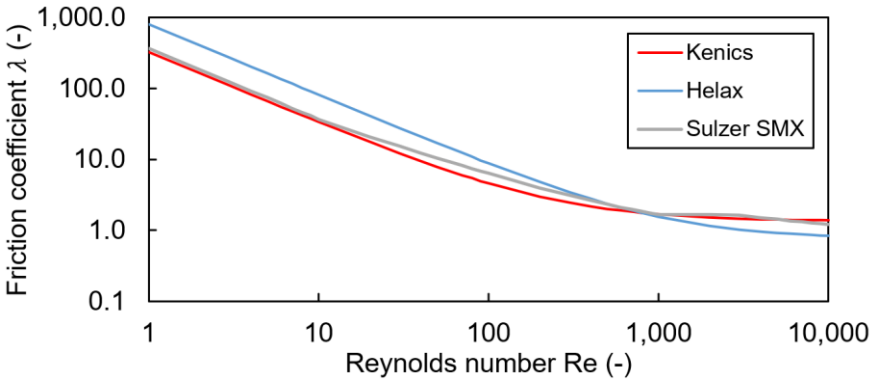

Fig. 8.3.3.1. Comparison of the friction coefficient of conventional static mixers.

The dimensionless friction coefficient of the static mixer λ_s can be derived from Darcy-Weissbach equation

$$\lambda_s = \frac{2 \cdot \Delta p_s \cdot d_h}{\rho \cdot L_s \cdot u^2} \tag{8.5}$$

where Δp_s (Pa) is the pressure drop of the static mixer, d_h (m) is the hydraulic diameter corresponding to the rectangular cross-section of the FP PBR chamber, L_s (m) is the length of the static mixer in the direction of medium flow, and u (m s^{-1}) is the mean velocity relative to the free rectangular cross-section of the chamber. Since the measurements were made for only one geometry of the FP PBR chamber, it is convenient to use a more general notation, i.e. the dependence of $\lambda_s(L_s/d_h)$ on *Re*. The dependence of this dimensionless parameter on the *Re* for the flow in the rectangular channel (Eq. (7.1)) is shown in Figure 8.3.3.2. It is evident that in the region of the lower turbulent *Re*, the dimensionless friction coefficient λ_s slightly decreases with increasing *Re*. Conventional tubular static mixers demonstrate a similar behavior at operating conditions approaching the critical *Re* defining the transition between laminar and turbulent flow regime (Figure 8.3.3.1). Also, the ***β*** power constant describing the dependence (Eq. (8.4)) is less than one in the case of a developed static mixer, which demonstrates comparable behavior to conventional static mixers.

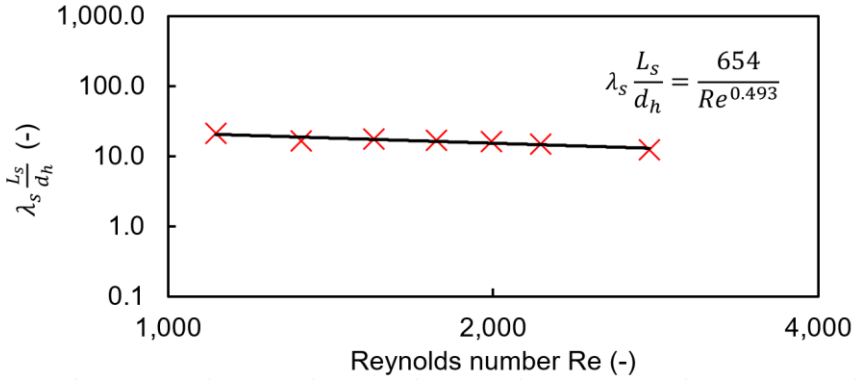

Fig. 8.3.3.2. Experimental dependence of friction coefficient on Reynolds number for the developed static mixer installed in the FP PBR chamber.

The assumptions of λ_s dependence on *Re* also correspond to the comparison of the ratio of the squares of the mean flow velocities in the chamber as the flow rate changes. This ratio should correspond to the ratio of the pressure loss during the flow rate change in the case of a fully developed turbulent flow. The ratio of the squares of the mean velocities at flow rates of 45 L min^{-1} and 63 L min^{-1} corresponds to 0.51. The same value is obtained for the ratio of analytically calculated pressure drops at flow rates of 45 L min^{-1} and 63 L min^{-1}, which assumes a fully developed turbulent flow. The pressure loss ratio based on the CFD simulation reaches a value of 0.47. In the case of experimental measurements, the ratio reaches the value of 0.57, confirming that the dimensionless friction coefficient λ in the empty chamber decreases with increasing flow rate.

8.3.4 Set of static mixers

To compare the configurations with single and double bottom inlet, it is possible to observe the effect of the medium inlet on the function of the static mixer. With a more stable inlet (double bottom inlet), there was also a more homogenous distribution of the mixed medium behind the static mixer. Conversely, in the case of a single bottom inlet configuration, the medium only flows into one part of the static mixer, which causes the medium to circulate in the area above the static mixer. In order to study the effect of a static mixer on the mixing of the medium, a model of a static mixer with a uniform inlet and outlet was created. The distance in front of and behind the static mixer was chosen so that the flow of the medium was fully developed and so that it was possible to study the hydrodynamic conditions behind the static mixer at the same time. From the experimental measurement and from the simulation of the flow velocity distribution, it can also be seen that the blades of the static mixer, which are perpendicular to the transparent walls of the FP PBR, direct the medium flow to the left side of the FP PBR chamber. In order to eliminate this imbalance and at the same time intensify the mixing of the medium in the chamber, another static mixer was created in the model at a distance of 200 mm. The second static mixer has the angle of inclination of the blades perpendicular to the transparent walls opposite to the first static mixer. The scheme of two static mixers installed in the FP PBR chamber is shown in Figure 8.3.4.1.

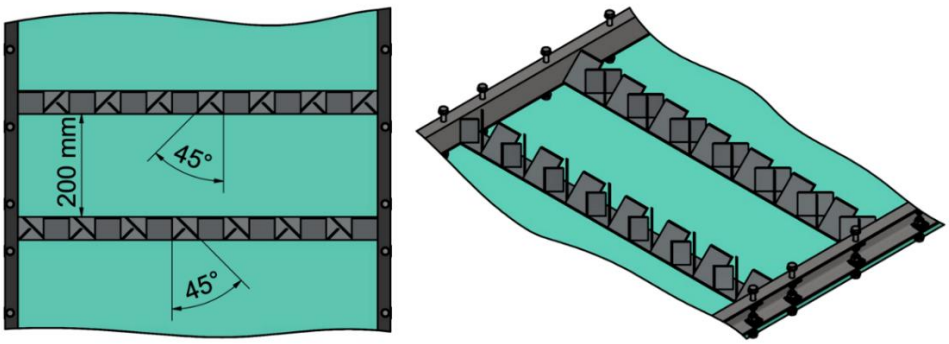

Fig. 8.3.4.1. 3D model of two static mixers installed in FP PBR chamber.

Using the created numerical model of two static mixers in the FP PBR chamber, a simulation of the medium flow velocity distribution was created. The distribution was created for three vertical cross-sections so that it was possible to investigate the function of the static mixer and its effect on the medium flow in the FP PBR chamber. The first cross-section was situated in the center of the chamber, i.e. at a distance of 25 mm from both transparent plates. In order to be able to observe the flow of the medium near the transparent walls, the remaining two cross-sections are located at a distance of 3 mm from the front and back transparent walls. The selected cross-sections of the geometry with two static mixers are shown in Figure 8.3.4.2.

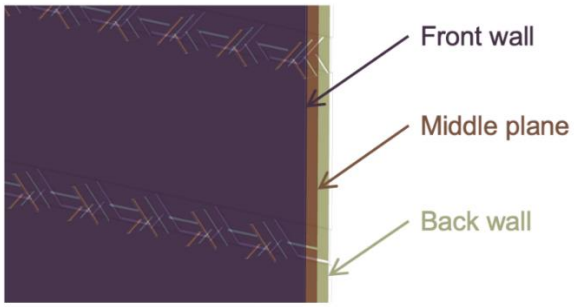

Fig. 8.3.4.2. Selected vertical cross-sections in geometry of FP PBR chamber with two static mixers – isometric view.

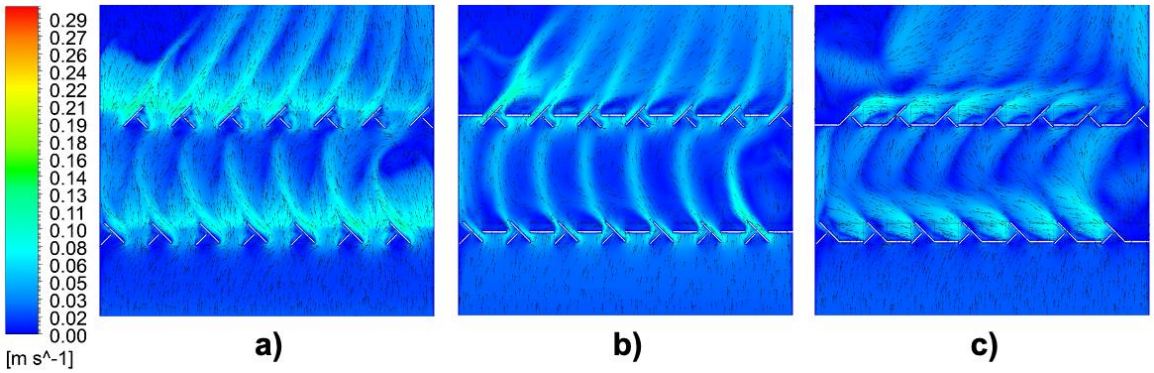

Fig. 8.3.4.3. Velocity distribution in FP PBR chamber with two static mixers – detail view, flow rate: 45 L min^{-1} – a) front wall, b) middle plane, c) back wall.

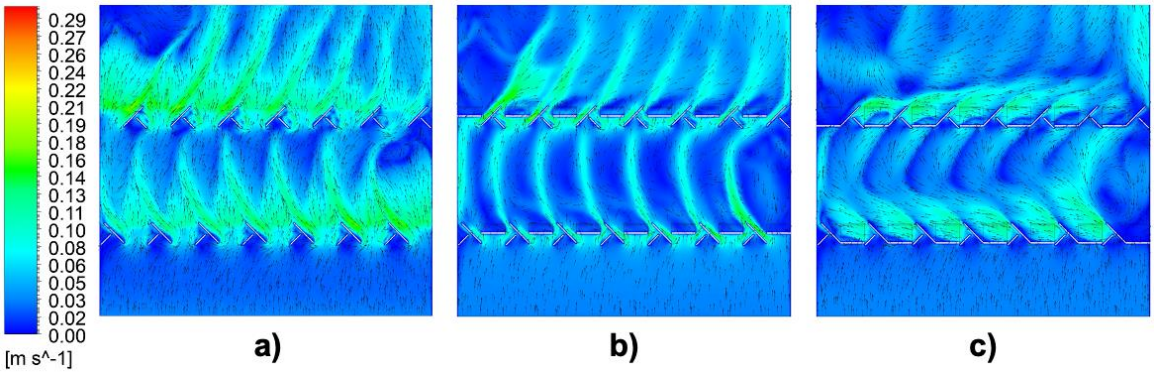

Fig. 8.3.4.4. Velocity distribution in FP PBR chamber with two static mixers – detail view, flow rate: 63 L min^{-1} – a) front wall, b) middle plane, c) back wall.

The highest values of the flow velocity were reached near the front wall (Figure 8.3.4.3a and Figure 8.3.4.4a). This was caused by the blades, which form an angle of 45° with the transparent wall and thus directs the flow towards the front wall. On the back wall (Figure 8.3.4.3c and Figure 8.3.4.4c) the flow was directed towards the side of the FP PBR chamber since the flow was influenced essentially only by the blades, which are perpendicular to the transparent walls. It can be seen from the distribution that a wake region was formed on the side of the FP PBR chamber and the backflow occurs here. Moreover, the flow rate was significantly lower here than in the rest of the chamber. Behind the blades, which form an angle of 45° with the transparent walls, a backflow in the wake region was also formed, which can be seen from the cross-section perpendicular to the transparent walls of the FP PBR (Figure 8.3.4.5). The medium was partially returned behind the blades, which intensify the mixing of the medium.

From the comparison of the velocity distribution in the middle plane in a chamber with two static mixers (Figure 8.3.4.3b and Figure 8.3.4.4b) and in a chamber with one static mixer (Figure 8.3.1.1), it can be observed that using multiple static mixers can compensate the flow on one side of the FP PBR chamber. The inverted inclination of the blades perpendicular to the transparent walls thus compensates the direction of the medium flow. Due to the opposite blade's inclination, the medium was more evenly distributed over the entire width of the chamber. Using the created CFD model, it would be possible to optimize the hydrodynamics according to the various operating conditions and design configurations of FP PBR.

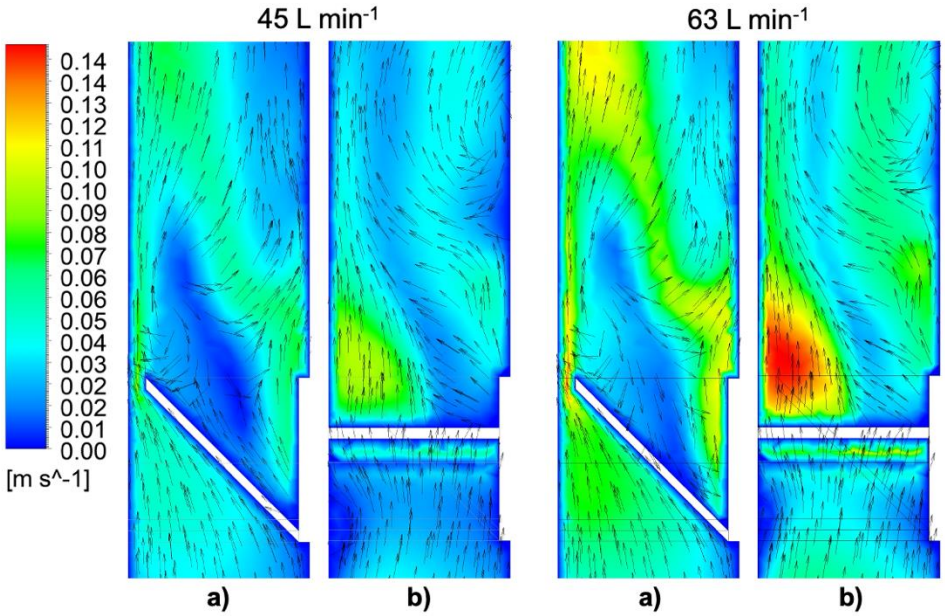

Fig. 8.3.4.5. Velocity distribution behind the static mixer in FP PBR chamber – a) cross-section of blade with an inclination of 45° to the transparent wall, b) cross-section of perpendicular blade to transparent wall. Note that all vertical cross-sections are perpendicular to transparent wall.

8.4 Conclusions

In order to homogenize and intensify the mixing of the culture medium stream, a static mixer was designed. The designed static mixer was installed in the FP PBR chamber and its influence on hydrodynamics at various operating settings was experimentally monitored using a tracer method. A numerical model was validated based on experimental measurement. A validated model can be used to examine individual hydrodynamic parameters more in detail.

For a single bottom inlet configuration, a circulation loop was formed in the bottom part of the chamber below the static mixer. It causes the medium to flow predominantly through the right part of the static mixer. The flow in the chamber above the static mixer was directed to the left side of the chamber, which consequently leads to the formation of dead zones. When the flow rate increases from 45 L min^{-1} to 63 L min^{-1}, the dead zones were partially eliminated, but they were not completely removed. In the double bottom inlet configuration, a more stable inlet to the static mixer was ensured. This makes the flow of medium behind the static mixer more uniform and homogeneous in the cross-section of the FP PBR chamber. The blades of the static mixer perpendicular to the transparent walls of the FP PBR slightly direct the flow to the left side of the chamber. In comparison to the single inlet configuration, the uniformity of flow was significantly more stable, and dead zones were thus almost eliminated.

Based on experimental measurements, the homogenization time for individual configurations was determined. Compared to the empty FP PBR chamber, the homogenization time was extended by 17 % in a single bottom configuration using a static mixer at a flow rate of 45 L min^{-1}. By increasing the flow rate to 63 L min^{-1}, the ratio between the empty chamber and the static mixer chamber was reduced to 4 %. The extension of the homogenization time was caused by the formation of dead zones in the part of the chamber above the static mixer. When using a double bottom inlet and a static mixer, the homogenization time was reduced by 17 % at a flow rate of 45 L min^{-1}, and by 34 % at a flow rate of 63 L min^{-1}. The double bottom inlet configuration with the static mixer ensures homogeneous flow in the FP PBR chamber and thus eliminates dead zones.

A comparison of the distribution of the turbulent Reynolds number shows that higher values were achieved locally in the empty FP PBR chamber. This was due to the uniform distribution and homogeneity of the flow in the cross-section of the FP PBR chamber with the static mixer. The highest values of wall shear stress were reached in part of the chamber below the static mixer. However, in the part of the chamber above the static mixer, the values were lower than in the case of an empty FP PBR chamber.

In order to further intensify the mixing of the processed medium and at the same time homogenize the flow in the cross-section of the FP PBR chamber, a model with two static

mixers was created. The static mixers were installed at a distance of 200 mm from each other. The static mixers have oppositely turned blades that are perpendicular to the transparent wall of the FP PBR. Using a developed numerical simulation in three different cross-sections of the FP PBR, more intense flow on the sides of the FP PBR chamber was eliminated. The highest flow velocities were achieved with the use of static mixers at the front transparent wall, which was caused by the geometry of the blades inclined at an angle of 45° to the transparent walls. The backflow acts on the back transparent wall, in the section just behind the static mixer. Part of the flowing medium returns behind the blades intensifying the mixing of the medium.

The use of a static mixer is more suitable compared to an empty chamber in terms of achieving a uniform HRT of the processed medium in the irradiated area FP PBR. The stable residence time in the irradiated area is more suitable for the microalgae cultivation process. Each microalgal cell receives an equivalent portion of the intensity from the light source. On the contrary, in terms of wall shear forces, which are associated with the stability of fixed biofilm on transparent walls, the configuration with an empty FP PBR chamber seems to be a more suitable variant. Therefore, for a cleaning regime or the prevention of biofilm formation on transparent walls, a configuration with an empty chamber seems to be a better option.

9
Conclusions

In this chapter, an overview of the main results and conclusions generated during the development of this thesis and the future research prospects were gathered together.

Nowadays, the majority of reactors for microalgae production are still on a laboratory scale or pilot scale. In general, the process of microalgae cultivation on a laboratory scale is already controllable, manageable, and widely described in the literature. However, the scale-up from the pilot or industrial scale is not easy. A limiting factor is the ability to guarantee comparable operating conditions on an industrial scale as well as in the laboratory. As the scale increases, a number of inhomogeneities occur in the culture medium. Specifically, the problem with irradiation of microalgae cells, which can reduce the efficiency of the microalgae cultivation process, can occur. Furthermore, temperature gradients can arise and inefficient utilization of nutrients and CO_2 can occur. Moreover, the formation of biofilm on the walls is a significant problem in pilot scale or industrial scale photobioreactors. It is difficult to irradiate the layer of culture medium through the formed biofilm, which reduces the overall production of microalgal biomass. Furthermore, contamination and degradation of the entire medium can occur during biofilm formation as well.

All parameters that affect the process of microalgae cultivation are influenced by hydrodynamic conditions in cultivation systems. Hydrodynamics has a significant effect on cultivation during the scaling-up of systems. The aim of this thesis was to study hydrodynamic conditions in two cultivation systems and propose the optimization of operating and/or design parameters. The first was a hybrid horizontal tubular photobioreactor that combines the specifics aspects of open and closed cultivation systems. The second cultivation system was a flat panel photobioreactor, which represents the typical closed system.

Numerical models simulating hydrodynamic conditions under different operating conditions were created for selected photobioreactor designs. The applicability of these models was subsequently validated based on the experimental measurements. Following the study of hydrodynamics, the operating conditions for both devices were optimized in order to intensify the microalgae cultivation process. The created numerical model proved its applicability for geometrically similar cultivation systems, which can be useful for optimization of the existing system, scaling-up, or for designing a novel photobioreactor.

9.1. Summary

The following conclusions can be drawn from the results obtained in this thesis.

- Based on intensive experimental measurements of HHT PBR performance, the mechanistic BIO_ALGAE model was calibrated and validated. The BIO_ALGAE can simulate the production of microalgae; however, the model does not consider the influence of hydrodynamic conditions and works with the assumption that the culture

medium is perfectly mixed. Experimental measurements of hydrodynamic conditions were performed on the same HHT PBR. Based on the results of hydrodynamic measurements, the CFD model hydrodynamic conditions were calibrated and validated. By increasing the flow rate of the culture medium, it was not possible to completely eliminate the formation of dead zones in open tanks. The intensification of mixing in the HHT PBR tubes due to the increasing flow rate (*Re*=23,700 to *Re*=46,200) results in an increase in shear stress on the transparent walls (0.3 Pa to 1 Pa). The wall shear forces are important in terms of elimination of biofilm formation, where the critical value avoiding the formation reaches 0.2 Pa. The movement of microalgal cells in transparent tubes was also simulated for different flow rates. Intensification of mixing (*Re*=23,700 to *Re*=46,200) results in a more frequent transition of cells between the dark and light zones (the light fraction increased to 0.678), which has a significant effect on production.

- The particle trajectory was subsequently integrated into a multi-physical model, which combines a mechanistic BIO_ALGAE model and a hydrodynamic CFD model. Using the created multi-physical model, it is possible to predict the influence of hydrodynamic conditions on the light attenuation in the culture medium and the subsequent microalgae production. The created multi-physical model showed an increase in the concentration of microalgae by 2 % due to the mixing intensification (*Re*=23,700 to *Re*=46,200). Increasing the flow rate to the maximum value (*Re*=174,700) may increase the concentration by 4.6 %. However, further intensification of mixing is limited by the operating and design parameters of HHT PBR and it would be necessary to optimize the system design by installing static mixers in transparent tubes.
- The hydrodynamic CFD model of FP PBR was calibrated and validated based on the experimental measurements. Hydrodynamic conditions in the FP PBR chamber were studied for different flow rates (45 and 63 L min^{-1}) and different configurations of inlet and outlet settings (top inlet, single bottom inlet, double bottom inlets). The most intensive mixing and homogenization of the culture medium in the FP PBR chamber occur in a double bottom inlet configuration, as the homogenization time (78 and 64 s for 45 and 63 L min^{-1} inflow) is lower than HRT (97 and 69 s). From the point of view of preventing the formation of biofilm on the transparent wall of FP PBR, a configuration with a single bottom inlet appears to be the most suitable. At a flow rate of 45 L min^{-1}, the wall shear stress on 70 % of the transparent wall of the FP PBR reaches a value lower than the critical value of the shear stress preventing the formation of biofilm (0.2 Pa). At a flow rate of 63 L min^{-1}, the area is reduced to 33 %. However, by increasing the flow rate, the formation of dead zones in any inlet configuration cannot

be prevented, and the flow of the culture medium needs to be more homogenized throughout the cross section of the FP PBR chamber.

- A static mixer was designed in order to intensify the mixing and homogenize the flow in the FP PBR chamber. For a single bottom inlet configuration, the installation of a static mixer did not shorten the homogenization time for any of the selected flow rates. However, in the double bottom inlet configuration, the homogenization time was reduced by 17 % at a flow rate of 45 L min^{-1} and 34 % at a flow rate of 63 L min^{-1}. The flow of the culture medium was homogeneous in almost the entire cross-section of the FP PBR chamber. By installing series-connected static mixers (vertical distance 200 mm) it was possible to eliminate the formation of dead zones in the FP PBR chamber.

9.2 Future research prospects

The aim of future research will be the application of created models to geometrically similar photobioreactors under full scale conditions. The influence of proposed operational and design optimizations on microalgae production will be further studied.

- An integrated multi-physical model describing the dependence of hydrodynamic conditions on microalgae production will be used especially in systems working with a larger layer of culture medium or in systems that achieve higher concentrations of microalgae. In those types of systems, mixing can significantly affect the irradiation of microalgal cells in the culture medium, which subsequently affects the overall biomass production. Application of the model to these systems could help to significantly affect their operation and overall productivity.
- A biofilm was significantly formed on the walls of HHT PBR during the winter season, which reduced the production of microalgae. The aim of further research should be to study the effect of hydrodynamic conditions on the disturbance of the stability of the formed biofilm or the prevention of its formation. Due to the limitation of operating conditions of HHT PBR, the static mixers installed in transparent tubes could be used to intensify the mixing of the culture medium.
- The influence of static mixers installed in the FP PBR chamber on the microalgae cultivation process should be deeper investigated. Based on different operating conditions, it would be possible to compare the effect of more intensive mixing and homogenization of the flowing culture medium on other operating parameters and the overall production of microalgal biomass.

References

Abu-Ghosh, S., Fixler, D., Dubinsky, Z., Iluz, D., 2016. Flashing light in microalgae biotechnology. Bioresour. Technol. 203, 357–363. https://doi.org/10.1016/j.biortech.2015.12.057

Acién Fernández, F.G., Fernández Sevilla, J.M., Sánchez Pérez, J.A., Molina Grima, E., Chisti, Y., 2001. Airlift-driven external-loop tubular photobioreactors for outdoor production of microalgae: Assessment of design and performance. Chem. Eng. Sci. 56, 2721–2732. https://doi.org/10.1016/S0009-2509(00)00521-2

American Public Health Association, American Water Works Association, Water Environment Federation, American Public Health Association (APHA), A.W.W.A. (AWWA) & W.E.F. (WEF), 2005. Standard Methods for the Examination of Water and Wastewater 21st Edition, Standard Methods.

Ansari, F.A., Singh, P., Guldhe, A., Bux, F., 2017. Microalgal cultivation using aquaculture wastewater: Integrated biomass generation and nutrient remediation. Algal Res. 21, 169–177. https://doi.org/10.1016/j.algal.2016.11.015

ANSYS Inc. (US), 2018. Ansys Users' Guide, Release 19.0. https://doi.org/10.1017/CBO9781107415324.004

Azov, Y., Shelef, G., Moraine, R., 1982. Carbon limitation of biomass production in high-rate oxidation ponds. Biotechnol. Bioeng. https://doi.org/10.1002/bit.260240305

Barros, A.C., Gonçalves, A.L., Simões, M., 2019. Microalgal/cyanobacterial biofilm formation on selected surfaces: the effects of surface physicochemical properties and culture media composition. J. Appl. Phycol. 31, 375–387. https://doi.org/10.1007/s10811-018-1582-3

Belohlav, V., Jirout, T., 2019. Design methodology of industrial equipment for microalgae biomass primary harvesting and dewatering. Chem. Eng. Trans. 76, 919–924. https://doi.org/10.3303/CET1976154

Belohlav, V., Jirout, T., Kratky, L., 2018. Possibilities of implementation of photobioreactors on industrial scale. Chem. List. 112, 183–190.

Belohlav, V., Zakova, T., Jirout, T., Kratky, L., 2020. Effect of hydrodynamics on the formation and removal of microalgal biofilm in photobioreactors. Biosyst. Eng. 200, 315–327. https://doi.org/10.1016/j.biosystemseng.2020.10.014

Bernardi, A., Nikolaou, A., Meneghesso, A., Chachuat, B., Morosinotto, T., Bezzo, F., 2015. A Framework for the Dynamic Modelling of PI Curves in Microalgae, in: Computer Aided Chemical Engineering. https://doi.org/10.1016/B978-0-444-63576-1.50108-4

Bird, R.B., Stewart, W., Lightfoot, E., 2002. Transport Phenomena, Second. ed, Journal of Chemical Education. John Wiley & Sons, Inc., Hoboken, New Jersey. https://doi.org/10.1021/ed038pa640

Bitog, J.P., Lee, I.B., Lee, C.G., Kim, K.S., Hwang, H.S., Hong, S.W., Seo, I.H., Kwon, K.S., Mostafa, E., 2011. Application of computational fluid dynamics for modeling and designing photobioreactors for microalgae production: A review. Comput. Electron. Agric. 76, 131–147. https://doi.org/10.1016/j.compag.2011.01.015

Blanken, W., Postma, P.R., de Winter, L., Wijffels, R.H., Janssen, M., 2016. Predicting microalgae growth. Algal Res. 14, 28–38. https://doi.org/10.1016/j.algal.2015.12.020

Bosma, R., de Vree, J.H.H., Slegers, P.M.M., Janssen, M., Wijffels, R.H.H., Barbosa, M.J.J., 2014. Design and construction of the microalgal pilot facility AlgaePARC. Algal Res. 6, 160–169. https://doi.org/10.1016/j.algal.2014.10.006

Brennan, L., Owende, P., 2010. Biofuels from microalgae-A review of technologies for production, processing, and extractions of biofuels and co-products. Renew. Sustain. Energy Rev. 14, 557–577. https://doi.org/10.1016/j.rser.2009.10.009

Callow, M.E., 2000. Algal biofilms, in: Biofilms: Recent Advances in Their Study and Control. https://doi.org/https://doi.org/10.1201/9781482284157

Camacho Rubio, F., Acién Fernández, F.G., Sánchez Pérez, J.A., García Camacho, F., Molina Grima, E., 1999. Prediction of dissolved oxygen and carbon dioxide concentration profiles in tubular photobioreactors for microalgal culture. Biotechnol. Bioeng. 62, 71–86. https://doi.org/10.1002/(SICI)1097-0290(19990105)62:1<71::AID-BIT9>3.0.CO;2-T

Cheng, W., Huang, J., Chen, J., 2016. Computational fluid dynamics simulation of mixing characteristics and light regime in tubular photobioreactors with novel static mixers. J. Chem. Technol. Biotechnol. 91, 327–335. https://doi.org/10.1002/jctb.4560

Chisti, Y., 2016. Large-Scale Production of Algal Biomass: Raceway Ponds, in: Algae Biotechnology. Springer, Cham, pp. 21–40. https://doi.org/10.1007/978-3-319-12334-9_2

Chisti, Y., 2007. Biodiesel from microalgae. Biotechnol. Adv. 25, 294–306. https://doi.org/10.1016/j.biotechadv.2007.02.001

Cicci, A., Stoller, M., Bravi, M., 2014. Analysis of microalgae growth in residual light: A diagnostics tool for low-cost alternative cultural media. Chem. Eng. Trans. 38, 79–84. https://doi.org/10.3303/CET1438014

de Godos, I., Arbib, Z., Lara, E., Rogalla, F., 2016. Evaluation of High Rate Algae Ponds for treatment of anaerobically digested wastewater: Effect of CO2 addition and modification of dilution rate. Bioresour. Technol. 220, 253–261. https://doi.org/10.1016/j.biortech.2016.08.056

Degen, J., Uebele, A., Retze, A., Schmid-Staiger, U., Trösch, W., 2001. A novel airlift photobioreactor with baffles for improved light utilization through the flashing light effect. J. Biotechnol. 92, 89–94. https://doi.org/10.1016/S0168-1656(01)00350-9

Díez-Montero, R., Belohlav, V., Ortiz, A., Uggetti, E., García-Galán, M.J., García, J., 2020. Evaluation of daily and seasonal variations in a semi-closed photobioreactor for microalgae-based bioremediation of agricultural runoff at full-scale. Algal Res. 47, 101859. https://doi.org/10.1016/j.algal.2020.101859

Ding, N., Li, C., Wang, T., Guo, M., Mohsin, A., Zhang, S., 2021. Evaluation of an enclosed air-lift photobioreactor (ALPBR) for biomass and lipid biosynthesis of microalgal cells grown under fluid-induced shear stress. Biotechnol. Biotechnol. Equip. 35, 139–149. https://doi.org/10.1080/13102818.2020.1856717

Douskova, I., Doucha, J., Livansky, K., MacHat, J., Novak, P., Umysova, D., Zachleder, V., Vitova, M., 2009. Simultaneous flue gas bioremediation and reduction of microalgal biomass production costs. Appl. Microbiol. Biotechnol. 82, 179–185. https://doi.org/10.1007/s00253-008-1811-9

García, J., Green, B.F., Lundquist, T., Mujeriego, R., Hernández-Mariné, M., Oswald, W.J., 2006. Long term diurnal variations in contaminant removal in high rate ponds treating urban wastewater. Bioresour. Technol. 97, 1709–1715. https://doi.org/10.1016/j.biortech.2005.07.019

García, J., Mujeriego, R., Hernández-Mariné, M., 2000. High rate algal pond operating strategies for urban wastewater nitrogen removal. J. Appl. Phycol. 12, 331–339. https://doi.org/10.1023/A:1008146421368

García, J., Ortiz, A., Álvarez, E., Belohlav, V., García-Galán, M.J., Díez-Montero, R., Álvarez, J.A., Uggetti, E., 2018. Nutrient removal from agricultural run-off in demonstrative full scale tubular photobioreactors for microalgae growth. Ecol. Eng. 120. https://doi.org/10.1016/j.ecoleng.2018.07.002

Gómez-Pérez, C.A., Espinosa, J., Montenegro Ruiz, L.C., van Boxtel, A.J.B., 2015. CFD simulation for reduced energy costs in tubular photobioreactors using wall turbulence promoters. Algal Res. 12, 1–9. https://doi.org/10.1016/j.algal.2015.07.011

Gutiérrez, R., Passos, F., Ferrer, I., Uggetti, E., García, J., 2015. Harvesting microalgae from wastewater treatment systems with natural flocculants: Effect on biomass settling and biogas production. Algal Res. 9, 204–211. https://doi.org/10.1016/j.algal.2015.03.010

Henze, M., Gujer, W., Mino, T., van Loosedrecht, M., 2015. Activated Sludge Models ASM1, ASM2, ASM2d and ASM3, Water Intelligence Online. https://doi.org/10.2166/9781780402369

Huang, J., Li, Y., Wan, M., Yan, Y., Feng, F., Qu, X., Wang, J., Shen, G., Li, W., Fan, J., Wang, W., 2014. Novel flat-plate photobioreactors for microalgae cultivation with special mixers to promote mixing along the light gradient. Bioresour. Technol. 159, 8–16. https://doi.org/10.1016/j.biortech.2014.01.134

Huang, Y., Xiong, W., Liao, Q., Fu, Q., Xia, A., Zhu, X., Sun, Y., 2016. Comparison of Chlorella vulgaris biomass productivity cultivated in biofilm and suspension from the aspect of light transmission and microalgae affinity to carbon dioxide. Bioresour. Technol. 222, 367–373. https://doi.org/10.1016/j.biortech.2016.09.099

Huesemann, M., Crowe, B., Waller, P., Chavis, A., Hobbs, S., Edmundson, S., Wigmosta, M., 2016. A validated model to predict microalgae growth in outdoor pond cultures subjected to fluctuating light intensities and water temperatures. Algal Res. 13, 195–206. https://doi.org/10.1016/j.algal.2015.11.008

Huo, S., Wang, Z., Zhu, S., Shu, Q., Zhu, L., Qin, L., Zhou, W., Feng, P., Zhu, F., Yuan, Z., Dong, R., 2018. Biomass accumulation of Chlorella zofingiensis G1 cultures grown outdoors in photobioreactors. Front. Energy Res. 6, 1–8. https://doi.org/10.3389/fenrg.2018.00049

Janssen, M., Tramper, J., Mur, L.R., Wijffels, R.H., 2003. Enclosed outdoor photobioreactors: Light regime, photosynthetic efficiency, scale-up, and future prospects. Biotechnol. Bioeng. 81, 193–210. https://doi.org/10.1002/bit.10468

Jerez, C.G., Enrique, N., Malpartida, I., Rico, R.M., Masojidek, J., Abdala, R., Figueroa, F.L., 2014. Hydrodynamics and photosynthesis performance of Chlorella fusca grown in a Thin-Layer Cascade (TLC) system. Aquat. Biol. 22, 111–122. https://doi.org/10.3354/ab00603

Kabátek, J., Ditl, P., Novák, V., 1989. Helax-a new type of static mixer-operation characteristics and comparison with other types. Chem. Eng. Process. 25, 59–64. https://doi.org/10.1016/0255-2701(89)80031-5

Katarzyna, L., Sai, G., Avijeet Singh, O., 2015. Non-enclosure methods for non-suspended microalgae cultivation: Literature review and research needs. Renew. Sustain. Energy Rev. 42, 1418–1427. https://doi.org/10.1016/j.rser.2014.11.029

Kunjapur, A.M., Eldridge, R.B., 2010. Photobioreactor Design for Commercial Biofuel Production from Microalgae. Ind. Eng. Chem. Res. 49, 3516–3526. https://doi.org/10.1021/ie901459u

Lan, S., Wu, L., Yang, H., Zhang, D., Hu, C., 2017. A new biofilm based microalgal cultivation approach on shifting sand surface for desert cyanobacterium Microcoleus vaginatus. Bioresour. Technol. 238, 602–608. https://doi.org/10.1016/j.biortech.2017.04.058

Levenspiel, O., 1999. Chemical Reaction Engineering - 3rd edition, Third Edit. ed. John Wiley & Sons, Inc., Hoboken, New Jersey.

Li, H.Z., Fasol, C., Choplin, L., 1997. Pressure drop of newtonian and non-newtonian fluids across a sulzer SMX static mixer. Chem. Eng. Res. Des. 75, 792–796. https://doi.org/10.1205/026387697524461

Li, J., Stamato, M., Velliou, E., 2015. Design and characterization of a scalable airlift flat panel photobioreactor for microalgae cultivation 75–86. https://doi.org/10.1007/s10811-014-0335-1

Lindblad, P., Fuente, D., Borbe, F., Cicchi, B., Conejero, J.A., Couto, N., Čelešnik, H., Diano, M.M., Dolinar, M., Esposito, S., Evans, C., Ferreira, E.A., Keller, J., Khanna, N., Kind, G., Landels, A., Lemus, L., Noirel, J., Ocklenburg, S., Oliveira, P., Pacheco, C.C., Parker, J.L., Pereira, J., Pham, T.K., Pinto, F., Rexroth, S., Rögner, M., Schmitz, H.J., Benavides, A.M.S., Siurana, M., Tamagnini, P., Touloupakis, E., Torzillo, G., Urchueguía, J.F., Wegelius, A., Wiegand, K., Wright, P.C., Wutschel, M., Wünschiers, R., 2019. CyanoFactory, a European consortium to develop technologies needed to advance cyanobacteria as chassis for production of chemicals and fuels. Algal Res. 41. https://doi.org/10.1016/j.algal.2019.101510

Loyseau, X.F., Verdin, P.G., Brown, L.D., 2018. Scale-up and turbulence modelling in pipes. J. Pet. Sci. Eng. 162, 1–11. https://doi.org/10.1016/j.petrol.2017.12.019

Marín, D., Ortíz, A., Díez-Montero, R., Uggetti, E., García, J., Lebrero, R., Muñoz, R., 2019. Influence of liquid-to-biogas ratio and alkalinity on the biogas upgrading performance in a demo scale algal-bacterial photobioreactor. Bioresour. Technol. 280, 112–117. https://doi.org/10.1016/j.biortech.2019.02.029

Martínez-Sanz, M., Garrido-Fernández, A., Mijlkovic, A., Krona, A., Martínez-Abad, A., Coll-Marqués, J.M., López-Rubio, A., Lopez-Sanchez, P., 2020. Composition and rheological properties of microalgae suspensions: Impact of ultrasound processing. Algal Res. 49, 101960. https://doi.org/10.1016/j.algal.2020.101960

Masojídek, J., 2014. Mass Cultivation of Freshwater Microalgae. Earth Syst. Environ. Sci. 1–13. https://doi.org/10.1016/B978-0-12-409548-9.09373-8

Massart, A., Mirisola, A., Lupant, D., Thomas, D., Hantson, A.L., 2014. Experimental characterization and numerical simulation of the hydrodynamics in an airlift photobioreactor for microalgae cultures. Algal Res. 6, 210–217. https://doi.org/10.1016/j.algal.2014.07.003

Mata, T.M., Martins, A.A., Caetano, N.S., 2010. Microalgae for biodiesel production and other applications: A review. Renew. Sustain. Energy Rev. 14, 217–232. https://doi.org/10.1016/j.rser.2009.07.020

Matamoros, V., Gutiérrez, R., Ferrer, I., García, J., Bayona, J.M., 2015. Capability of microalgae-based wastewater treatment systems to remove emerging organic contaminants : A pilot-scale study. J. Hazard. Mater. 288, 34–42. https://doi.org/10.1016/j.jhazmat.2015.02.002

Michels, M.H.A., van der Goot, A.J., Vermuë, M.H., Wijffels, R.H., 2016. Cultivation of shear stress sensitive and tolerant microalgal species in a tubular photobioreactor equipped with a centrifugal pump. J. Appl. Phycol. 28, 53–62. https://doi.org/10.1007/s10811-015-0559-8

Milano, J., Ong, H.C., Masjuki, H.H., Chong, W.T., Lam, M.K., Loh, P.K., Vellayan, V., 2016. Microalgae biofuels as an alternative to fossil fuel for power generation. Renew. Sustain. Energy Rev. 58, 180–197. https://doi.org/10.1016/j.rser.2015.12.150

Mohd Udaiyappan, A.F., Abu Hasan, H., Takriff, M.S., Sheikh Abdullah, S.R., 2017. A review of the potentials, challenges and current status of microalgae biomass applications in industrial wastewater treatment. J. Water Process Eng. 20, 8–21. https://doi.org/10.1016/j.jwpe.2017.09.006

Molina, E., Fernández, J., Acién, F.G., Chisti, Y., 2001. Tubular photobioreactor design for algal cultures. J. Biotechnol. 92, 113–131. https://doi.org/10.1016/S0168-1656(01)00353-4

Munson, B., Young, D., Okiishi, T., Huebsch, W., 2009. Fundamentals of fluid mechanics, Third. ed. John Wiley & Sons, Inc., Hoboken, New Jersey. https://doi.org/10.1017/CBO9781107415324.004

Nikolaou, A., Booth, P., Gordon, F., Yang, J., Matar, O., Chachuat, B., 2016. Multi-Physics Modeling of Light-Limited Microalgae Growth in Raceway Ponds. IFAC-PapersOnLine 49, 324–329. https://doi.org/10.1016/j.ifacol.2016.12.147

Olivieri, G., Salatino, P., Marzocchella, A., 2014. Advances in photobioreactors for intensive microalgal production: Configurations, operating strategies and applications. J. Chem. Technol. Biotechnol. 89, 178–195. https://doi.org/10.1002/jctb.4218

Papacek, S., Jablonsky, J., Petera, K., 2018. Advanced integration of fluid dynamics and photosynthetic reaction kinetics for microalgae culture systems. BMC Syst. Biol. 12, 1–12. https://doi.org/10.1186/s12918-018-0611-9

Paul, E.L., Atiemo-Obeng, V.A., Kresta, S.M., 2004. Handbook of Industrial Mixing. John Wiley & SOns, Inc., Hoboken, New Jersey.

Perner-Nochta, I., Posten, C., 2007. Simulations of light intensity variation in photobioreactors. J. Biotechnol. 131, 276–285. https://doi.org/10.1016/j.jbiotec.2007.05.024

Phillips, J.N., Myers, J., 1954. Growth rate of Chlorella in flashing light. Plant Physiol. 152–161.

Pires, J.C.M., Alvim-Ferraz, M.C.M., Martins, F.G., 2017. Photobioreactor design for microalgae production through computational fluid dynamics: A review. Renew. Sustain. Energy Rev. 79, 248–254. https://doi.org/10.1016/j.rser.2017.05.064

Posadas, E., Morales, M. del M., Gomez, C., Acién, F.G., Muñoz, R., 2015. Influence of pH and CO2 source on the performance of microalgae-based secondary domestic wastewater treatment in outdoors pilot raceways. Chem. Eng. J. 265, 239–248. https://doi.org/10.1016/j.cej.2014.12.059

Rossi, D., Gargiulo, L., Valitov, G., Gavriilidis, A., Mazzei, L., 2017. Experimental characterization of axial dispersion in coiled flow inverters. Chem. Eng. Res. Des. 120, 159–170. https://doi.org/10.1016/j.cherd.2017.02.011

Schädler, T., Thurn, A.-L., Brück, T., Weuster-Botz, D., 2021. Continuous Production of Lipids with Microchloropsis salina in Open Thin-Layer Cascade Photobioreactors on a Pilot Scale. Energies 14, 500. https://doi.org/10.3390/en14020500

Schnurr, P.J., Espie, G.S., Allen, D.G., 2014. The effect of light direction and suspended cell concentrations on algal biofilm growth rates. Appl. Microbiol. Biotechnol. 98, 8553–8562. https://doi.org/10.1007/s00253-014-5964-4

Schreiber, C., Behrendt, D., Huber, G., Pfaff, C., Widzgowski, J., Ackermann, B., Müller, A., Zachleder, V., Moudříková, Š., Mojzeš, P., Schurr, U., Grobbelaar, J., Nedbal, L., 2017. Growth of algal biomass in laboratory and in large-scale algal photobioreactors in the temperate climate of western Germany. Bioresour. Technol. 234, 140–149. https://doi.org/10.1016/j.biortech.2017.03.028

Sforza, E., Enzo, M., Bertucco, A., 2014. Design of microalgal biomass production in a continuous photobioreactor: An integrated experimental and modeling approach. Chem. Eng. Res. Des. 92, 1153–1162. https://doi.org/10.1016/j.cherd.2013.08.017

Slade, R., Bauen, A., 2013. Micro-algae cultivation for biofuels: Cost, energy balance, environmental impacts and future prospects. Biomass and Bioenergy 53, 29–38. https://doi.org/10.1016/j.biombioe.2012.12.019

Slegers, P.M.M., van Beveren, P.J.M.J.M., Wijffels, R.H.H., van Straten, G., van Boxtel, a. J.B.J.B., 2013. Scenario analysis of large scale algae production in tubular photobioreactors. Appl. Energy 105, 395–406. https://doi.org/10.1016/j.apenergy.2012.12.068

Solimeno, A., 2017. Numerical modelling of microalgae systems for wastewater treatment. Universitat Politécnica de Catalunya, BarcelonaTech.

Solimeno, A., Acíen, F.G., García, J., 2017a. Mechanistic model for design, analysis, operation and control of microalgae cultures: Calibration and application to tubular photobioreactors. Algal Res. 21, 236–246. https://doi.org/10.1016/j.algal.2016.11.023

Solimeno, A., García, J., 2019. Microalgae and bacteria dynamics in high rate algal ponds based on modelling results: Long-term application of BIO_ALGAE model. Sci. Total Environ. 650, 1818–1831. https://doi.org/10.1016/j.scitotenv.2018.09.345

Solimeno, A., Parker, L., Lundquist, T., García, J., 2017b. Integral microalgae-bacteria model (BIO_ALGAE): Application to wastewater high rate algal ponds. Sci. Total Environ. 601–602, 646–657. https://doi.org/10.1016/j.scitotenv.2017.05.215

Solimeno, A., Samsó, R., Uggetti, E., Sialve, B., Steyer, J.P., Gabarró, A., García, J., 2015. New mechanistic model to simulate microalgae growth. Algal Res. 12, 350–358. https://doi.org/10.1016/j.algal.2015.09.008

Solórzano, L., 1968. Determination of ammonia in natural waters by the phenolhypochlorite method. Limnol. Oceanogr.

Souliès, A., Pruvost, J., Castelain, C., Burghelea, T., 2016. Microscopic flows of suspensions of the green non-motile Chlorella micro-alga at various volume fractions: Applications to intensified photobioreactors. J. Nonnewton. Fluid Mech. 231, 91–101. https://doi.org/10.1016/j.jnnfm.2016.03.012

Su, Z., Kang, R., Shi, S., Cong, W., Cai, Z., 2010. Study on the destabilization mixing in the flat plate photobioreactor by means of CFD. Biomass and Bioenergy 34, 1879–1884. https://doi.org/10.1016/j.biombioe.2010.07.025

Suh, I.S., Lee, S.B., 2003. A light distribution model for an internally radiating photobioreactor. Biotechnol. Bioeng. 82, 180–189. https://doi.org/10.1002/bit.10558

Theron, F., Sauze, N. Le, 2011. Comparison between three static mixers for emulsification in turbulent flow. Int. J. Multiph. Flow 37, 488–500. https://doi.org/10.1016/j.ijmultiphaseflow.2011.01.004

Tilzer, M.M., 1987. Light-dependence of photosynthesis and growth in cyanobacteria: Implications for their dominance in eutrophic lakes. New Zeal. J. Mar. Freshw. Res. 21, 401–412. https://doi.org/10.1080/00288330.1987.9516236

Ting, H., Haifeng, L., Shanshan, M., Zhang, Y., Zhidan, L., Na, D., 2017. Progress in microalgae cultivation photobioreactors and applications in wastewater treatment: A review. Int. J. Agric. Biol. Eng. https://doi.org/10.3965/j.ijabe.20171001.2705

Uggetti, E., García, J., Álvarez, J.A., García-Galán, M.J., 2018. Start-up of a microalgae-based treatment system within the biorefinery concept: from wastewater to bioproducts. Water Sci. Technol. 78, 114–124. https://doi.org/10.2166/wst.2018.195

Vanysacker, L., Boerjan, B., Declerck, P., Vankelecom, I.F.J., 2014. Biofouling ecology as a means to better understand membrane biofouling. Appl. Microbiol. Biotechnol. https://doi.org/10.1007/s00253-014-5921-2

Vasumathi, K.K., Premalatha, M., Subramanian, P., 2012. Parameters influencing the design of photobioreactor for the growth of microalgae. Renew. Sustain. Energy Rev. 16, 5443–5450. https://doi.org/10.1016/j.rser.2012.06.013

Wang, B., Lan, C.Q., Horsman, M., 2012. Closed photobioreactors for production of microalgal biomasses. Biotechnol. Adv. 30, 904–912. https://doi.org/10.1016/j.biotechadv.2012.01.019

Wang, C., Lan, C.Q., 2018. Effects of shear stress on microalgae – A review. Biotechnol. Adv. 36, 986–1002. https://doi.org/10.1016/j.biotechadv.2018.03.001

Wang, L.L., Tao, Y., Mao, X.Z., 2014. A novel flat plate algal bioreactor with horizontal baffles: Structural optimization and cultivation performance. Bioresour. Technol. 164, 20–27. https://doi.org/10.1016/j.biortech.2014.04.100

Weissman, J.C., Goebel, R.P., Benemann, J.R., 1988. Photobioreactor design: Mixing, carbon utilization, and oxygen accumulation. Biotechnol. Bioeng. https://doi.org/10.1002/bit.260310409

Xu, L., Weathers, P.J., Xiong, X.-R., Liu, C.-Z., 2009. Microalgal bioreactors: Challenges and opportunities. Eng. Life Sci. 9, 178–189. https://doi.org/10.1002/elsc.200800111

Zakova, T., Jirout, T., Kratky, L., Belohlav, V., 2019. Hydrodynamics as a tool to remove biofilm in tubular photobioreactor. Chem. Eng. Trans. 76, 451–456. https://doi.org/10.3303/CET1976076

Zeriouh, O., Reinoso-Moreno, J.V., López-Rosales, L., Cerón-García, M. del C., Sánchez-Mirón, A., García-Camacho, F., Molina-Grima, E., 2017. Biofouling in photobioreactors for marine microalgae. Crit. Rev. Biotechnol. 37, 1006–1023. https://doi.org/10.1080/07388551.2017.1299681

Zhang, Q., Wu, X., Xue, S., Liang, K., Cong, W., 2013. Study of hydrodynamic characteristics in tubular photobioreactors. Bioprocess Biosyst. Eng. 36, 143–150. https://doi.org/10.1007/s00449-012-0769-2

Zhang, Y., 2017. Critical transition Reynolds number for plane channel flow. Appl. Math. Mech. 38, 1415–1424. https://doi.org/10.1007/s10483-017-2245-6

Zhu, J., Rong, J., Zong, B., 2013. Factors in mass cultivation of microalgae for biodiesel. Chinese J. Catal. 34, 80–100. https://doi.org/10.1016/s1872-2067(11)60497-x

Zippel, B., Neu, T.R., 2005. Growth and structure of phototrophic biofilms under controlled light conditions. Water Sci. Technol. 52, 203–209. https://doi.org/10.2166/wst.2005.0202

On-line database of cyanobacterial genera. 2018. Cyano DB Classification. [ONLINE] Available at: http://www.cyanodb.cz. [Accessed 16 November 2018].

Servei Meteorològic de Catalunya. 2018. meteo.cat. [ONLINE] Available at: https://www.meteo.cat/observacions/xema/dades. [Accessed 15 December 2018].

A European Green Deal. 2020. European Commission. [ONLINE] Available at: https://ec.europa.eu/info/strategy/priorities-2019-2024/european-green-deal_en. [Accessed 5 November 2020].

The Paris Agreement. 2020. United nations Climate Change. [ONLINE] Available at: https://unfccc.int/process-and-meetings/the-paris-agreement/the-paris-agreement. [Accessed November 2020].

The Katowice climate package: Making the Paris Agreement work for all. 2020. United nations Climate Change. [ONLINE] Available at: https://unfccc.int/process-and-meetings/the-paris-agreement/katowice-climate-package. [Accessed November 2020].

Curriculum vitae

Vojtech Belohlav was born in Prague, (Czech Republic), in 1990. He obtained his undergraduate degree in the School of Agricultural Engineering specialized in Food and Bioprocess Engineering at the Universitat Politècnica de Catalunya-BarcelonaTech in 2015. In 2016 he obtained an undergraduate degree in the Faculty of Mechanical Engineering specialized in Process Engineering at the Czech Technical University in Prague. In 2016, he started his double degree PhD research at the Department of Process Engineering in the Czech Technical University in Prague and in the Group of Environmental Engineering and Microbiology in the Universitat Politècnica de Catalunya-BarcelonaTech.

Articles in refereed journals

Belohlav, V., Uggetti, E., García, J., Jirout, T., Kratky, L., Díez-Montero, R. (2021) Assessment of hydrodynamics based on Computational Fluid Dynamics to optimize the operation of hybrid tubular photobioreactors, *Journal of Environmental Chemical Engineering*, 9, 105768.

Belohlav, V., Jirout, T., Kratky, L. (2021) Optimization of hydrodynamics by installation of static mixer in flat panel photobioreactor. *Chemical Engineering Transactions*, 86, 139-144.

Belohlav, V., Zakova, T., Jirout, T., Kratky, L. (2020). Effect of hydrodynamics on the formation and removal of microalgal biofilm in photobioreactors. *Biosystems Engineering*, 200, 315–327.

Díez-Montero, R., Belohlav, V., Ortiz, A., Uggetti, E., García-Galán, M. J., García, J. (2020). Evaluation of daily and seasonal variations in a semi-closed photobioreactor for microalgae-based bioremediation of agricultural runoff at full-scale. *Algal Research*, 47, 101859.

Belohlav, V., Jirout, T. (2019). Design methodology of industrial equipment for microalgae biomass primary harvesting and dewatering. *Chemical Engineering Transactions*, 76, 919–924.

Belohlav, V., Jirout, T., Kratky, L. (2018). Possibilities of implementation of photobioreactors on industrial scale. *Chemické Listy*, 112 (3), 183–190.

García, J., Ortiz, A., Álvarez, E., Belohlav, V., García-Galán, M. J., Díez-Montero, R., Álvarez, J. A., Uggetti, E. (2018). Nutrient removal from agricultural run-off in demonstrative full scale tubular photobioreactors for microalgae growth. *Ecological Engineering*, 120.

Zakova, T., Jirout, T., Kratky, L., Belohlav, V. (2018). Hydrodynamics as a tool to remove biofilm in tubular photobioreactor. *Chemical Engineering Transactions*, 76, 451–456.

Belohlav, V., Jirout, T., Kratky, L., Uggetti, E., Díez-Montero, R., García, J. (in preparation). Integration of hydrodynamics in cultivation model of hybrid horizontal tubular photobioreactor.

Belohlav, V., Jirout, T., Kratky, L., Uggetti, E., Díez-Montero, R., García, J. (in preparation). Mutual hydrodynamics and light regime influence on microalgae biomass production in a hybrid horizontal tubular photobioreactor.

Conference proceedings

Belohlav, V., Jirout, T., Kratky, L. (2017). Operational and design parameters of microalgae cultivation systems for its application in industrial scale. In European Biomass Conference and Exhibition Proceedings; ETA – Florence, pp 1990–1997.

Belohlav, V., Uggetti, E., Montero, R. D., García, J., Jirout, T., Kratky, L. (2018). Numerical investigation of hydrodynamic conditions in a pilot tubular photobioreactor. In European Biomass Conference and Exhibition Proceedings; ETA – Florence, pp 183–190.

Belohlav, V., Jirout, T. (2019). Equipment for microalgae primary dewatering and separation using gravitational and centrifugal forces. In European Biomass Conference and Exhibition Proceedings; ETA – Florence, pp 1957–1962.

Belohlav, V., Jirout, T., Kratky, L., Uggetti, E., Díez-Montero, R. (2019). Numerical analysis of hydrodynamic conditions in pilot flat-panel photobioreactor: operating and design parameters influence on the microalgae cultivation. In European Biomass Conference and Exhibition Proceedings; ETA - Florence, pp 255–260.

Belohlav, V., Jirout, T., Kratky, L. (2021). Integration of hydrodynamics into a biokinetic model for the simulation of microalgae cultivation in a photobioreactor. In European Biomass Conference and Exhibition Proceedings; ETA – Florence, Proceedings Pre-proof.

Conference contribution

Oral communications

Uggetti E., Belohlav V., García-Galán M.J., García J. (2018). A biorefinery approach in a microalgae-based wastewater treatment plant: from wastewater to bioproducts. In 8th International Conference on Algal Biomass, Biofuels & Bioproducts 2018 – Seattle.

Belohlav V., Jirout T., Kratky L. (2018). Numerical simulation of hydrodynamic conditions in hybrid tubular photobioreactor. In Conference on Energy from Biomass, ENBIO 2018 – Lednice.

Belohlav, V., Jirout, T., Kratky, L. (2019). Hydrodynamics as a tool for elimination of biofilm formation in flat panel photobioreactor. In Conference on Energy from Biomass, ENBIO 2019 – Lednice.

Posters

Belohlav, V., Jirout, T., Kratky, L. (2017). Operational and design parameters of microalgae cultivation systems for its application in industrial scale. In European Biomass Conference and Exhibition, EUBCE 2017 – Stockholm.

Belohlav, V., Jirout, T., Kratky, L. (2017). Possibilities of photobioreactors applications in industrial scale. In Týden vědy a inovací pro praxi a životní prostředí, TVIP 2017 – Hustopeče.

Belohlav, V., Uggetti, E., Montero, R. D., García, J., Jirout, T., Kratky, L. (2018). Numerical investigation of hydrodynamic conditions in a pilot tubular photobioreactor. In European Biomass Conference and Exhibition, EUBCE 2018 – Copenhagen.

Belohlav, V., Jirout, T., Kratky, L. (2018). Numerical investigation of hydrodynamic conditions in pilot flat panel photobioreactor. In AlgaEurope Conference 2018 – Amsterdam.

Belohlav, V., Jirout, T., (2019). Design methodology of industrial equipment for microalgae biomass primary harvesting and dewatering. In 22nd conference of Process Integration, Modelling Optimisation for Energy Saving and Pollution Reduction, PRES'19 – Crete.

Belohlav, V., Jirout, T. (2019). Equipment for microalgae primary dewatering and separation using gravitational and centrifugal forces. In European Biomass Conference and Exhibition, EUBCE 2019 – Lisbon.

Belohlav, V., Jirout, T., Kratky, L., Uggetti, E., Díez-Montero, R. (2019). Numerical analysis of hydrodynamic conditions in pilot flat-panel photobioreactor: operating and design parameters influence on the microalgae cultivation. In European Biomass Conference and Exhibition, EUBCE 2019 – Lisbon.

Belohlav, V., Jirout, T., Kratky, L. (2019). Elimination of biofilm formation in flat panel photobioreactor by hydrodynamics. In International Conference on Chemical Technology, ICCT 2019 – Mikulov.

Belohlav, V., Jirout, T., Kratky, L. (2021). Integration of hydrodynamics into a biokinetic model for the simulation of microalgae cultivation in a photobioreactor. In European Biomass Conference and Exhibition, EUBCE 2021 – online conference.

Belohlav, V., Jirout, T., Kratky, L. (2021). Homogenization and mixing of flow in flat panel photobioreactor. In International Conference on Chemical Technology, ICCT 2021 – online conference.

Utility model

Jirout, T., Belohlav, V. Static mixer, especially into a plate reactor chamber, U1 34 865 CZ, Feb 23, 2021.

European patent

Jirout, T., Belohlav, V. Static mixer, especially into a plate reactor chamber (submitted).

Participation in R&D projects

- Innovative eco-technologies for resource recovery from wastewater - INCOVER (GA 689242), EU H2020, 2016-2019.
- Research Center for Low Carbon Energy Technologies, EF16_019/0000753, 2018-2022.
- Design of separation technology for radioactive mash processing, CZ.01.1.02/0.0/0.0/16_084/0010286, 2017-2020.
- Design of structural arrangement of expansion head of extruder and flash separator for flash distillation of PET waste, Client: EGIPLUS, 2017.
- Design of technical solution for hydraulic separation of slag from process water, Client: VVV MOST, 2019.
- Research and development project on material recovery technology of waste plastics and tires in the refining and petrochemical industry (PYREKOL), Client: ORLEN UniCRE, 2021.

Courses

PhD Summer School (12-25 August 2019) - Affordable Energy Transition: technological solutions and socio-economic constraints. Shanghai Jiaotong University, Zhejiang University Hangzhou, China.